

2016

A statistical mechanical model of economics

<https://hdl.handle.net/2144/19754>

Boston University

BOSTON UNIVERSITY
GRADUATE SCHOOL OF ARTS AND SCIENCES

Dissertation

A STATISTICAL MECHANICAL MODEL OF ECONOMICS

by

NICHOLAS EDWARD WILLIAMS LUBBERS

B.S., Colorado School of Mines, 2008

M.A., Boston University, 2012

Submitted in partial fulfillment of the
requirements for the degree of
Doctor of Philosophy
2016

© Copyright by
NICHOLAS EDWARD
WILLIAMS LUBBERS
2016

Approved by

First Reader

William Klein, Ph.D.
Professor of Physics
Boston University

Second Reader

Pankaj Mehta, Ph.D.
Associate Professor of Physics
Boston University

For the spirit of collective improvement; for all those who change the world for the better, be those changes great or small.

Acknowledgments

All you happy people

A STATISTICAL MECHANICAL MODEL OF THE ECONOMY

NICHOLAS LUBBERS

Boston University Graduate School of Arts and Sciences, 2016

Major Professor: William Klein, Professor of Physics

ABSTRACT

Statistical mechanics pursues low-dimensional descriptions of systems with a very large number of degrees of freedom. I explore this theme in two contexts.

The main body of this dissertation explores and extends the Yard Sale Model (YSM) of economic transactions using a combination of simulations and theory. The YSM is a simple interacting model for wealth distributions which has the potential to explain the empirical observation of Pareto distributions of wealth. I develop the link between wealth condensation and the breakdown of ergodicity due to nonlinear diffusion effects which are analogous to the geometric random walk. Using this, I develop a deterministic effective theory of wealth transfer in the YSM that is useful for explaining many quantitative results.

I introduce various forms of growth to the model, paying attention to the effect of growth on wealth condensation, inequality, and ergodicity. Arithmetic growth is found to partially break condensation, and geometric growth is found to completely break condensation. Further generalizations of geometric growth with growth inequality show that the system is divided into two phases by a tipping point in the inequality parameter. The tipping point marks the line between systems which are ergodic and systems which exhibit wealth condensation.

I explore generalizations of the YSM transaction scheme to arbitrary betting functions to develop notions of universality in YSM-like models. I find that wealth

condensation is universal to a large class of models which can be divided into two phases. The first exhibits slow, power-law condensation dynamics, and the second exhibits fast, finite-time condensation dynamics. I find that the YSM, which exhibits exponential dynamics, is the critical, self-similar model which marks the dividing line between the two phases.

The final chapter develops a low-dimensional approach to materials microstructure quantification. Modern materials design harnesses complex microstructure effects to develop high-performance materials, but general microstructure quantification is an unsolved problem. Motivated by statistical physics, I envision microstructure as a low-dimensional manifold, and construct this manifold by leveraging multiple machine learning approaches including transfer learning, dimensionality reduction, and computer vision breakthroughs with convolutional neural networks.

Contents

1	Introduction and Background	1
1.1	What is Econophysics?	1
1.2	The dissertation in brief	3
1.3	Pareto Laws in Income and Wealth Distribution	6
1.3.1	On analyzing data of high inequality	8
1.4	Issues with non-interacting models of Economics	9
1.5	Asset Exchange Models	11
1.5.1	The Yard Sale Model	13
1.6	Ergodicity	13
1.7	Structure of this Dissertation	15
1.7.1	Chapter 1: Introduction and Background	15
1.7.2	Chapter 2: The Yard Sale Model without growth	15
1.7.3	Chapter 3: Theoretical descriptions of the YSM	16
1.7.4	Chapter 4: The YSM with arithmetic growth	16
1.7.5	Chapter 5: The YSM with geometric growth	16
1.7.6	Chapter 6: Generalized framework for wealth condensation . .	17
1.7.7	Chapter 7: Concluding remarks and future work	17
1.7.8	Chapter 8: Faithful Dimensionality Reduction of Materials Mi- crostructure using Convolutional Neural Networks	17

2	The Yard Sale Model without growth	18
2.1	Purpose of this chapter	18
2.2	Postulates of Asset Exchange	18
2.3	The Model	19
2.4	Conservation of Wealth	21
2.5	Rescaling Invariance	22
2.6	Simulation Findings	23
2.6.1	Wealth Condensation	23
2.6.2	The thermodynamic limit and scaling with system size	24
2.6.3	Scaling with α	27
2.6.4	Mobility	30
2.6.5	Ergodicity	33
2.6.6	Evolution of the Wealth Distribution	36
3	Theoretical descriptions of the YSM	39
3.1	Purpose of this chapter	39
3.2	Theoretical Treatments	39
3.2.1	Geometric Random Walk	39
3.2.2	Master Equation Approach	41
3.2.3	Mean Trade Theory	47
3.2.4	Connection between MT, GRW, and master equation	51
3.2.5	Solution to bare YSM under MT	52
3.3	Generalized return distributions	53
4	The YSM with arithmetic growth	55
4.1	Form of the Growth and Dimensional Considerations	55

4.2	Developing steady-state	55
4.3	Varying α	57
4.4	Pareto Index	60
4.5	Mobility	60
4.5.1	Rank Correlation	60
4.5.2	Rank-Rank transfer data	61
4.5.3	TM metric	64
4.6	Arithmetic growth in the MT approximation	67
4.7	Skewed arithmetic growth	68
4.7.1	Constrained arithmetic growth	68
4.7.2	Unconstrained growth	69
4.7.3	On physical expectations for the growth	70
5	The YSM with geometric growth	71
5.1	Uniform geometric growth	71
5.1.1	Wealth distribution	72
5.2	Skewed Growth	75
5.2.1	Duality with wealth tax	76
5.2.2	Dynamical phases	77
5.2.3	System sensitivity to μ, α	80
5.3	Ergodicity	83
5.3.1	Wealth distribution approaching the transition	86
5.4	MT with geometric growth	87
6	Generalizations	93
6.1	Generalized Wealth Condensation	93

6.1.1	Diffusion in Wealth Space	94
6.1.2	Dynamics near betting function zeros	96
6.1.3	The next-to-poorest agent and so on	104
6.1.4	The thermodynamic limit and the emergence of wealth con- densation	105
6.1.5	Measuring Inequality	106
6.1.6	Inequality evolution and Jensen’s Inequality	107
6.1.7	Drift Terms, Growth, and Trade bias: Condensation stability .	111
6.1.8	Example system simulations	112
7	Concluding remarks and further directions	115
7.1	The Yard-Sale Model	115
7.2	Extending the Yard-Sale Model with growth:	117
7.2.1	Arithmetic growth	117
7.2.2	Geometric growth	119
7.3	Extensions to generalized trading schemes	120
7.4	Future directions	121
8	Part II: Inferring low-dimensional microstructure representations using convolutional neural networks	125
8.1	Introduction	125
8.1.1	Structure of this chapter	128
8.2	Background	129
8.2.1	Convolutional Neural Networks for image processing	129
8.3	Methods	130
8.3.1	Baseline method: Power spectrum for texture characterization	130

8.3.2	CNNs for texture characterization	131
8.3.3	Manifold Learning with Multidimensional Scaling	133
8.4	Tasks	134
8.4.1	Image generation process	134
8.4.2	Angle reconstruction task	135
8.4.3	Three dimensional manifold reconstruction task	141
8.5	Discussion	146
8.5.1	Power spectrum performance	146
8.5.2	CNN performance	148
8.6	Conclusions and future directions	153
Appendices		155
A Mean Trade Equations Approaching the Phase Transition		156
A.1	Scaling of the richest agent	156
A.2	Solution to the scaling form near the phase transition	158
Bibliography		161
Curriculum Vitae		179

List of Tables

- 8.1 R^2 coefficients for linear regression between the manifold coordinates
and generating parameters for varying embedding dimensions. . . . 145

List of Figures

1.1	A schematic of the typical structure of a wealth distribution.	7
2.1	The wealth condensation phenomenon.	23
2.2	YSM time scaling with system size.	25
2.3	Comparison of wealth density evolution for $N = 1000$ and $N = 10,000$	26
2.4	The fraction of the richest agents that hold a given fraction of the wealth against time.	27
2.5	The fraction of agents that are richer than the initial wealth versus time plotted for various values of the trade size parameter α	28
2.6	Richest fractions above various thresholds versus scaled time, showing condensation scaling.	29
2.7	Rank correlation against time and against rescaled time, showing scal- ing collapse.	31
2.8	The number of bankrupt agents in time.	32
2.9	Permutation correlation against time and rescaled time.	33
2.10	The Thirumalai-Mountain metric applied to the YSM.	35
2.11	Exponential wealth decay by rank.	37
2.12	Cumulative wealth against time.	38
4.1	The evolution of the wealth distribution with arithmetic growth.	56
4.2	Evolution of very rich agents under arithmetic growth.	57

4.3	The arithmetic growth steady state distribution for various trading parameters.	58
4.4	Scaling collapse of the steady state distribution for various trading parameters.	59
4.5	Rank correlations against time for arithmetic growth.	61
4.6	Rank-Rank transfer plots for various α over various time scales. . . .	62
4.7	Unmodified TM metric for arithmetic growth.	65
4.8	Modified TM metric for arithmetic growth.	66
5.1	The wealth distribution under geometric growth shown for several times.	72
5.2	The rescaled wealth distribution under geometric growth shown for several times, showing rescaled steady state.	72
5.3	The rescaled steady state for various trading and growth parameters.	73
5.4	Wealth against shifted rank, showing the quality of the mean trade solution.	74
5.5	Scaling of the median wealth for geometric uniform growth.	75
5.6	The standardized moments of the log-wealth distribution.	76
5.7	The wealth distribution for γ approaching 1, showing a slow approach to rescaled steady state.	77
5.8	The wealth in the richest segments of the economy for various growth skew parameters.	79
5.9	The wealth of the richest agent approaching the phase transition, plotted for various system sizes.	79
5.10	The timescale associated with the approach to steady state as the skew parameter is varied.	80
5.11	The method for obtaining steady-state times.	81

5.12	The steady-state timescale against the growth skew for different values of trade and growth parameters.	81
5.13	The steady-state timescale against different values of the trading parameter.	82
5.14	The steady-state timescale against different values of the growth rate.	83
5.15	The TM metric for skewed geometric growth for different values of the skew parameter.	84
5.16	The mixing time against the skew parameter and the regression fits used to determine the mixing time.	85
5.17	Demonstration of the mean trade scaling relations in numerical solution of mean trade and in trading simulations.	88
5.18	The collapse function which indicates convergence to the mean trade scaling solution.	91
5.19	A top-down view of the collapse function.	92
6.1	A diagram of wealth space.	94
6.2	An example betting function	95
6.3	Types of betting functions.	99
6.4	Types of potential functions.	101
6.5	Wealth quantiles versus time for various types of wealth condensation.	113
6.6	The number of nonbankrupt agents versus time for each type of model.	114
6.7	The uncondensed wealth versus time for each type of models.	114
7.1	The 2013 Forbes Global 2000 dataset	123
8.1	Texture synthesis of materials microstructures using a convolutional neural network.	127

8.2	The space of synthetic textures, generated by three tunable parameters.	135
8.3	Sample images at different noise values and the corresponding power spectra.	136
8.4	Reconstructions of the angle image manifold.	138
8.5	The reconstruction error of the angle reconstruction task as a function of noise.	139
8.6	The MDS stress of the embedding into two dimensions for the angle reconstruction task as a function of noise.	140
8.7	The MDS embedding stress for the three dimensional manifold reconstruction as a function of embedding dimension.	142
8.8	The three dimensional embedding of the three dimensional image manifold.	143
8.9	Axis-aligned view of the 3-D embedding.	143
8.10	Images of the 3-D image manifold embedded into four dimensions. . .	144
8.11	Projection from the six dimensional embedding into the two dimensions which best capture scale and noise variations using linear regression.	145

Chapter 1

Introduction and Background

1.1 What is Econophysics?

The body of work contained here is predominantly categorizable as *Econophysics* research, research which aims to tackle questions of an economic nature, and whose methods are inspired by traditional physics research. My particular economic interest is in studying the distribution of wealth and income in society.

Bulk properties of human populations have been of interest to mankind for quite some time. In fact, the historical origin of the word “statistics” is in studying the properties of the *state* [1]. In physics, the development of statistical mechanics by Ludwig Boltzmann hailed a new era of tackling physical problems using probability theory and the assumption of the interaction of simple, identical components. Econophysicists seek to turn the resulting body of mathematics back at the original social setting of statistics.

Econophysics is a young discipline [2–4], usually characterized as originating in the 1990’s, formed in part by a dissatisfaction with the results of mainstream economics [2–6]. Many concerns are cited regarding the Economist’s methodology. Perhaps foremost is the development of models based on *a priori* expectations when empirical data disagrees with these expectations [6–10]—e.g. the efficient market hypothesis, the rational agent hypothesis, and general equilibrium theory. Econo-

physicists established themselves by successfully applying techniques from physics to financial markets [2–4], in particular defying the a typical economic assumption of normally distributed returns.

However, Econophysics has not been well-received by economists, who in return have criticized the econophysicist’s methodology. Gallegati *et al.* [5] raise several objections: They decry the ignorance of physicists to the large body economic literature, lament the differences in statistical methodology, raise concerns over whether the ‘universal’ facts taken by econophysicists are in fact universal, and perhaps above all argue that physics models are not appropriate to economic situations, in particular the invocation of conservation laws and transaction-only models. (This dissertation deals in a model which addresses that concern.)

McCauley [6] reply from the econophysicists perspective, point by point addressing their perceived flaws in economics. In particular, while they agree that physicists use different statistical methodology, they argue that relevant economic models are plagued by too many variables to produce meaningful results on the amount of data available, and this demands that researchers focus on simpler models and on the falsifiability of these models. They do agree that there is a danger in over-simplifying and that economics presents situations fundamentally different from physics: The bare units of the model can make intelligent decisions, the decisions rules may dynamically respond to the state of the system.

The difficulty, then, is in producing simplified models which have meaningful and reasonable economic interpretations (or what a physicist would call a physical interpretation) that incorporate the flexibility of economic entities. These models must be amenable to analysis, and they must be in some way comparable to data. From this perspective, the aim of the research in this dissertation is twofold. The basis of the

dissertation is a very simple model (the Yard Sale Model) which contains reasonable assumptions and compelling dynamics (Wealth condensation), but does not capture empirical phenomena. The first aim is to extend the dynamics in order to investigate the potential to capture empirical data on wealth distributions. The second aim is to generalize the framework of the Yard Sale Model in order to investigate whether or not the compelling results can be said to be generally true.

1.2 The dissertation in brief

The economic focus of the research herein is the distribution of wealth. Empirical studies of wealth distributions [11, 12]. have shown a consistent structure demonstrated in a variety of domains—in different places, different times, and different metrics of wealth (see section 1.3 for more details). The wealth distribution is divided into two regimes. The richest economic entities follow a power-law distribution known as a Pareto law, after Vilfredo Pareto [13, 14]. The richest agents here constitute somewhere between 1% and 10% of the economy, with fluctuations in this number being governed both by the shape of the distribution and by the fitting methods being applied. The bulk of the agents deviate markedly from the power law, with various authors arguing for Boltzmann distributed or Log-normal distributed wealth.

In particular, I am focused on agent-based modeling of wealth exchange (see section 1.5) These models treat wealth as a scalar quantity which is transferred from agent to agent via stochastic rules. For the most part, I have focused on a particular model of wealth exchange known as the *Yard Sale Model* [15] (YSM) (See section 1.5.1). The wealth exchange takes place between random pairs of agents, and the quantity of wealth traded is a fixed fraction of the wealth of the poorer agent in the trade. This parcel of wealth is then traded either from the richer to the poorer,

or the other way around, according to a fair coin flip.

The YSM is valuable for many reasons. Foremost it is a simple model, which itself has many advantages. Conceptually simple models are easy to explain, and so they are intrinsically valuable for interdisciplinary communication—many of the concepts of statistical mechanics are foreign to the ecosystem of (pure) economics research, and so simplicity is especially a virtue in these interdisciplinary pursuits. Models with few parameters are most easily amenable to analysis; The fewer the buttons and dials which can be adjusted, the easier it is to determine which parameters control the state of the system, and how.

A particular aspect of this simplicity is that the model is scale-free; the bare model's only parameter is a dimensionless fraction of wealth, reflecting multiplicative exchange dynamics. Real economies often exhibit multiplicative fluctuations, both in the aggregate and when looking at individual components; A good example here is the stock market [16–18]. Thus, multiplicative wealth exchange is a good ground on which to build a model which exhibits multiplicative fluctuations. The scale-free nature of the trading is a good set-up to explain the power-distributed Pareto law. Moreover, multiplicative betting not only reflects empirical fluctuations, but is in certain cases is theoretically justified as the strategic choice which optimizes an individual's the long-term growth rate [19].

Another advantage of the YSM is that it is an interacting model. Many economic models seek to explain wealth distributions by allowing an ensemble of agents which fluctuate independently in a fixed background (see section 1.4). Conceptually, then, the analysis seeks to solve a simple one-body inverse problem: What background landscape gives rise to a given steady-state distribution? The answer to this question gives little insight into the economic processes at hand, as *a priori* any background

landscape is allowed, because the landscape need not be consistent with the action and evolution of the agents. In addition, this type of model assumes from the outset that the economy can be described by an equilibrium process. A more coherent model realizes the structure of the landscape via interactions within the economy—this closes the loop of cause and effect, so that the wealth distribution is generated by a mechanism, not just by another distribution.

I seek to explore the potential of the YSM to explain the structure of empirical wealth distributions. Previous work [15,20–22] has established that the YSM exhibits *wealth condensation*; Over time, the wealth condenses onto a single agent in the system. I present further analysis of and extensions to the YSM. I establish that the dynamics of the model are essentially dissipative, ergodicity-breaking dynamics, and that these mathematical properties are the origin of wealth condensation.

I also introduce a new framework for conceptualizing and solving the model based on the stochastic drift of individual agents, conceptualizing bridging this interacting model with the autoregressive, independent-agent formulations from economic literature. This framework is useful for considering dynamics which are essentially a function of an agent’s rank in the economy, and is in this regard readily interpretable, giving insight into the effective dynamics for each strata of an econophysics model.

While real-world wealth is not quite so monopolized, it is also not in a steady state, but rather growing in time [23]. So, I consider driving the system with external sources of growth in a driven-dissipative fashion, with an eye on the ergodicity of the model as well as wealth condensation. Growth allows the model to break wealth condensation and support various nontrivial wealth distributions. Different forms of growth are explored and compared to the known structure of empirical wealth distributions.

Finally, using this new framework, I consider the possibility of wealth condensation in more generalized asset exchange models, whose dynamics are given by a more general function of the poorer agent's wealth, as opposed to the strictly multiplicative YSM. Using an effective theory of wealth transfer, I find that wealth condensation in the absence of growth is a general phenomena, and that the rate of wealth condensation can be partitioned into slow models and fast models. The YSM turns out to be the critical system which marks the dividing line between these cases.

1.3 Pareto Laws in Income and Wealth Distribution

The primary motivator for much of econophysics is a remarkable empirical fact first observed by Pareto [13]: The distribution of wealth and income in society has a universal form. His work established the power law distribution of wealth, now known as the Pareto distribution, given as a probability distribution function $p(w)$ or a cumulative distribution function $C(w)$:

$$p(w) \propto w^{-1-\alpha} \quad (1.1)$$

$$C(w) \propto w^{-\alpha} \quad (1.2)$$

The exponent α , called the *Pareto Index* or *Pareto Exponent* of the distribution, characterizes the inequality of the distribution. Pareto found approximately $\alpha = 1.5$, but it is now known that the Pareto index is a fluxuating quantity over time and regions, usually somewhere between 1.5 and 2.5, and almost always between 1 and 3. While Pareto originally believed this distribution to apply to the whole of society, it is now understood that the power-law distribution of wealth applies only to to the richest segment of society, usually between 1% and 10%. The bulk of the

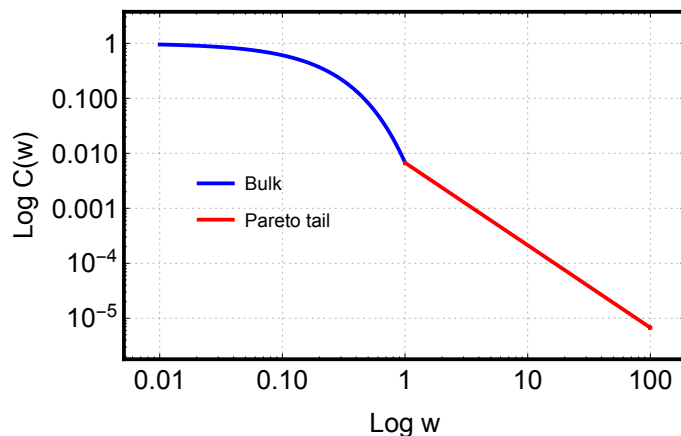


Figure 1.1: A schematic of the typical structure of a wealth distribution.

society follows a more centralized distribution, often characterized an exponential distribution (e.g. e.g. [11]), but sometimes as a log-normal distribution (e.g. [12, 24])—see Fig. 1.1 for a schematic.

This structure has been observed in many societies over a fairly wide spectrum of time and space: Atkinson *et al.* [25] surveys studies of Pareto indices and inequality in over twenty countries throughout the twentieth century, broadly finding inequality decreased during the period of the world wars, but has been increasing in the last few decades. There is modern data on the United States [26,27], Japan [24,26], the United Kingdom [11,28], India [29], Germany [28]. Looking back in time, there are historical studies finding Pareto exponents for 19th century Prussia and England [12], 18th century Peru [12], 15th and 16th century Augsburg [12], medieval Hungary [30] (using the number of serfs owned as a proxy for wealth), and even ancient Egypt [31] (using property area as a proxy for wealth). Internationally, the Forbes 400 data [27,32] have been analyzed. The Pareto law has even been found in the modern electronic Bitcoin crypto-currency [33].

1.3.1 On analyzing data of high inequality

Many statistical models are given in the context of distributions which are relatively symmetric and centralized (with a tail that decays exponentially or faster). However, the power law distributions present both in the statistical physics of phase transitions and in economics thwart both of these common assumptions. In this case, averaging summary statistics such as the mean and standard deviation may formally diverge. In the context of finite data sets, this results in a population mean and standard deviation which is highly dependent on the particular sample drawn. The practical consequence of this is that any wealth data which one examines should be summarized with more robust statistical measures, else one risks results which depend crucially on the precise wealths of the wealthiest entities.

One common and viable approach is to use the median to characterize the central tendency, and quantiles to determine the approximate spread. This approach is non-parametric, and the median is insensitive to monotonic, invertible transformations of the quantity in question. This is in line with the economic concept of *utility*, which postulates that economics can be explained by the supposition that the *value* of wealth depends on how much wealth one currently has, i.e. added value is a marginal function.

Several related approaches to economic modeling, including the one in this dissertation, treat economic agents as undergoing some type of random multiplicative process. In this case it is appropriate to examine the logarithm of wealth as a statistical summary- in particular, the typical wealth *scale* can be thought of as $e^{\langle \log w \rangle}$ [34].

In economics, this school of thought is embodied in *Theil's L measure* [35] of inequality, $L = \log \langle w \rangle - \langle \log w \rangle$. Theil's economic measures were motivated by Shannon's information theory [36], and *Theil's T measure*, $T = \langle w \log w \rangle$, is the

negative of Shannon's information entropy, which was recognized in its inception as connected to the theory of statistical mechanics. Shannon and Theil were interested in measures of spread which obeyed certain axioms appropriate to complexity and econometrics. On the other hand, statistical mechanical entropy concerns itself with the measure of the number of microscopic states that may be taken by a system subject to macroscopic constraints. Theil's measure can then be reconciled as measuring the scale of the partitioning of wealth among various economic agents—the maximum equality is given by the maximum entropy condition, wherein wealth is divided equally among the agents, and greater inequality can be understood as partitions of the wealth in which the total wealth is dominantly owned by fewer agents.

1.4 Issues with non-interacting models of Economics

Modeling of wealth and income distributions begins with with Gibrat's law of proportional effect [37]. This scheme assumes that firms will grow and shrink with fluctuations which are proportional to the size of the firm. This leads to a non-stationary log-normal distribution of firm sizes. A conspicuous aspect of this scheme is that it makes predictions on the assumption that firms can be thought to be completely independent of each other—hence I refer to these models as non-interacting models or one-body models. The second conspicuous aspect of the model is that it is a Markov process—growth at one time is not influenced by growth in the past. Econophysicists have more recently characterized the growth of firms and found an interesting structure that disobeys Gibrat's fundamental assumption—empirical growth percentages are dependent on firm size. [38]

Champernowne [39] gave a more detailed model which provides an equilibrium distribution—indeed, to solve his model he prescribes that it must have an equilibrium.

He discretizes the income spectrum into discrete bins and postulates a Markov chain model for income. The essential difference between his approach and Gibrats is the assumption of the lower-boundedness of income. Similar approaches have been made many times since [16, 26, 40–51], with many approaches following the Kesten process [52], which is the continuous analogue for the discrete Markov chain model of Champernowne. The unifying aspect of these approaches is that agents fluctuate purely in a background. The sources of these fluctuations are not clarified; they are parameteric functions of random variables. Like Gibrat, they assume a particular form of recurrence in wealth fluctuations (indeed, many of them make exactly the same multiplicative supposition as Gibrat) but without further physical or empirical justification.

There are two interrelated reasons why this approach is problematic. The first is the assumption of equilibrium. The continually growing economy of the real world assures that no wealth distribution is in equilibrium, even in the case that the economy appears roughly static over a short period of time (these particular periods are sometimes cherry-picked when analyzing data [53]). In fact, studies have explicitly refuted the markov property for income mobility [54–56] and there have been numerous calls in recent years to avoid blind assumption of equilibrium [7, 8, 57]. To be careful about the issue, let me note that many non-interacting analyses do derive whether or not their mathematical model is in equilibrium—the problem is the assumption that equilibrium results are the ones pertinent to the real world.

The second problematic aspect is the nature of the fluctuations. In non-interacting models models, agents fluctuate being coupled to a noise source which is presumed to represent a bath—the economy as a bulk—which gives the prescription for how a single agent in the system will fluctuate. An equilibrium system (of sufficient size)

can be modeled in such a way, and the nature of the bath is to capture fluctuations induced in a single agent by way of interactions with other agents. An interacting economy allows only self-consistent baths—the bath governs the agents, but the bath is determined by the spectrum of agents and their interactions. The spectrum of agents is itself governed by the interactions, and so the *causal* nature of the model is clear—everything originates from the interactions. A non-interacting model suffers an enormous difficulty in these regards. If one specify the bath (instead of the interactions), then one can assert kinetic properties of agents (in the sense that kinematics describes the motion of objects but not the origin of those motions)—that is, one can recover a (possibly evolving) wealth distribution—but one cannot understand how that wealth distribution should give rise to the bath, nor even whether it is possible for the wealth distribution to give rise to the bath.

A self-consistent requires needs the bath to be determined by the interactions—the bath is a dynamic environment which is determined collective motions of the agents, which are in turn a product of their individual interactions. It is only in an interacting picture of the economy that the concept of equilibrium can be established (rather than presumed) and investigated. This is a key reason for investigating kinetic models of wealth, usually termed Asset Exchange Models.

1.5 Asset Exchange Models

The most direct background to this dissertation is the field of asset exchange models. These interacting models of the economy arose out of the work of Angle [58] and of Ispolatov *et al.* [59] They conceive of the Economy in a purely interacting fashion, such that economic motions consist entirely of exchanges between agents. Ispolatov *et al.* treat two basic models: additive exchange and multiplicative exchange. In the

additive method, two traders are selected, and a fixed unit of wealth is transferred between them. In the multiplicative model, the amount of wealth exchanged is a percentage of the losing agent's wealth. They furthermore specialize to random exchange and greedy exchange—in random exchange, the winner of the selected pair is random, but in greedy exchange, it is always the richer agent. One of the key limitations of this work is the notion that when rich agents lose the exchange, they can very easily increase the wealth of the poorer agent by a factor of several.

Further work along these lines was considered by [60], which treat a similar multiplicative model. By relating their model to polymer physics, they are able to include several extensions, including the agents additionally coupled stochastically and multiplicatively to a bath, which represents various external investment markets and taxes, as well as agent connectivity. Results here show the renormalized wealth distribution can give power-laws with exponential cutoffs, and they demonstrate wealth condensation in certain parameter regimes.

A similar conception which relates the market to ideal gas collisions was developed by Dragulescu and Yakovenko [61]. They consider bare interactions between agents which randomly split wealth between the agents. These results lead to distributions of wealth which follow the Boltzmann distribution, with temperature corresponding to the average wealth. They consider as well the effect of thermodynamic machines upon such a wealth distribution. Chakraborti and Chakrabarti [62] augment this conception with the concept of *saving propensity*, whereby agents elect only to enter some fraction of their wealth into the process. In some sense this represents multiplicative trading, and this results in markets where the most probable wealth is non-zero. This was further extended by Chatterjee *et al.* [63], who incorporate random (fixed) saving propensity for each agent, and discover Pareto tails in the

wealth distribution. Slanina [64] produced a similar phenomenology with inelastic mean-field Maxwellian mixing of wealth between agents. An early review on these types of models was given by Chatterjee [65].

1.5.1 The Yard Sale Model

A key economic constraint was added to the picture with the invention of the YSM, realized independently (and with slight variations) by Chakraborti [66] and Hayes [15]. The constraint is the notion that traders are willing to risk fractions of their wealth at most, however, they are not willing to risk more than their trading partner. This ties the scale of economic transactions to the poorer agent. However realistic, it also proved fatal to the notion of a steady-state economy. Impoverished agents are no longer rescued by occasional large donations by the rich, and over time poverty compounds upon itself.

Since then, the YSM has been re-examined [20, 67] and extend many times, including such factors as heterogeneity [68], biased trade direction probabilities [21, 69], stochastic wealth fractions involved in the betting process [22], and wealth exchange on networks [70, 71]. A short paper with my collaborators which highlights some aspects of the work in this dissertation is available [72].

1.6 Ergodicity

A key concept in statistical physics is *ergodicity* [73–76]. In loose terms, an ergodic system is one which does not contain any long-term memory. If a system is ergodic, the long-term behavior of the system is independent of the details of its history—the system exhibits a sort of stability and mixing. In statistical mechanics, ergodicity is a prerequisite for thermodynamic equilibrium; If a system is not ergodic, then it is

in some sense either unstable or does not thoroughly mix its components. Ergodicity is of considerable interest to the problem of wealth and income distributions, as in an ergodic system there can be some notion of long-term fairness between identical agents; over long enough times, it does not matter whether or not an individual was born rich or poor. However, if the proper model is not ergodic, then an agent may be born into such a condition that they might never escape their origins.

Formally speaking, ergodicity can be expressed as the statement that time averages are equivalent to ensemble averages, so that averaging the measurement of a quantity over the trajectory of the system is equivalent to measuring that quantity over an ensemble of systems. Boltzmann introduced ergodicity to statistical physics as a hypothesis which was necessary in order to use statistical ensembles in order to describe the behavior of a single system. Mathematicians have subsequently analyzed this assumption and found that for some systems, it is effectively true. However, it is now recognized that arbitrary systems are not necessarily ergodic.

Ergodicity for Markov chains is not difficult to establish [75, 77, 78]. A Markov chain is ergodic if it is irreducible and has an aperiodic state. Irreducible means that it is possible to get from any state to any other state in the chain; it cannot be factored into spaces such that any space is absorbing or disconnected. Any state which has a positive self-transition probability is aperiodic, which is a fairly easy condition to fulfill in practice when concerning wealths or incomes binned into classes. In fact, Champernowne [39] cites the convergence of Markov chains and associated analytical simplicity as one of his motivations for studying such models, and explicitly neglects economic growth, owing to the complications of such an analysis.

Ergodicity is less trivial for interacting systems in continuous domains is much more complex, owing to the more sensitive dependence of the model's evolution on

its state space. Here we will find ourselves concerned with *effective ergodicity*—the question of whether time averages tend towards ensemble averages, and if so, how much time is required for said convergence. Effective ergodicity is a necessary but not sufficient condition for formal ergodicity. Even in formally ergodic systems, ergodicity is connected to the relaxation time of the system—time averages over very short times will certainly not be representable by ensemble averages over configurations; Sufficient time must pass for the system to sample the distribution of available configurations. The timescale of effective ergodicity is also of economic interest, for individual agents may only exist for a human lifespan. If the relaxation timescale is on the same scale or larger, then the economy will appear non-ergodic to the agents as individuals, that is, individual agents will experience limited mobility. Thirumalai and Mountain [79, 80] developed a simple, tractable measure to examine the timescale of effective ergodicity which are used here to probe relaxation timescales for the YSM.

1.7 Structure of this Dissertation

Chapter 1 gives background information useful for examining

1.7.1 Chapter 1: Introduction and Background

This chapter introduces the content and context of the dissertation, explaining the structure of the dissertation, the empirical study of wealth distributions, and previous econophysics models of wealth.

1.7.2 Chapter 2: The Yard Sale Model without growth

This chapter explores the Yard Sale Model (YSM) of an economy in some detail, with attention to the features found in model simulations.

1.7.3 Chapter 3: Theoretical descriptions of the YSM

This chapter develops theoretical tools for understanding evolution of the wealth distribution in the YSM. I make connections with the geometric random walk, a kinetic equation approach, and a mean-field-like approximate interaction. These tools will be used throughout the work in order to shed light on the results uncovered by direct simulation.

1.7.4 Chapter 4: The YSM with arithmetic growth

This chapter explores the addition of growth to the YSM in the simplest possible form—growth which is additive and constant in time, which I call arithmetic growth. This growth partially breaks wealth condensation—in the long-time limit, a single agent absorbs all of the growth. However, the remaining agents are left with finite non-zero wealth, and so there is still a wealth distribution to speak of. In the simplest form of growth this distribution does in fact follow a power law, which is explained using the theoretical tools outlined in chapter 2.

1.7.5 Chapter 5: The YSM with geometric growth

Explores geometric growth terms, such that the total wealth grows exponentially in time. This slightly more complicated form of growth more closely mimics the growth in the real world. Here, the wealth distribution approaches a rescaled steady state— that is, a steady distribution multiplied by a global growth factor. The wealth distribution corresponds to a power-law with an upper cutoff, which again can be explained in terms of the tools outlined in chapter 2. Introducing skewed growth, which allows for growth to depend dynamically on the current wealth, gives rise to interesting phenomenology: A phase transition between the rescaled steady state,

which is shown to be effectively ergodic, and a wealth condensation state, which is non-ergodic. The transition has similar properties to a thermodynamic phase transition, including power law divergences, critical slowing down, and scaling collapse.

1.7.6 Chapter 6: Generalized framework for wealth condensation

Here I examine other generalized asset exchange models. Of particular interest is the result that a large class of asset exchange models exhibit wealth condensation. This class is characterized by “fair” (zero-expectation value) exchange between agents, and monotonically increasing agent risk. I show how condensation emerges by using the Itô calculus.

1.7.7 Chapter 7: Concluding remarks and future work

This chapter includes a summary of results and potential guidelines for more work in the same field.

1.7.8 Chapter 8: Faithful Dimensionality Reduction of Materials Microstructure using Convolutional Neural Networks

This chapter details my work developing applications for data analysis for materials science. I use state of the art Machine Learning algorithms for computer vision, Convolutional Neural Networks (CNNs), to automatically compute distance between texture images in a way that reflects the relevant structural parameters of the image. A collection of related images is found to be highly amenable to dimensionality reduction, so that each image can be given a coordinate in a low-dimensional space. I compare this with a baseline procedure using the Fourier content of the image, and find the CNN-based approach to be far superior.

Chapter 2

The Yard Sale Model without growth

2.1 Purpose of this chapter

This chapter will explore the YSM without growth in detail. We cite and explain results known from the literature, and give others which are new developments. This chapter will likewise develop the language of the mathematics which we use to characterize the system.

2.2 Postulates of Asset Exchange

An asset exchange model is an economic model of wherein *wealth* (assets) is exchanged between *agents*. An economic agent is an entity capable of holding wealth—An individual, a corporation, or perhaps a nation.

Less concrete is the notion of *wealth*. In the real world, wealth is a complicated construct; There are many types of assets one may hold, and many ways to call upon those assets. The economic nature of an asset implies that it has monetary value. While the precise, detailed process of ascribing a monetary value to each and every asset would prove very difficult, if we allow some error the process is possible; more concretely, I may not be able to tell you the exact value of a certain pair of shoes, but I may be able to tell you with reasonable confidence that they are worth between 50 and 60 dollars. Applying the process in serial to an agent's various possessions and

summing the result produces a mathematical representation of wealth as a scalar number. This is the notion of wealth used in this work—as a real number which characterizes the sum total of the value of the assets of the agents.

Transactions between agents, then, consist of exchange of assets. If the values of the assets exchanged between two individuals are equal, then the wealths of the agents do not change. However, when the values of the assets exchanged are not equal, then there is an *exchange of wealth*, and one agent will gain wealth, while the other loses wealth.

Implicit in the previous paragraph is the idea that the exchange takes place between two agents. Mathematically speaking, it is simple to write down more complicated models in which wealth exchange takes place between three or more agents. We limit ourselves to two-agent exchanges, though, on the dual grounds that it seems to be the predominant form of economic activity, and that becomes a much more difficult problem mathematically.

Another aspect of the model is *stochasticity*. This means that while the model has rules, the rules will have a degree of randomness or unpredictability. Practically speaking, this means that we assume that transactions depend on variables which do not need to be in the model. That is to say that a given asset exchange model will assume some set of facts about wealth exchange, but it will also acknowledge that there are other variables that are not within the model which give rise to the transactions. It presumes that these other factors can be usefully modeled by randomness.

2.3 The Model

The yard sale model (YSM), introduced in [15], is a pair-wise asset exchange model. The model economy consists of N agents who own varying quantities of wealth. The

model is initialized in a state where all the agents have equal wealth.

The agents exchange wealth according to the following scheme: We select two agents at random and exchange a fraction α of the poorer person's wealth. As a fraction, the physically acceptable values of α range from 0 to 1. We refer to this model, without growth or modification to the trading rule, as the *bare* YSM. The justification for this scheme is that the size of the economic transaction must be limited by the wealth of the poorer agent. Moreover, as the wealth of an agent increases, the agent is more likely to engage in transactions at a higher scale; The wealthier the agent is, the larger the value of assets in their transactions.

Mathematically speaking, this only gives rise to the constraint that trades are monotonic with the wealth of the agents. However, the simple assumption that the rate of growth of the scale of trade is proportional to the assets of the agent is the most parsimonious way to invoke the monotonicity because it means that the YSM does not have any implicit wealth scale, which we explore more carefully in the next section.

Another of the assumptions built into the model is that the economy is fully connected: Each agent is equally likely to be picked for each trade, and so all possible pair of agents are equally likely to trade. Thus, there are many extensions to this model wherein the trading is given more structure. This is possible by, for example, placing the agents on a network structure. It is also possible to extend the model such that the probability for picking agents for each trade is not equal. Broadly speaking, there are two categories of extensions to the structure of the trading: static and dynamic. A static trading structure is quenched or “frozen in” to the agents, thereby distinguishing the agents from each other. This type of mathematics may help model situations where there are inherent differences between the agents, e.g.

agents which lie embedded on a geometric surface and can only trade with other agents within a certain distance. The contrasting category of dynamic models, on the other hand, allows us to account for various economic effects associated with the wealth of the agents. An example here is to explore the possibility that richer agents trade more or less frequently than poorer agents. In this way, we can explore a multitude of possible feedback relations between the economic landscape and behavior of the agents within that landscape.

The bare YSM uses an unbiased coin to indicate the direction of trade, so that each agent is equally likely to win the exchange. While this assumption may seem simplistic, it is important that it is virtually the most charitable assumption for the poorer agent of the trade, for a great many of economic transactions are carried out by vendors, whose economic transactions so constructed as to systematically be profitable.

2.4 Conservation of Wealth

Wealth in the YSM is *conserved*: it is neither generated nor destroyed by any process, but transferred from agent to agent. Clearly, then, the YSM fails to capture economic activity which produces or destroys wealth, but rather is intended to capture the dynamical effects of which are the result of transactions. We emphasize this for two reasons:

- 1) Physically, the total wealth in the system is a constant of motion and is unaffected by the dynamics.

- 2) Economically, we expect that wealth is created and destroyed by processes associated with human activity and the passage of time: The harvesting of resources, the consumption of food, and others. Thus, if the YSM fails to describe the econ-

omy on its own, it may still provide a useful model of trading processes within an economy. Thus the mechanisms uncovered and conclusions drawn can still be useful as a description of those aspects of the economy associated with trade. We likewise expect that extensions to the yard-sale may be necessary to provide a more complete description, but find this not to be a failure of the model, but rather relegate it contextually; incomplete does not mean outright wrong.

2.5 Rescaling Invariance

In the YSM, the global wealth scale is arbitrary. The act of global wealth rescaling commutes with the trading transactions, because each trade will also rescale by the same fraction. That is, if we rescale all wealths by a factor R ,

$$w \rightarrow w' = Rw \implies \Delta w \rightarrow \Delta w' = R\Delta w \quad (2.1)$$

If we define the collection of wealths in the system as $\{w_i\}$ and a rescaling operator \mathcal{R} and a trading operation by \mathcal{T} , then $\mathcal{R}\mathcal{T}\{w_i\} = \mathcal{T}\mathcal{R}\{w_i\}$.

The first use of this property is that it tells us that the overall wealth scale of the bare YSM is a free parameter. Hence, we may normalize the total wealth $W = \sum_i w_i$ in the system as we deem appropriate: generally to either $W = 1$ or $W = N$, so that the initial wealth for each agent is $1/N$ or 1 , respectively. Moreover, we are free to switch between normalizations at will, as the overall wealth scale is decoupled from the dynamics. Additionally, we will also find this property to be of good use in growing systems, wherein the typical (or total) wealth of the system grows in a predictable way, and this overall growth factor can be scaled out.

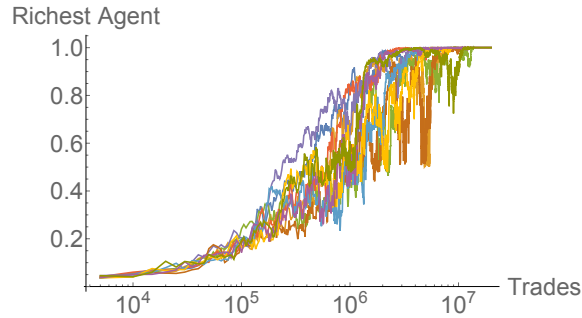


Figure 2.1: The wealth condensation phenomenon. The fraction of wealth held by the richest agent in the system is plotted as a function of the number of trade for ten independent runs. $N = 100$, $\alpha = 0.1$

2.6 Simulation Findings

We begin by exploring the YSM via explicit simulation without recourse to theoretical treatment. After, in the subsequent section, we will explore theoretical arguments which explain these facts via mathematics.

2.6.1 Wealth Condensation

One of the most conspicuous and immediate properties of the bare YSM is that after a large number of exchanges, a single agent will hold nearly all of the wealth in the system [15], as shown in Fig. 2.1. Statistically, the longer the system is run, the greater the fraction of wealth which is held by the largest agent, increasing towards 1 as $t \rightarrow \infty$. This property has been termed *Wealth Condensation* [60]. Likewise, every other agent will continue to decrease in wealth, asymptotically approaching 0 over time. At first glance, this is surprising, as every trade is fair in the sense of an expectation value. Nonetheless, we will find in the following sections that the compounding effect of multiple trades is systematically biased against poorer agents.

The wealth condensation phenomenon establishes the bare YSM as a nonergodic model; we cannot follow the time trajectory of a single agent in order to sample

the ensemble of agents. This is in itself quite remarkable from the perspective of academic economics, which often posits *a priori* that the economy can be described by an ergodic process (q.v. Sec 1.4). Thus the YSM shows that this assumption can be violated by even a very simple non-equilibrium model.

2.6.2 The thermodynamic limit and scaling with system size

Statistical mechanical formulations generates systems which generally converge towards a distribution in the thermodynamic limit, as the system size N grows to ∞ . The most prototypical example of this is the central limit theorem, which demonstrates that average of (well-behaved i.e. short-tailed) random variables converges to the average of the variables, with fluctuations which shrink predictably as $N^{-1/2}$ as N grows larger. Or, conversely, the existence of the thermodynamic limit can in some circumstances be seen as a consequence of the central limit theorem.

Because our model is fully connected and not embeded geometrically, increasing the size of the system is accomplished simply by increasing N , the number of agents in the system. Hence, to establish a notion of thermodynamic limit for our system, we need to identify what variables converge as N becomes very large.

Figure 2.2 shows the evolution of the richest, median, and poorest agents in the system for various numbers of agents. The first conspicuous property the data indicates is that after a large number of trades, the median and poorest agents lose wealth exponentially. Secondly, the data indicates that the evolution of the richest agent over time scales with N^2 , while the median and poorest agents scale with N . This paradoxically seems to indicate that a time-step for the system ought to be given by both N^2 trades and N trades, respectively. Thirdly, we note that by inspection the wealth fraction for the median agents is approximately multiplicatively lower

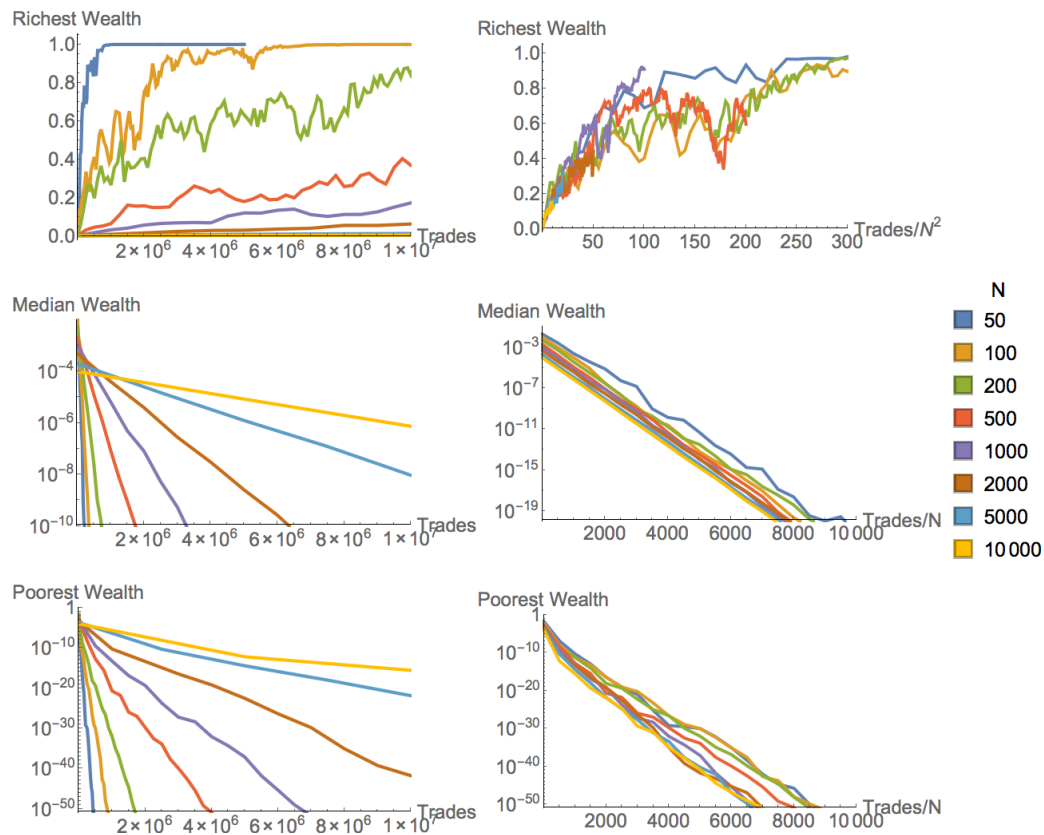


Figure 2.2: YSM time scaling with system size for $N = 50$ up to $N = 10^4$. Left: The plots show the maximum, median, and minimum wealth in the system as a function on the number of trades. Right: The same data plotted against the number of trades divided by N^2 , N , and N , respectively. $\alpha = 0.1$

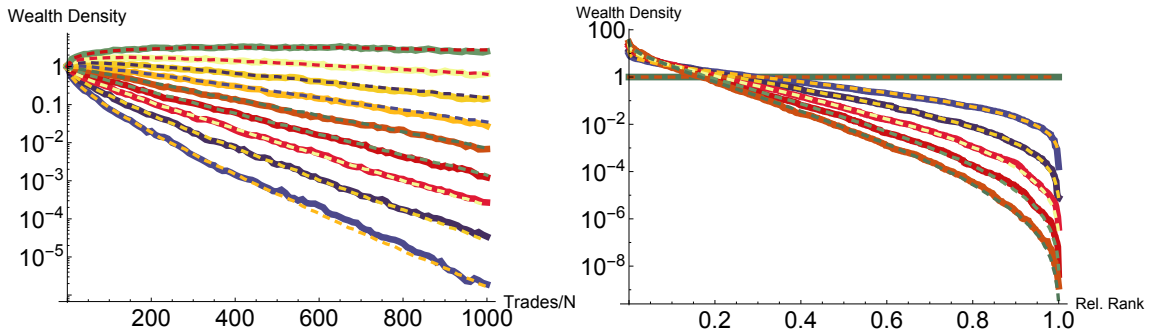


Figure 2.3: Comparison of wealth density evolution for $N = 1000$ (Solid) and $N = 10,000$ (Dashed). Left: Rank slices in the economy over time every 10th percentile from 10 to 90. Right: The same run, viewed in snapshots of the wealth density as a function of rank for times from $t = 0$ to 1000 in increments of 200. $\alpha = 0.1$

with increasing N , reflecting the persistence of the initial wealth, which scales as $1/N$.

The resolution to the paradox can be found in tandem with the third observation by viewing the wealth as moving through the strata of the economy which are defined by the relative rank in the economy: That is, the i th richest agent has relative rank i/N . Likewise, we change normalizations from wealth fraction to *wealth density*, such that each agent begins with wealth $w_{init} = 1$ regardless of system size.

Figure 2.2 shows that under this normalization scheme, two large systems of differing sizes follow approximately the same evolution. We thus define a single time-step for the system to consist of N trades and an associated time variable $t = (\# \text{ of trades})/N$.

We choose the terminology *wealth density* in light of this convergence; since for large N , the wealth as a function of relative rank becomes independent of N , we are motivated to seek a description of the system in terms of a *wealth density function*, $w(x, t)$, where the relative rank x varies quasi-continuously from $x = 0$ to $x = 1$. The wealth density can be integrated across ranks to obtain a quantity of the total wealth

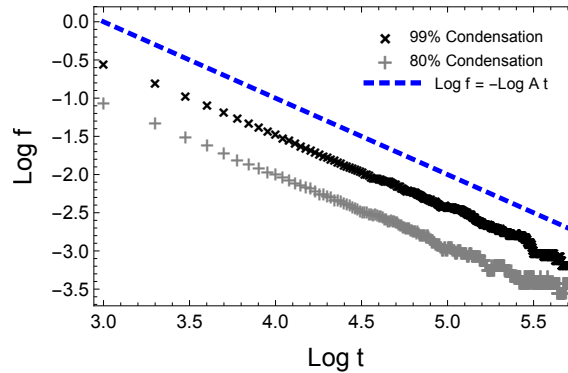


Figure 2.4: The fraction of the richest agents, f , that hold a given fraction of the wealth against time for condensation fractions of 80% and 99%. The dashed blue line is included to guide the eye, and represents a power law with exponent -1 . $\alpha = 0.1$, $N = 10,000$.

in the system. The wealth density function can then be subject to the normalization constraint $\int_0^1 w(x, t) dx = 1$, also independent of N .

Under this scheme, we see in figure 2.4 that the wealth in the system collapses to a small fraction of the agents f in a number of trades that scales with $\frac{N}{f}$. In examining only the richest agent in the system for different system sizes, the fraction f of the economy being examined scales down as $f \sim \frac{1}{N}$, so that the number of trades for the wealth to condense to a single agent scales approximately with N^2 , resolving the paradox from figure 2.2.

2.6.3 Scaling with α

We now turn to investigate the role of the trade fraction parameter α on the dynamics of the system, and to answer the following questions: What phenomena are independent of α , and what phenomena are dependent on α ? How do the latter change with α ? The answer to these questions is paramount in light of the not only of the fact that the appropriate value of α to model the real world is yet unknown, but also that it seems quite possible that α may vary from time to time, place to

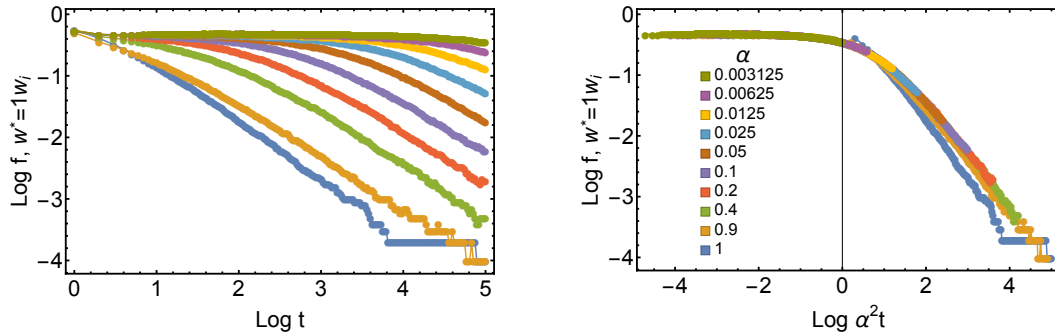


Figure 2.5: The fraction of the agents that are richer than the initial wealth, plotted for various trade fractions α . α varies from 1 to 0.003125, a factor of about 300. Right: The same data plotted against the scaled time $\alpha^2 t$, showing a scaling collapse for values of α which are not close to 1. Small deviations from the scaling collapse are just visible for $\alpha = 0.9$ and clear for $\alpha = 1$. $N = 10,000$

place, and market to market. It's furthermore realistic that α may vary stochastically from trade to trade, a possibility which we will address in section. 3.3.

Intuitively speaking, since α scales the amount of wealth traded in each trade, one expects that increasing α will increase the overall rate of wealth transfer through the economy. Figure 2.4 demonstrates this by plotting the fraction of agents above the initial wealth in the system: The larger α , the faster agents lose wealth and fall below the mean wealth. But moreover, we find also that these rates can be aligned via a reparameterization of time from t to $\alpha^2 t$. It is worthy of note that this collapse takes place only when α is not close to 1, however, the collapse is fairly good even up to $\alpha = 0.9$.

In figure 2.4, we see that the same collapse is visible regardless of the wealth threshold examined. This indicates that within the collapse regime, the only effect of α is to speed up time by a factor α^2 .

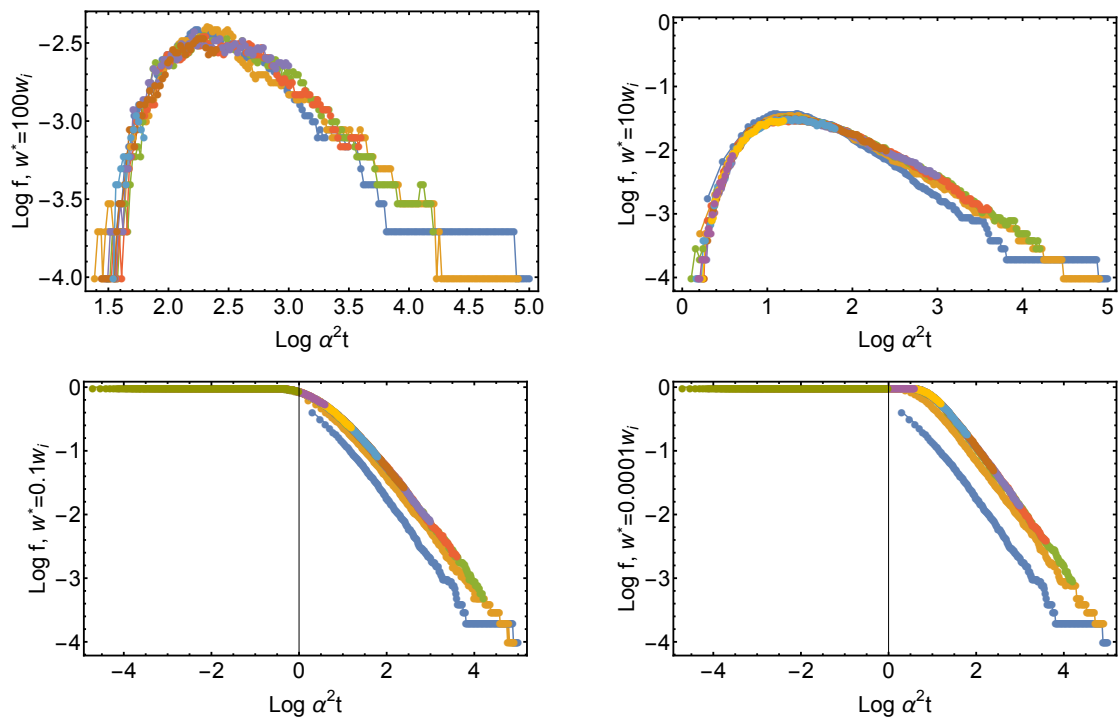


Figure 2.6: Richest fractions above thresholds versus scaled time, showing condensation scaling with α^2 . Threshold values: $10^2, 10, 10^{-1}, 10^{-4}$. $N = 10,000$

2.6.4 Mobility

Rank Correlation Function

Another interesting economic variable to be examined is the *mobility* of agents within the economy, that is, how the rank of an agent will fluctuate in time. One simple way to characterize the mobility is to analyze the correlation of agent rank. At time t_1 , the internally labeled agents, i , are sorted by wealth and given a rank, n_i , from 1 to N . The ranks are recalculated at t_2 , and the rank correlation for the two sets of ranks n_i and m_i is then given by the Pearson Correlation coefficient for the ranks, also known as Spearman's rank correlation coefficient [81]:

$$C(t_1, t_2) = \sum_{i,j=1}^N \frac{(n_i - \bar{n}_i)(m_j - \bar{m}_j)}{(\sigma_n \sigma_m)^{\frac{1}{2}}} \quad (2.2)$$

This makes for a useful measuring of mobility for a few reasons. Firstly, the correlation function is invariant under rescaling of the data, and so is the same whether or not we examine the ordinal ranks of the agents or the relative ranks, $x_i = n_i/N$. In the same vein, a function of rank will be insensitive to the distribution of the data, leading to the easily computed limit of $C(t_1, t_2) = 1$ when the ranks of the agents have not changed from t_1 to t_2 . This is particularly important in our case as functions of the *wealth* of the agents tend weight agents vary differently. We can then compare the correlation between t and $t + \Delta t$ to examine the mobility as a function of time:

$$C'_{\Delta t}(t) = C(t, t + \Delta t) \quad (2.3)$$

This is shown in figure 2.7. The data indicate that over time, the system decorrelates more and more slowly, asymptotically approaching a fixed-rank economy,

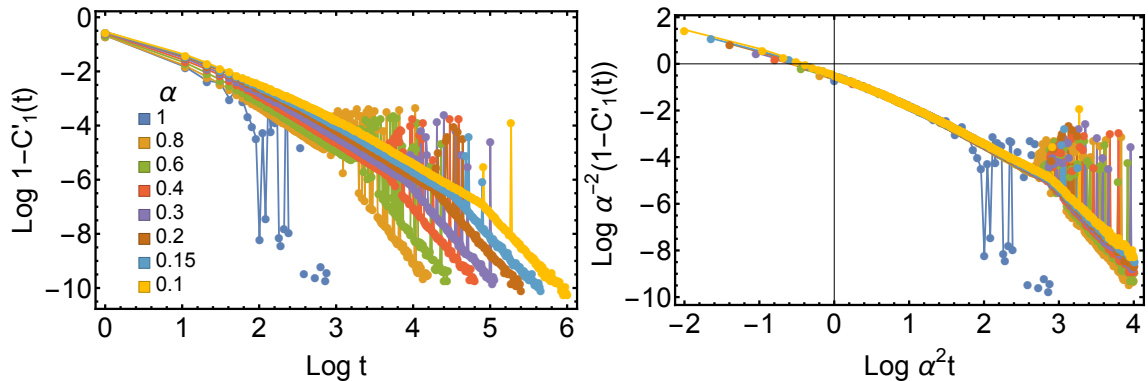


Figure 2.7: Rank correlation $C'_1(t)$ against time and against rescaled time $\alpha^2 t$ for various α . Right: The data asymptotically approach total correlation roughly as a power law, with a kink around $\alpha^2 t = 10^3$, associated with bankrupt agents (see figure 2.8 $N = 10,000$)

with agents effectively quenched (in the sense of fixed) to static ranks in the economy. There is a noticeable kink and other erratic behavior in the data around $\alpha^2 t = 10^3$, which can be attributed to bankrupt agents; those whose wealth has undergone underflow below the minimum representable wealth, approximately 10^{-308} . Bankruptcy causes the presence of multiple agents at the same wealth, and this causes agent rank to become not well-defined. Idiosyncracies of the sorting algorithm may then over or underestimate agent correlation, depending on how the agents at zero wealth are ordered.

Bankruptcy

We likewise show bankruptcy for the agents in fig 2.8, demonstrating that agents do become bankrupt around $\alpha^2 t = 10^3$, giving rise to the second order discontinuity in fig 2.7. For $\alpha = 1$, the number of bankrupt agents is much larger; this is to be expected, as in this limit of the model, every time a poorer agent loses, they become bankrupt. Thus approximately half of the agents are bankrupted per time-step,

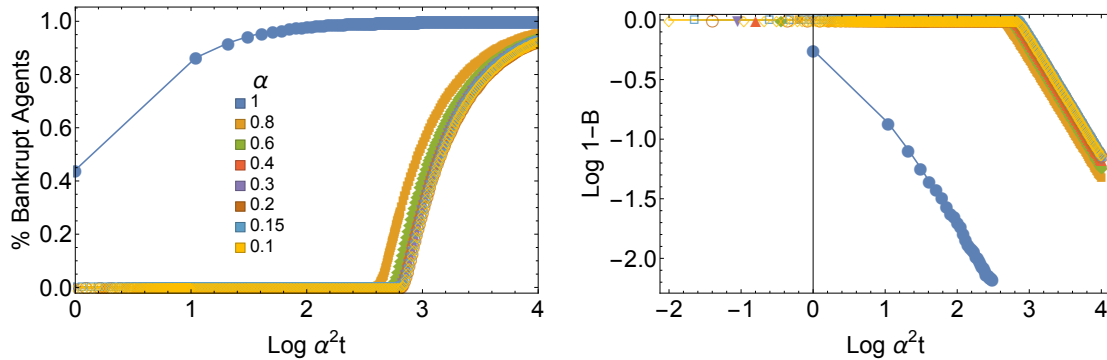


Figure 2.8: The number of bankrupt agents in time.

leading to the scaling $1 - B(t) \approx 2^{-t}$.

Permutation correlation

The permutation correlation is the correlation of the permutation of the agents which ranks those agents; that is, it is the inverse function R^{-1} of the rank function $R(l) = n$; $L = R^{-1}$ gives the label of the agent at a specified rank. The value of the permutation function is that it is sensitive to agents who have not changed rank whatsoever, however, for agents which have changed rank, since the agent labels are arbitrary, the permutation function essentially gives a random number. In this way, the permutation correlation function allows us to see when agents have become *frozen in* to a set place with unchanging rank. Mathematically, it is written

$$P(t, t') = \sum_{i,j=1}^N \frac{(L(t)_i - \bar{L}(t)_i)(L_j(t') - \bar{L}(t')_j)}{(\sigma_{L(t)} \sigma_{L(t')})^{\frac{1}{2}}} \quad (2.4)$$

and we adopt the same notation for the differential correlation:

$$P'_{\Delta t}(t) = P(t, t + \Delta t) \quad (2.5)$$

This is shown in figure 2.9. The data indicate that initially, all permutation

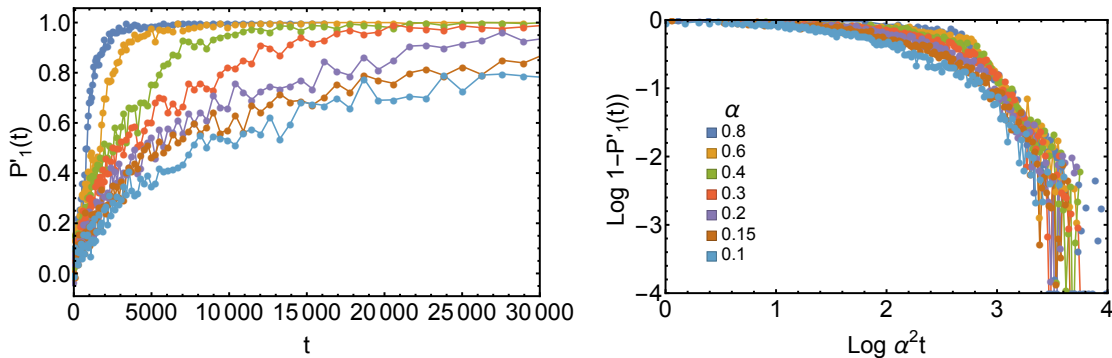


Figure 2.9: Permutation correlation $P'_{250}(t)$ against time and against rescaled time $\alpha^2 t$ for various α . Right: The data asymptotically approach total correlation, $P'(t) = 1$, as a power law in time with exponent -1 . $N = 10,000$

correlations are erased in a time shorter than $\Delta t = 250$; Indicating that no agents are frozen over a timescale of 250 time steps. As time passes, correlations in the permutation appear, indicating that some of the agents are “frozen in” to their ranks in the economy. At larger still times, the entire system becomes frozen; such that they are roughly perfectly correlated between two times 250 time steps apart. Further transformation reveals that the correlation is approached inversely with time, that is, as a power law with exponent -1 .

2.6.5 Ergodicity

The TM metric and effective ergodicity.

Related to the mobility is the ergodicity of the model, which we address by way of the Thirumalai-Mountain (TM) metric. [80] The metric is formulated in terms of energy variable E_i for particles in a fluid. In its original context, the metric provides a test for *effective ergodicity* by comparing the ensemble average of e to the time average. The time average energy for each particle is given by

$$e_i = \frac{1}{t} \int_0^t ds E_i(s), \quad (2.6)$$

and the ensemble average of this is given by

$$\bar{e} = \frac{1}{N} \sum_{i=1}^N e_i. \quad (2.7)$$

The energy metric is then given by the average square deviation between the time averages and the ensemble averages:

$$\Omega(t) = \frac{1}{N} \sum_{i=1}^N (e_i - \bar{e})^2 \quad (2.8)$$

This quantity can be related to the time correlation function of energy fluctuations averaged over the particles. Thirumalai and Mountain reason that an ergodic system, this correlation function is, in the long term, independent of the origin of time, and hence only a function of the time difference $t_2 - t_1$ between the times t_1 and t_2 which are being examined for correlation. This allows them to derive the long term scaling

$$\Omega(t) \sim 1/t \quad (2.9)$$

The presence of this scaling relation is an indication that the energy variable is self-averaging [80], that is that measurements on a limited sample will coincide with calculations performed over an ensemble average. In this way, the presence of the scaling relation indicates that the system is *effectively ergodic*, that is, that it is not distinguishable from an ergodic system under this metric. Effective ergodicity is thus a necessary but not sufficient condition for a system to be ergodic; this is an inevitable result of assessing ergodicity through any single aggregate variable.

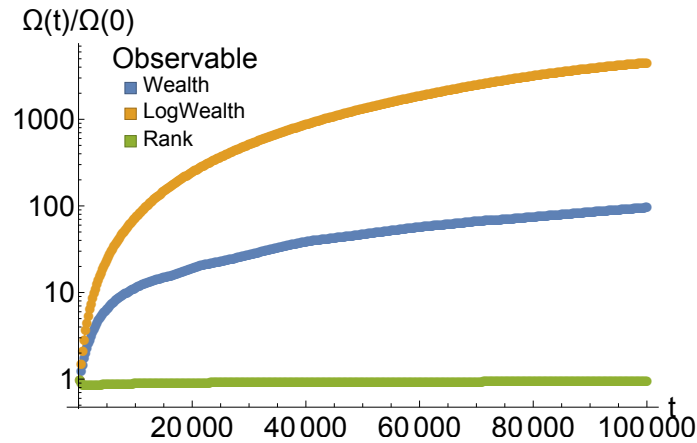


Figure 2.10: The TM metric applied to three observables: The wealth of the agents, the log-wealth of the agents, and the rank of the agents. The fact that the metric does not fall to zero in time indicates that indeed, the system is not self-averaging. $N = 10,000$, $\alpha = 0.1$

Applying the metric

The TM metric provides a useful structure to examine the properties of the YSM. The fluctuation metric Ω need not be applied to an energy *per se*; Any instantaneous observable of the particles (agents, here) will do. We thus examine the effective ergodicity for three agent observables: *Wealth*, *Log(Wealth)*, and *Rank*.

We implement the metric in the case of discrete sampling, constructing time averaged variables sampled at regularly spaced time intervals t_j :

$$e_i(t_j) = \frac{1}{j} \sum_{k < j} E_i(t_k) \quad (2.10)$$

The data is shown in figure 2.10. Far from decaying in time, the growth of the metric for wealth and log-wealth indicates that deviations from the system-wide average are in fact growing with time. The rank metric is asymptotically constant, much in line with the result for rank correlations, which show that agents become ordered after long times. These results are hardly surprising given the wealth

condensation phenomenon we have already witnessed, however, we give them for comparison with our results on the system with growth in the subsequent chapters.

2.6.6 Evolution of the Wealth Distribution

Moukarzel [22] shows that when agents are well-ordered into ranks, and separated enough in wealth such that poorer agents can be neglected, the typical wealth of an agent evolves as

$$w(x, t + \Delta t) \approx w(x, t) \exp(-\beta x \delta t), \quad (2.11)$$

where β is a parameter extracted from the trading scheme, which we will examine more carefully in the next chapter. The wealth for various ranks is shown in figure 2.11. We see that this exponential decay form appears to hold eventually, however, it (deliberately) neglects profits from poorer agents., meaning that it does not describe the flow of wealth upwards into the rich agents in the economy. Since $\log(w) \sim \beta x t$, we plot $\frac{1}{x} \log(w)$, confirming that the exponential decay rate is given by the appropriate form as a function of rank and time for some parameter β . Crucial, here, is that the onset time for this scaling depends heavily on the rank of the agents- lower ranks take much longer to reach this scaling regime. In mathematical parlance, it appears that the convergence to the scaling regime is not uniform convergence.

Theoretical arguments, given in the next chapter, establish that we can understand the data more coherently by examining the cumulative wealth distribution, $C(x, t)$, of the wealth at or below a given rank. We will show that the cumulative wealth scales with the same relation,

$$C(x, t + \Delta t) \approx C(x, t) \exp(-\beta x \Delta t), \quad (2.12)$$

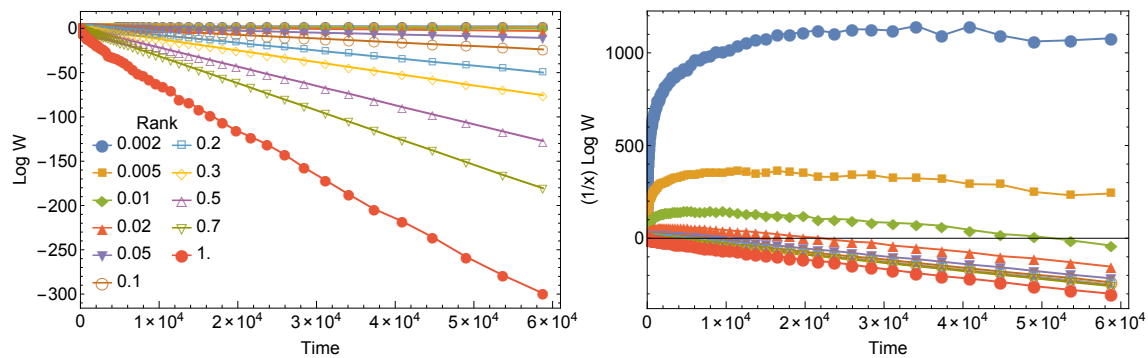


Figure 2.11: Exponential wealth decay per rank. Left: The log-wealth for various ranks in the economy. The poorest agents fall to astronomically low wealths, given enough time. Right: By scaling the log-wealths by agent rank x , we verify the asymptotic wealth decay as $\exp(-\beta xt)$. $N = 10,000, \alpha = 0.1$

but that this relation is accurate for much shorter times, even for extremely small ranks. This is shown from simulation data in figure 2.12.

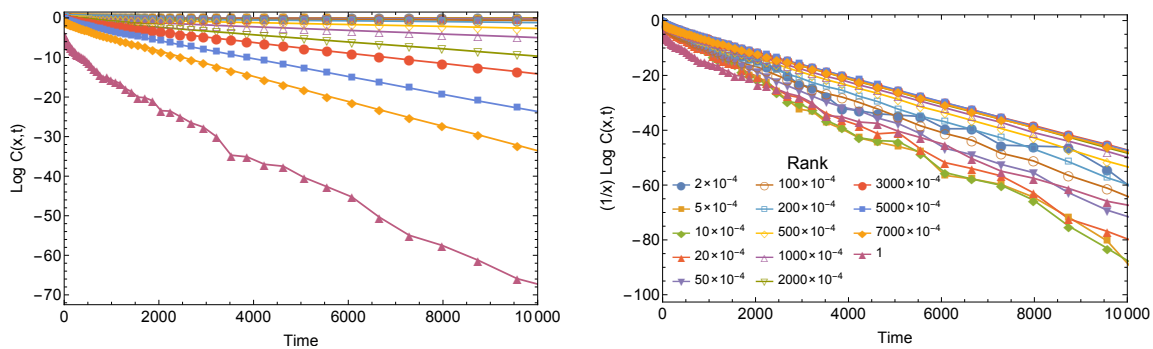


Figure 2.12: Left: The cumulative log-wealth for various ranks in the economy, which begin to decay exponentially much faster than the wealth in each rank. Right: By scaling the log-cumulative-wealths by agent rank x , we verify the asymptotic wealth decay as $\exp(-\beta xt)$ in a few thousand time steps. $N = 10,000, \alpha = 0.1$

Chapter 3

Theoretical descriptions of the YSM

3.1 Purpose of this chapter

We will also develop theoretical tools and perspectives which will aid in the analysis of extensions to the basic model here and in other chapters.

3.2 Theoretical Treatments

3.2.1 Geometric Random Walk

To understand at heart why the trading mechanism alone is nonergodic, we first consider a simplified, two-agent system. Furthermore, suppose that the two agents have wealths on different orders of magnitude, so that the poorer agent is likely to remain poorer after many time steps. In this case, the poorer agent is undergoing a Geometric Random Walk (GRW); a random walk wherein the steps are multiplicative, as opposed to additive.

In this limiting case, the poorer trader's wealth after T trades is given by

$$w_p(T) = (1 + \kappa_T)(1 + \kappa_{T-1})\dots(1 + \kappa_1)w_p(0), \quad (3.1)$$

where κ is a random variable. (In the bare YSM, $\kappa \in \{-\alpha, +\alpha\}$) Determining the distribution of the trader's wealth after a long time is complicated by the fact that

the incremental changes in later steps are dependent on those in earlier trades; as such we cannot simply examine each step independently and invoke central limit theorem. However, the logarithm of the agent's wealth is more amenable to analysis:

$$\ln w_p(t) = \ln [(1 + \kappa_T)(1 + \kappa_{T-1})\dots(1 + \kappa_1)w_p(0)] \quad (3.2)$$

$$= \sum_{i=1}^T \ln(1 + \kappa_i) + \ln w_p(0) \quad (3.3)$$

Thus, $\ln w$ can be treated as undergoing an arithmetic random walk. By examining the total growth $g(t) = \ln \frac{w_p(T)}{w_p(0)}$, provided the distribution of κ is well-behaved enough to apply the central limit theorem, the agent will have an effective step-wise drift $\mu = \langle \ln 1 + \kappa \rangle$, and variance $\sigma^2 = \langle (\ln 1 + \kappa)^2 \rangle$. After many steps, the distribution of the agent will be peaked near $\ln \frac{w(T)}{w(0)} = \mu T$. We can use the elementary series for $\ln(1 + \kappa)$ to find

$$\mu = - \left\langle \sum_{n=1}^{\infty} (-1)^n \frac{\kappa^n}{n} \right\rangle \quad (3.4)$$

$$= - \sum_{n=1}^{\infty} (-1)^n \frac{\langle \kappa^n \rangle}{n} \quad (3.5)$$

The typical (poorer) trader, then, will have wealth in the vicinity of $w(T) = w(0)e^{\mu T}$. There is an important observation to make here: Given fair trades (those such that neither trader is expected to gain or lose in a signal trade), $\langle \kappa \rangle = 0$, and the leading term to μ is negative definite. The negative-definiteness extends to all orders for symmetric trading, such that the amount traded between the agents is independent from which agent is likely to win. Thus, even presented with a fair trading scheme, compounding effect of multiplicative trading will typically lead to the

poorer agent losing wealth over time. Nonetheless, as the trading is fair, the formal average of the poorer trader's wealth remains stationary over time. This is reconciled by the fact that there are exponentially rare trajectories in which the poorest agent wins a large fraction of the time, gaining wealth exponentially. The rareness of these trajectories balances with the grandeur of their winnings to give a finite contribution to the average. However, as these trajectories are exponentially rare, they do not typically appear, and finite collections of trajectories will on average lose wealth over time, as detailed in [82]. If the trading is biased enough in favor of the poorer agent such that μ is positive, the system will not exhibit wealth condensation. For more details surrounding this phenomenon, see [22].

The time step is defined by N total trades, giving the poorer trader 2 trades per time step, we switch definitions from the growth per trade μ to the effective loss per time $\beta = -\mu/2$, so that the typical trajectory at time t is near $w(t) = w(0)e^{-\beta t}$.

For the YSM, the effective loss rate is $\beta = \alpha^2 + \frac{\alpha^4}{2} + \dots$. This is consistent with the analagous continuous-time analog, geometric Brownian motion [82], wherein the multiplicative noise term σ gives rise to an overall growth term $-\sigma^2$ via the Itô calculus (see chapter 6).

3.2.2 Master Equation Approach

Here, we formulate the master equation approach to the agent density function $P(w, t)$, starting as given by Moukarzel. [22] This generates an integral expression for the evolution of the density, $\dot{P}(w, t)$. We then extend this approach to show that this expression can be written as an expansion over moments of the return distribution. The truncation of this expansion to various orders gives rise to the Mean Trade approximation, detailed in section 3.2.3, and the differential equation approach given

in [67]. By using a generic return distribution, we extend the equation found in [67] to more generic models. Finally, the higher order terms of the series give a route to numerical solutions of higher accuracy, as well as a more concrete understanding of the error involved in truncation.

Master Equation

We begin with the process defined by

$$w_{min} \rightarrow w_{min}(1 + \kappa) \quad (3.6)$$

$$w_{max} \rightarrow w_{max} - \kappa w_{min} \quad (3.7)$$

where κ is a random variable between -1 and 1 with distribution $\pi(\kappa)$.

We construct a master equation for the density of agents $P(w, t)$ at a wealth w . We presume that the two-agent distribution function $P(x, y, t)$ can be written as a product $P(x, t)P(y, t)$ of one agent density functions. The master equation then has the form

$$\dot{P}(w, t) = \int \pi(\kappa) d\kappa \int dy dz P(y) P(z) I(w, y, z, \kappa) \quad (3.8)$$

where $I(w, y, z, \kappa)$ gives the probability function for the agents entering the trade with wealth y and z to leave the trade with wealth w , and the factors $P(y)dy$ and $P(z)dz$ account for the probability for the agents entering the trade to have wealths y and z . For notational brevity we introduce $\dot{P}(w, t|\kappa)$ as the second integral, so that $\dot{P}(w, t) = \left\langle \dot{P}(w, t|\kappa) \right\rangle_{\kappa}$. We can assume without loss of generality that $z > y$; The transfer terms for $y > z$ will be the same, but for the relabeling of y and z . Since the probability factors are identical in this relabeling, the contributions due to both of

these labelings are identical.

$$I(w, y, z, \kappa) = \Theta(z - y)\{\delta(w - (1 + \kappa)y) + \delta(w - z + \kappa y) - \delta(w - y) - \delta(w - z)\} \quad (3.9)$$

The first two terms correspond to gain of agents at wealth w , and the second two correspond to loss of agents at w .

Straightforward integration in the above equation produces the expression

$$\dot{P}(w, t|\kappa) = -P(w) + \frac{1}{1 + \kappa} P\left(\frac{w}{1 + \kappa}\right) A\left(\frac{w}{1 + \kappa}\right) + \int_0^{\frac{w}{1 - \kappa}} P(y)P(w + \kappa y)dy \quad (3.10)$$

where

$$A(w) = \int_w^\infty P(y)dy \quad (3.11)$$

gives the number of agents richer than a wealth value w . The first term in equation 3.10 is due to the local loss of agents who are trading. The second term is due to the increase of poorer agents moving to wealth w due to gaining wealth percent κ , and the third term is due to the increase of richer agents moving to wealth w due to losing wealth.

Comparing this expression to equation 19 in [67], we see that the equations are not precisely the same; the third term appearing here differs in the sign of κ . This apparent discrepancy is resolved when averaging over the two values of κ ; The treatment in [67] treats the cases of an agent gaining and losing wealth separately, and as such is only consistent when the probability for those possibilities is equal. The treatment in [22] and here is thus more general and can be applied to more general return distributions for which $\pi(\kappa) \neq \pi(-\kappa)$.

Expansion by orders in κ

As in [67], we can expand this equation to second order in κ . Explicitly doing so in equation 3.10 produces the cumbersome result:

$$\begin{aligned}
\dot{P}(w, t|\kappa) = & + 0 \\
& + \kappa \left(wP'(w)A(w) + P(w)A(w) - 2wP(w)^2 - P'(w) \int_0^w yP(y)dy \right) \\
& + \frac{\kappa^2}{2} \left(w^2P''(w)A(w) + 2xP'(w)A(w) \right. \\
& \left. - xP(w)^2 + 2P(w)A(w) + P''(w) \int_0^w y^2P(y)dy \right)
\end{aligned} \tag{3.12}$$

As in [67], the second order term can be rewritten as

$$+ \frac{\kappa^2}{2} \left(\frac{\partial}{\partial w} \right)^2 ([w^2A(w) + M_2(w)] P(w)), \tag{3.13}$$

where the set of partial moment integrals are defined by $M_n \equiv \int_0^x y^n P(y)dy$. Motivated by this form, we find one can rewrite the first order term as

$$+ \kappa \left(\frac{\partial}{\partial w} \right) ([-wA(w) + M_1(w)] P(w)) \tag{3.14}$$

This indicates a general form. However, confirming this form by expanding equation 3.10 is quite cumbersome due to the complicated dependence on κ . It turns out that it is much easier to do this expansion in equation 3.8, before integrating. Expanding in a Taylor series,

$$\dot{P}(w, t|\kappa) = \int dydz P(y)P(z) \sum_{n=0}^{\infty} \frac{\kappa^n}{n!} \left[\left(\frac{\partial}{\partial \alpha} \right)^n I(w, y, z, \alpha) \right]_{\beta=0}. \tag{3.15}$$

Notice that the model is only consistent when $|\kappa| \leq 1$, so that there is some hope that in practice we can truncate the series at finite n , and that the later terms in the series are not paramount and may be neglected. This will depend, however, on the form of $P(w)$. By taking derivatives here, we find that the 0th order term is zero as expected, and that the higher order terms are

$$\begin{aligned}
\left[\left(\frac{\partial}{\partial \alpha} \right)^n I(w, y, z, \alpha) \right]_{\alpha=0} &= \theta(z-y) [(-y)^n \delta^{(n)}(w - (1+\alpha)y) + y^n \delta^{(n)}(w - z + \alpha y)]_{\alpha=0} \\
&= \theta(z-y) [(-y)^n \delta^{(n)}(w - y) + y^n \delta^{(n)}(w - z)] \\
&= \theta(z-y) \left(\frac{\partial}{\partial w} \right)^n [(-y)^n \delta(w - y) + y^n \delta(w - z)],
\end{aligned} \tag{3.16}$$

where $\delta^{(n)}$ is the n^{th} derivative of the Dirac delta function. Inserting this into our series expansion and integrating over the delta functions, we find

$$\dot{P}(w, t|\kappa) = \sum_{n=1}^{\infty} \frac{\kappa^n}{n!} \left(\frac{\partial}{\partial w} \right)^n [(-w)^n A(w) + M_n(w)] P(w). \tag{3.17}$$

Physical interpretation of the series

Let us consider the first order term:

$$\dot{P}_1(w, t|\kappa) = \kappa \frac{\partial}{\partial w} [(-w)A(w) + M_1(w)] P(w) \tag{3.18}$$

This can be interpreted as a current equation:

$$\frac{\partial P}{\partial t} = -\frac{\partial}{\partial w} J_1(w) \tag{3.19}$$

$$J_1(w) = \kappa ([wA(w) - M_1(w)] P(w)) \tag{3.20}$$

Which can further be decomposed in terms of the velocity of the agents through wealth space:

$$J_1(w) = v_1(w) \cdot P(w) \quad (3.21)$$

$$v_1(w) = \kappa(wA(w) - M_1(w)) \quad (3.22)$$

Where the velocity of the agents at w is given in terms of the wealth distribution via

$$\dot{w} = \kappa(wA - M_1(w)). \quad (3.23)$$

Here each agent here agent gains a return fraction κ of their wealth for each richer agent they trade with, and loses a corresponding amount due to the the poorer agents they trade with. When we average over the distribution of κ , the first order term gives the net motion of agents due to the expected value wealth transfer due to all possible trades.

The second order term is

$$\frac{\partial P}{\partial t} = \frac{\kappa^2}{2} \frac{\partial^2}{\partial w^2} ([w^2 A(w) + M_2(w)] P(w)) \quad (3.24)$$

Writing this as above in the form of a current, we have

$$\begin{aligned} J_2(w) &= -\kappa^2 \frac{\partial}{\partial w} ([w^2 A(w) + M_2(w)] P(w)) \\ &= -\kappa^2 A(w) P(w) + \kappa^2 \left(\frac{w^2}{2} A(w) + \frac{1}{2} M_2(w) \right) \frac{d}{dw} P(w) \end{aligned} \quad (3.25)$$

This suggests a fluid velocity $v_2(w) = \kappa^2 w A(w)$; this term corresponds to the typical wealth loss due to the geometric random walk of poorer agents relative to richer agents. The second term is a nonlinear diffusion with diffusion coefficient $D_2(w) = \kappa^2 (\frac{w^2}{2} A(w) + \frac{1}{2} M_2(w))$

Truncation of the series

3.2.3 Mean Trade Theory

Herein we develop the Mean Trade theory (MT) approach to analyzing the YSM. The MT approach is somewhat akin to a mean field theory of classical statistical mechanics; We examine an agent from the ensemble and consider the collective action of the interactions which involve that agent. We then construct an effective theory by replacing the statistically fluctuating interactions with their typical behavior, which is then treated behaving deterministically (with no fluctuations). A key difference between the MT model for the YSM and a Mean Field theory is that the agent's rank in wealth space is retained in the MT model as a relevant parameter. This means that agents are not all equivalent, so that the MT can retain the character of rich-poor interactions.

As we discussed in section 3.2.1 concerning the GRW, when two agents trade many times, the poorer agent will typically lose a fraction of their wealth. The first basic ansatz of the MT is to assume we do not lose too much information about the wealth distribution by replacing the trading scheme with a simpler one wherein the poorer agent always loses a wealth fraction which, for future parsimony, we call $\beta/2$:

$$w_{poor} \rightarrow (1 - \frac{\beta}{2})w_{poor}, \quad w_{rich} \rightarrow w_{rich} + \frac{\beta}{2}w_{poor} \quad (3.26)$$

Although this scheme is deterministic, it still requires knowledge of (a) which agent

is poorer and (b) how much wealth the poorer agent has in order to compute the amount traded.

The second assumption of MT is that although the interactions take place between randomly selected pairs of agents, due to the large number of trades taking place, we can apply the process evenly to all agents at once. The normalization of N trades per time step fixes this rate such that each agent is expected to undergo 2 trades per time step.

Together these assumptions generate the process which evolves wealths under the MT of the YSM. The wealths update as follows:

$$w_i \rightarrow w_i \left(1 - \frac{R_i}{N}\beta\right) + \frac{\beta}{N} \sum_{j:w_j < w_i} w_j, \quad (3.27)$$

where $R_i = \sum_{j:w_j > w_i} 1$ is the rank of agent i - the number of agents richer than agent i . Equation 3.27 fixes the normalization of β such that β represents the loss fraction per time step that an agent experiences due to trades with richer agents; the factor R_i/N accounts for the probability of trading with a richer agent. We will see by comparison to YSM simulations that the MT process in equation 3.27 provides a useful description of the wealth distribution of the system.

One of the most important practical consequences of these assumptions is that agent rank in the MT is preserved. From the perspective deriving analytical tractability, this is a good thing. On the other hand, this means that MT does not contain information about the mobility of agents within the economy; to obtain estimates of these variables, we will have to supplement MT.

In considering a system composed of a large number of agents, it will be useful to consider a representation of the system which, in the limit as $N \rightarrow \infty$, is independent of N ; in essence, we seek to deal with a thermodynamic variable. We rescale wealth

so that the total wealth at time $t = 0$ is fixed at $W(0) = 1$ and rescale rank to the continuous rank $x = R_i/N$, which varies between 0 and 1. Then, the wealth distribution of the system is described by a ranked wealth density function $w(x, t)$ – that is, the wealth in any given segment of the economy is given by the integral over w . At $t = 0$, each agent has the same wealth, so that $w(x, 0) = 1$. Converting the mean trade process into the continuum language, we obtain the mean trade differential equation:

$$\frac{dw(x, t)}{dt} = -x\beta w(x, t) + \beta \int_x^1 w(x', t) dx'. \quad (3.28)$$

Notice that we have implicitly treated time as a continuous variable as well. The treatment of these variables as continuous is not problematic, as the appropriate discrete version of any results can be recovered by straightforward conversion, correct up to correction terms which vanish as $N \rightarrow \infty$.

Matching β

An advantage of the MT approach is that it captures universal properties of multiplicative trade models; Regardless of details, a YSM model with any general return distribution $\pi(\kappa)$ can *only* generate wealth drift that is in proportion to the wealth of the poorer agent, because there are no dimensionful parameters. Moreover, statements that can be made independent of the value of β will be true for a large class of models, as MT theory captures the behavior of the system due to this generalized net drift. The only parameter in MT is the typical loss fraction β . As in the analogous mean field theory, there are many asset exchange models which may map to the same MT behavior; Since β must characterize the whole of the return distribution $\pi(\alpha)$ (see section 3.3), many return distributions will match to the same value of β . While

within the domain of the validity of MT, the distribution of the wealth will behave similarly. However, the individual agents themselves will behave differently; for example they may exhibit higher or lower mobility or wealth variation over time. The MT approximation scheme will most accurately return distributions with low variability; the extreme limit being the “Greedy” multiplicative model of [59], wherein the poorer agent always loses. In this case, under our normalization, $\beta = 2\alpha$. However, the MT scheme will break down as the expected variability of an agent’s wealth increases, as detailed in [22], if the trades are sufficiently biased in favor of the poorer agent, there is eventually a phase transition as the effective drift β passes through zero. At $\beta = 0$, the MT approach predicts no change in the wealth distribution—all effects, then, are diffusive or higher order. Near $\beta = 0$, the diffusive effects will dominate. When $\beta < 0$, MT predicts that the wealth distribution collapses to a delta function at the mean agent wealth, whereas the actual system converges to a steady-state whose shape, then, depends on the diffusive motion.

The matching in the bare YSM can be determined by examining the GRW; Since a poorer agent will typically lose a fraction $\alpha^2/2$ per trade, the appropriate matching is $\beta = \alpha^2$, as given in the theory of the GRW with a finite number of agents [82]. In MT, the picture presumes that this lost wealth is distributed equally over the richer agents; this maintains the conservation of total wealth by trading, and reflects the fact that the wealth of the richer agent does not affect the trading process. This assumption may break down when the trading agents are close enough in wealth that they may change rank with one another.

3.2.4 Connection between MT, GRW, and master equation

Here, we give show how the three theoretical approaches are related. The MT approach to solving the system is closely connected to the master equation given in section [refsection]; The smooth, fluid-like flow of the mean-trade picture given by the wealth evolution equation $\dot{w} = -x\beta w + \beta \int_x^1 w$ is equivalent to the smooth flow from the first order effects of unfair trading, with β being the mean wealth fraction $\langle \kappa \rangle = \int_{-1}^1 \kappa \pi(\kappa) d\kappa$ lost by the poorer agent. In the bare model with a fair coin, this term does not contribute.

However, the second order of the master equation also contains a similar loss term—one with coefficient κ^2 (see section 3.2.2). This is precisely the loss expected due to the nonlinear stochasticity of the geometric random walk. However, the gain term which balances this loss is buried in the nonlinear diffusion coefficient- implying that the wealth gain is local to the wealth loss- while typical agents at wealth w lose wealth due to the loss term, there are rare agents at the same wealth w which gain enough wealth to balance the loss, netting wealth conservation.

However, the locality of this effect (that both processes occur at the same wealth w) is an artifact of the fact that the master equation presumes infinite ensemble of agents. To see this, consider the formal average of the wealths in the *infinite* ensemble of the GRW, of which the time average is indeed zero. Typical agents lose wealth, but (exponentially) few gain an exceptionally large amount of wealth, such that the net is zero. However, this is an oversight—in any *finite* GRW ensemble, the agents are expected to lose wealth. If they are undergoing this random walk by trading with a more wealthy ensemble of agents, then clearly the richer agents will gain wealth lost by the poorer agents. Moreover, the nature of the system implies that all of the rich agents are equally likely to absorb the wealth from the poor ensemble. Motivated

by this, the MT approach takes the wealth lost by poorer agents in a GRW fashion, and distributes it evenly among the richer agents.

We can summarize by saying that the MT approach takes the wealth from agents as predicted by the GRW and master equation approaches, and distributes it as prescribed by the *finite* ensemble GRW. This approach is very sensible when there are not exponentially many agents in any given region of wealth space. [82] As such we expect that the MT approach will not necessarily be valid very near the initial condition given by wealth equality for all agents.

3.2.5 Solution to bare YSM under MT

The MT differential equation for the bare YSM (3.28) can be solved for its time dependence by examining the cumulative function $W(x, t) = \int_x^1 w(x', t) dx'$; $W(x, t)$ counts the total wealth of all the agents poorer rank x . In terms of the cumulative function, Eq. 3.28 becomes

$$\frac{\partial}{\partial x} \dot{W}(x, t) = -\beta \frac{\partial}{\partial x} (xW(x, t)) \quad (3.29)$$

Using the boundary condition $W(1, t) = 0$, we can integrate this equation to get

$$\dot{W}(x, t) = -\beta x W(x, t). \quad (3.30)$$

The transformation to the cumulative ranked wealth, $W(x, t)$, has resulted in a local differential equation, which is much easier to work with. This equation is solved by

$$W(x, t) = W(x, 0)e^{-\beta xt}, \text{ or} \quad (3.31)$$

$$w(x, t) = w(x, 0)e^{-\beta xt} + \beta W(x, 0)te^{-\beta xt}. \quad (3.32)$$

The first term in (3.32) represents the loss of initial wealth due to richer agents, and the second term represents wealth gained due to poorer agents. The principle advantage of this treatment over the one given in Refs. [21, 22] is that we no longer neglect the wealth gain experienced by the richer agents in a trade, which has a substantial effect on the richest agents.

In the long-time limit, as $t \rightarrow \infty$, $w(x) \rightarrow 0$, and the economy becomes impoverished. However, to properly recover the wealth of the richest agent, we must remember that although the economy may be quite large, it is inevitably finite. The wealth of the richest agent is the wealth contained between 0 and $dx = 1/N$. Thus, the wealth of the richest agent is given by

$$w_{richest} = W(0, t) - W(dx, t) = W(0, 0) - \sum_{i \neq 0} w_i(0) e^{-\beta t/N}. \quad (3.33)$$

That is, the richest agent exponentially relaxes to having all of the wealth. This confirms that number of trades required for wealth condensation to complete scales with N^2 .

3.3 Generalized return distributions

One can very easily consider a more general family of asset exchange models. A good formulation for doing so is as in Ref. [22] by introducing a return distribution which characterizes the probability for fractional wealth change by the poorer agent in an exchange. The return distribution $\pi(\kappa)$ is the probability distribution for the poorer agent to gain a wealth fraction κ . In order guarantee that the wealths in the system are always positive, $-1 \leq \kappa \leq 1$. For example, in the bare YSM, the distribution is $\pi(\kappa) = \frac{1}{2}\delta(\kappa - \alpha) + \frac{1}{2}\delta(\kappa + \alpha)$.

Biased coin The introduction of a biased coin introduces two possibilities. When the coin is biased towards the richer agent, the resulting wealth distribution is quite similar to the unbiased coin. This can be reconciled under the mean trade model in section 3.2.3. The dynamics, however, are faster-scaling with α instead of α^2 . When the coin is biased towards the poorer agent, the wealth distribution stabilizes.

Chapter 4

The YSM with arithmetic growth

4.1 Form of the Growth and Dimensional Considerations

Here, we study arithmetic growth, wherein the growth is additive and constant in time. We begin by generating the growth uniformly across the agents, so that each agent gains a wealth g after each time step. Recalling that the YSM trading mechanism does not itself invoke any wealth scales, the only wealth scales in the system are the initial wealth w_0 for each agent, and the growth per agent per time step, g . We use the normalization such that $g = 1$ and vary w_0 to explore the evolution of the system for different initial wealths. Using $w_0 \sim g$ corresponds to fast growth, and using $w_0 \gg g$ corresponds to slow growth.

4.2 Developing steady-state

Regardless of the value of w_0 , the input growth stabilizes the YSM, by preventing agents from falling to zero wealth. Figure 4.1 demonstrates the ranked wealth distribution as a function of time for large and small w_0 .

For small initial wealth, the typical agent wealth grows, with the poorest agents leveling off much more quickly than the richer agents. The distribution settles towards a power-law form in this way; from the poorest agents up. Starting with a large initial wealth presents a similar but reflected picture: The typical wealth in the

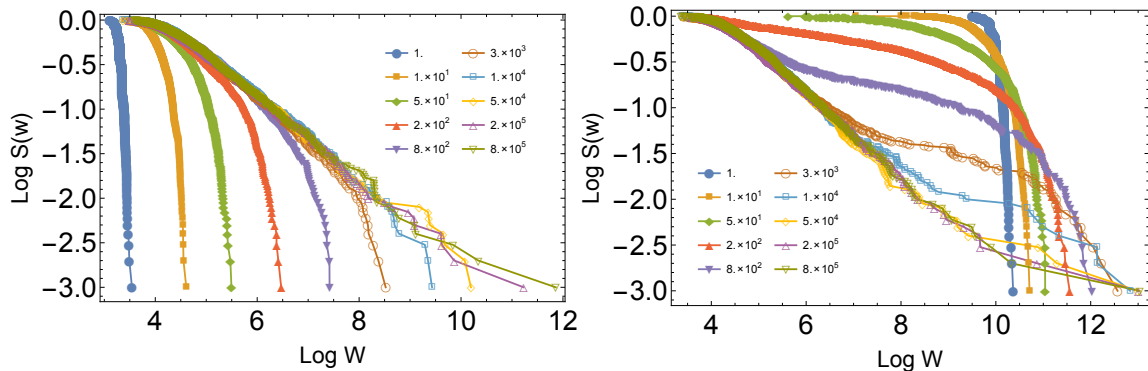


Figure 4.1: The evolution of the wealth distribution for arithmetic growth shown through the survival function. On the left, the initial wealth in the system is equal to the growth per time step. On the right, the initial wealth is much larger than the growth, $w_0 = 10^7 g$. The distribution appears approximately the same for long times. Note also the power law form of the distribution. $N = 1000$, $\alpha = 0.25$

system shrinks, with the poorest agents more quickly converging to the power-law form. We thus see that the long-term form of the wealth distribution is independent of the initial wealth. This is at odds with the notion that the total wealth in the two systems is different. The difference is accounted for by the wealth of the richest few agents.

In the long-term limit, all of the growth in the system is absorbed by the richest agent, whose growth remains even when the second agent has reached steady state, as shown in figure 4.2. Thus, the economy has not reached an equilibrium *per se*, but rather has a *steady-state* form resulting from an effective driven-dissipative system, where the driving force is provided by the growth, and the dissipation is provided *from within the trading model* by the richest agent. Justification of this picture implies the time-independence of the long-time form of wealth distribution.

Furthermore, since this late-time distribution is a residual, finite amount of wealth, it goes to show that in some sense wealth condensation is not broken. On the other

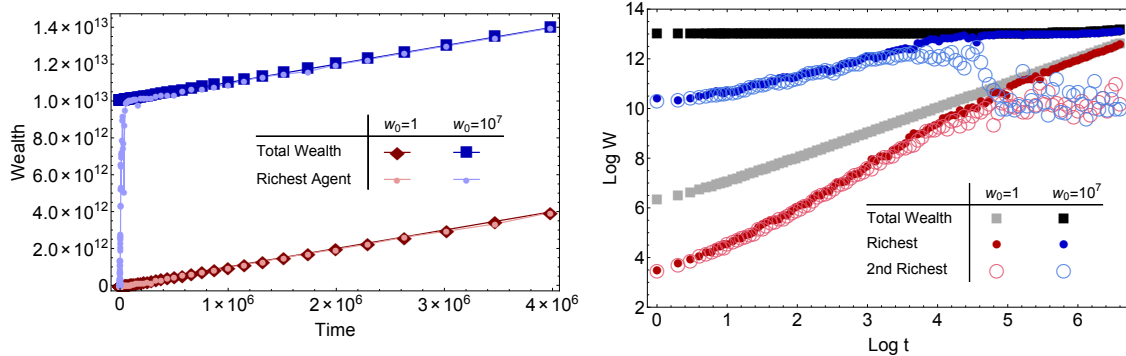


Figure 4.2: Evolution of very rich agents under arithmetic growth. Left: In the long term, the richest agent grows approximately linearly and asymptotically approaches having all of the wealth in the system, regardless of the initial wealth in the system. Right: The evolution of the total wealth, the richest person’s wealth, and the second richest person’s wealth for large and small values of the initial wealth. This shows the time scale at which the second richest agent reaches a steady state, around $t = 10^5$ time steps. $N = 1000$, $\alpha = 0.25$

hand, the wealth condensation has been weakened, in the sense that in the thermodynamic limit, all but a set of measure zero of the agents belong to a steady-state wealth distribution, the nature of which we proceed to investigate.

4.3 Varying α

How does the trading parameter α affect the shape of the steady state distribution? Simulations, shown in figure 4.3, show that the shape of the distribution is fairly consistent across a wide range of α : a power law with approximate index $-1/2$. However, the *scale* of the distribution varies noticeably with α .

We can find this wealth scale by simple dimensional analysis on the parameters of the system. The parameter list is small: only g , w_0 , and α . However, since the steady state of the system does not depend on w_0 , it cannot factor into any formula for the scale of the system in steady state. The dimension of g is $\frac{\text{wealth}}{\text{time}}$. α is formally dimensionless, but we know that it generates a wealth decay timescale such that

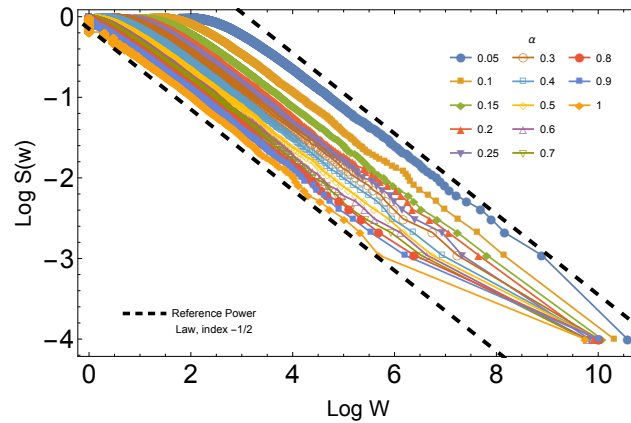


Figure 4.3: The arithmetic growth steady state distribution for various α . The data indicate that regardless of the value of α , the rich agents follow a power law distribution with cumulative exponent roughly equal to $-1/2$. The data was recorded at a time given approximately by $t = 20000/\alpha^2$ to ensure that the systems had reached the steady-state regime. $N = 10,000$

α^2 has dimension of *time* from the MT and other theoretical arguments given in chapter 3. Thus, the only viable wealth scale to be built of the parameters is a wealth which scales as

$$w \sim \frac{g}{\alpha^2}. \quad (4.1)$$

By scaling the wealth thusly, the distributions approximately collapse, as shown in figure 4.4. Economically, this scaling gives credence to the simple logic that since poor agents suffer under the YSM wealth exchange, when the exchange is slowed down, they are able to save up more of their growth. We also note the more counter-intuitive result that scaling this applies to the rich agents as well, as their position is buoyed by the wealth of the poor ones. Nonetheless, many measures of inequality in the system, such as the Gini coefficient and the Pareto Index will remain roughly invariant through changes in α , since the distribution only changes by a scaling factor. The only agent who suffers, then, is the richest agent, whose domination is

delayed until the growth has supplied sufficient wealth to the rest of the system.

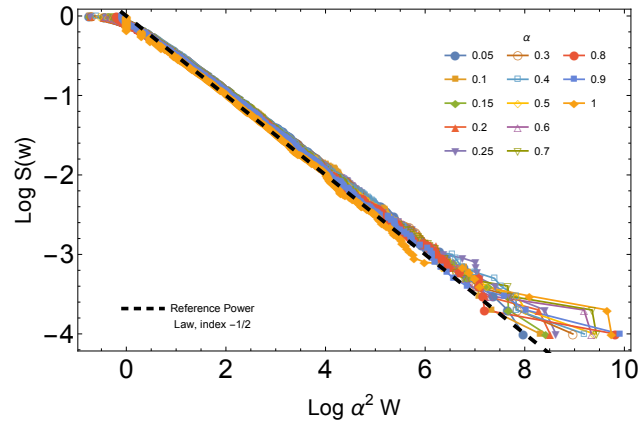


Figure 4.4: Scaling collapse of the steady-state distributions for various α , demonstrating that trading in smaller amounts actually benefits the bulk of the economy. $N = 10,000$

Changing the value of α also adjusts the time-scale for approach to steady state in much the same way. The length of time it takes to approach steady state is dictated by the slowest time scale in the system. It is important to note that the multiplicative motion of richest, low rank portion of the economy is slower than that of the typical, poor agents. The timescale t scales with the rank x as $t \sim 1/x$, as to the *rate* at which an agent trades with a richer agent is proportional to $1/x$.

This consideration by itself explains why the richest agent does not reach steady state; the richest agent does not undergo any multiplicative motion, and hence there is no combination of parameters to generate a time scale to reach steady state.

Likewise, as $N \rightarrow \infty$, the rank of the second richest agent diverges. This means that in the thermodynamic limit, the time scale for the system as a whole to reach steady-state is ill-defined. However, we can still define an effective time-scale for a specific nonzero rank of the economy to reach steady state.

4.4 Pareto Index

Removing the richest agent, this steady-state wealth distribution carries a Pareto index just under $k = 0.5$ over the bulk of the distribution. As seen in figure 4.4, the value of the index does not depend strongly upon α , the trading percentage. The MT approach for this system predicts an exponent of $k = 0.5$, as shown in section 4.6.

The value of $k \approx 0.5$ is far too low (skewed towards the wealthy) to fit the empirical data for a real economy. Realistic Pareto indices for income form a range from about 1.5 to 2.5, and for wealth closer towards 1, as described in section 1.3.

4.5 Mobility

For the bare YSM, we found that the mobility of the agents decreased steadily in time. The quasi steady-state nature of the YSM with arithmetic growth coupled with the wealth fluctuations induced by trading allow for the economy to exhibit mobility. The richest agent is excepted from this as this as their wealth grows apart from the economy.

4.5.1 Rank Correlation

While the structure of the wealth distribution remains largely unaffected with changes in α , the mobility of the economy is strongly dependent on α . This is visible in figure 4.5, which plots the rank correlation between adjacent time-steps for various α . In steady state, the decorrelation rate is approximately proportional to α^2 .

The structure of figure 4.5 shows that initially, agents decorrelate very quickly. The correlation function then approaches a maximum value, whereupon it decreases somewhat to the steady state. The interpretation of this is as follows: Initially, the diffusive motion of the agents and their localization in wealth space allow an agent

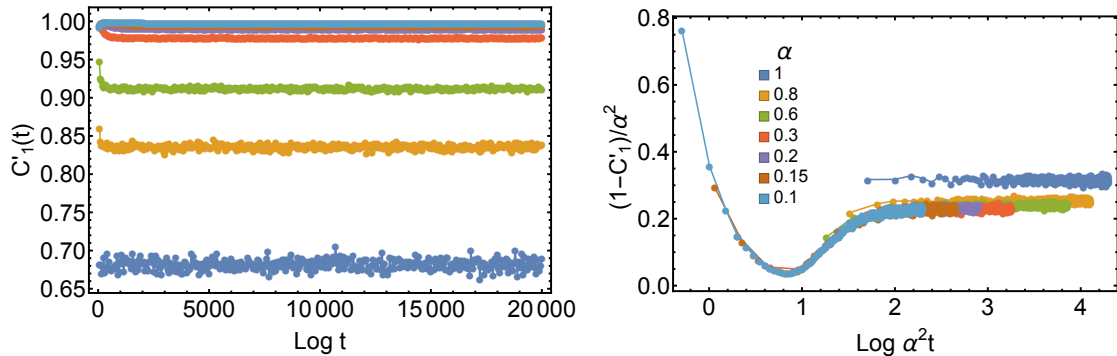


Figure 4.5: Rank correlations against time for arithmetic growth. Left: $C_1'(t)$, the correlation of agent ranks in adjacent time-steps. Right: Rescaling, we find that the residual decorrelation is proportional to α^2 .

to traverse large ranks with only a few trades. As the agents spread in time, the spreading effect of the YSM trading enhances correlations, as the YSM dynamics tend all ranks to distinctly different wealth scales. However, this trend is inhibited when the poorer agents approach their steady-state wealth, as in this state, a non-trivial fraction of the economy, the poorest end, is actually 1) fairly localized in wealth space and 2) undergoing multiplicative fluctuations.

4.5.2 Rank-Rank transfer data

In order to better visualize these facts, we give plots of the rank of the agents between two times. A completely immobile economy has a rank structure which is static in time, giving a diagonal line; the deviations in these rank-rank plots from a diagonal demonstrate mobility in the economy.

We have overlain these rank-rank plots for increasing time intervals in figure 4.6. This gives a sense of the mixing time for agents to become decorrelated; when the agents fill the plot uniformly, they have completely decorrelated.

Striations are visible in figure 4.6 across one time-step. These striations are

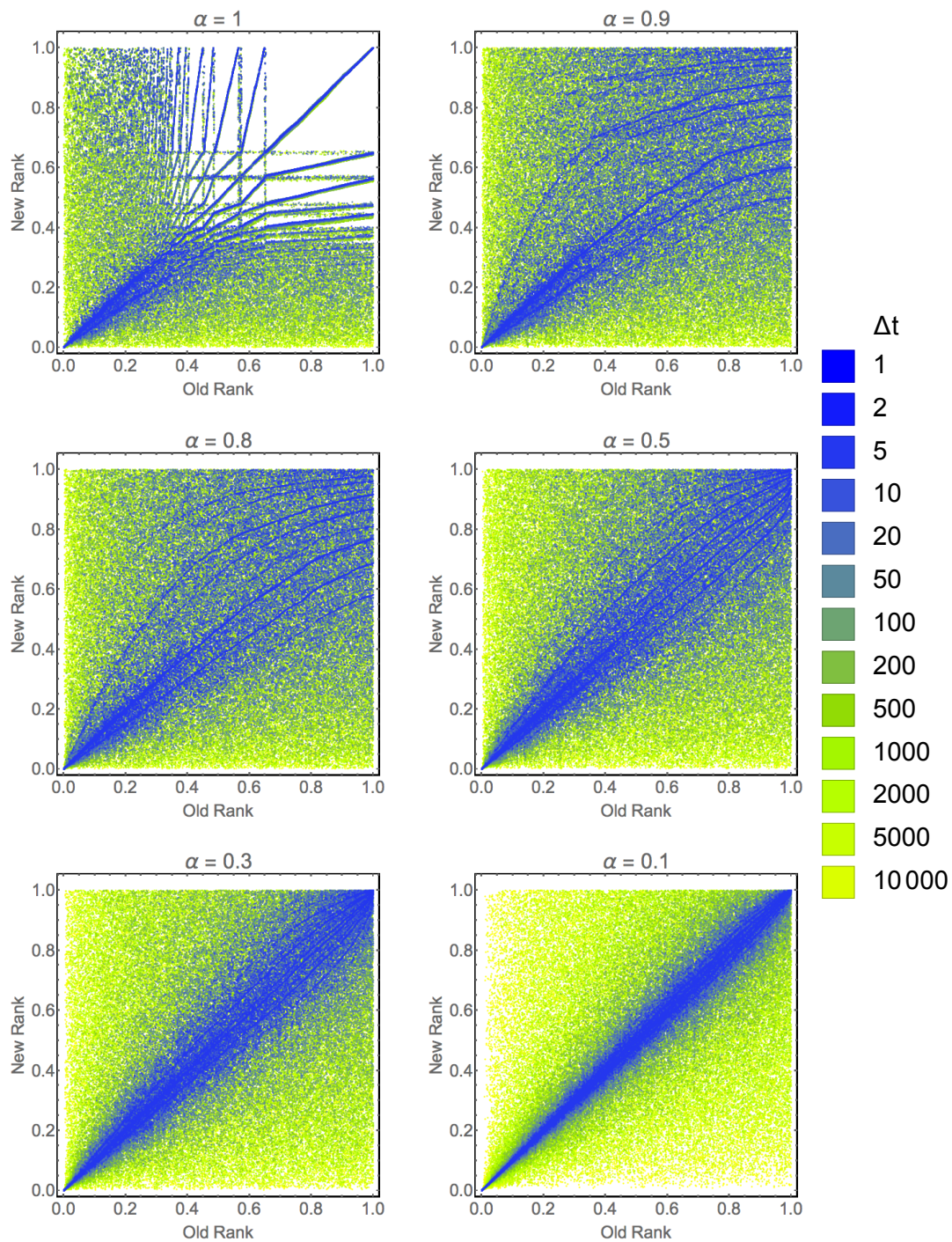


Figure 4.6: Rank-Rank transfer plots for various α over various time scales. Each graph shows the migrations of agents through ranks by comparing their ranks at a reference time to a time Δt later.

present due to the discrete formula which dictates wealth transfer in the economy; Since the economy is in steady-state, if two agents of both either win or lose in trading, then they will be transferred to approximately the same rank; as agents with slightly different wealths will then map to slightly different wealths in a continuous fashion; This is a reflection of the continuity of the functions $w \rightarrow (1 + \alpha)w$ and $w \rightarrow (1 - \alpha)w$.

For $\alpha \ll 1$, these striations are nearly symmetrical, indicating that a losing agent will lose about as many ranks as a winning agent will win. On the other hand, for α near or equal to 1, there is a strong asymmetric in the striations. This is a reflection of the multiplicative asymmetry of the process for larger values of α ; For $\alpha = 0.9$, an agent can nearly double their wealth by winning against a richer agent, but on the other hand, on losing, loses an entire order of magnitude of wealth. This is visible as well for $\alpha = 1$ as a cloud of agents in the upper-left quadrant which have become impoverished in only one time-step.

The graph for $\alpha = 1$ is remarkable in itself and deserves some special treatment. In this case, the wealths in the economy are nearly quantized, as a poorer agent losing will fall to zero wealth, accruing a discrete amount when growing. Various diagonal lines on the rank-rank transfer plot represent transitions between the wealth tiers; vertical and horizontal lines which are aligned with the ends of the diagonal lines represent the ranks which mark the division between the wealth tiers. Thus the strict geometrical character of the plot is somewhat of an artifact of the artificial constant growth in the system. Nonetheless, these lines give us some insight into the motion of the agents between the wealth tiers and by examining their density, length, and other characteristics we could probe the structure of the economic mobility in this economy as a set of transitions between bands of states. For the wealthy agents, a striation is

visible below the main diagonal—this is the counterpart to the impoverished agents in the upper left, showing winning agents which are able to climb up the ranks somewhat slowly.

Thus, for large α , the economy is not characterized by symmetric drift, but rather by (relatively) slow climbs and sudden impoverishing failures. A similar picture is available for the plots of $\alpha = 0.9$ and $\alpha = 0.8$.

For smaller α , the diagonal symmetry of the plots gives us the opposite picture: Over many time steps, an agent is roughly equally likely to drift up compared to drifting down, giving a sense of symmetric diffusive mobility.

Regardless of α , it is clear in all of the plots that poorer ranks are generally more mobile than richer ranks. There are two reasons for this. The first is that poor ranks are more likely to undergo larger, multiplicative fluctuations than richer ranks, who predominantly trade with agents poorer than themselves. The second is that the poorer agents are more closely spaced than the richer; we can see from the striations in this plot as well as figure 4.4 that a multiplicative change in w translates to a much larger change in rank for a poor agent than for a rich agent; so it must go with any heavy-right-tailed wealth distribution.

4.5.3 TM metric

We can likewise examine the TM metric on a system incorporating arithmetic growth after a suitable equilibration time. Figure 4.7 shows the TM for wealth, log-wealth, and rank on a system with $\alpha = 1$. The metric grows linearly for wealth. The absorption of the growth by the richest agent explains the wealth metric- the average wealth in the system is growing, but most of the agents are not. Thus, the deviations from the mean are growing, and so likewise with the time-averaged deviations and

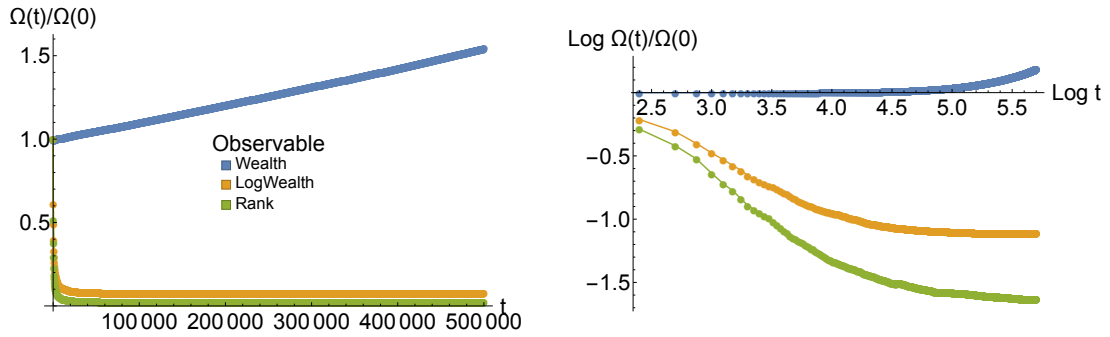


Figure 4.7: Unmodified TM metric for $\alpha = 1$, $N = 1000$, indicating limited economic mobility.

thus the metric. For log-wealth and rank, the metric shrinks in time; however, the decrease is very slow—slower than a power law—indicating that the metric for these quantities is likely asymptotically approaching a constant. We interpret this as also connected to the richest agent, who presents a small but finite persistent deviation from the system averages.

In light of this possibility, we modify the TM metric Ω to a metric $\bar{\Omega}$ which examines the fluctuations in the bulk of the system, ignoring the richest agent. The results are shown in figure 4.8.

The wealth metric fluctuates greatly, regardless of α . This is due to the highly unequal distribution of wealth in the system and the long times that would be necessary for each agent to become rich. The log-wealth and rank metrics are more tame, as they do not weight this inequality so severely. These metrics are also shrinking in time, indicating that fluctuations in the system are steadily erased by the dynamics; agents are completely mobile throughout the system.

As indicated in section 2.6.5, an effectively ergodic system will have a TM metric which decays as $1/t$. This scaling behavior is evident and present to some extent. For $\alpha = 1$ it is evident that this is not the case for agent rank, which resembles

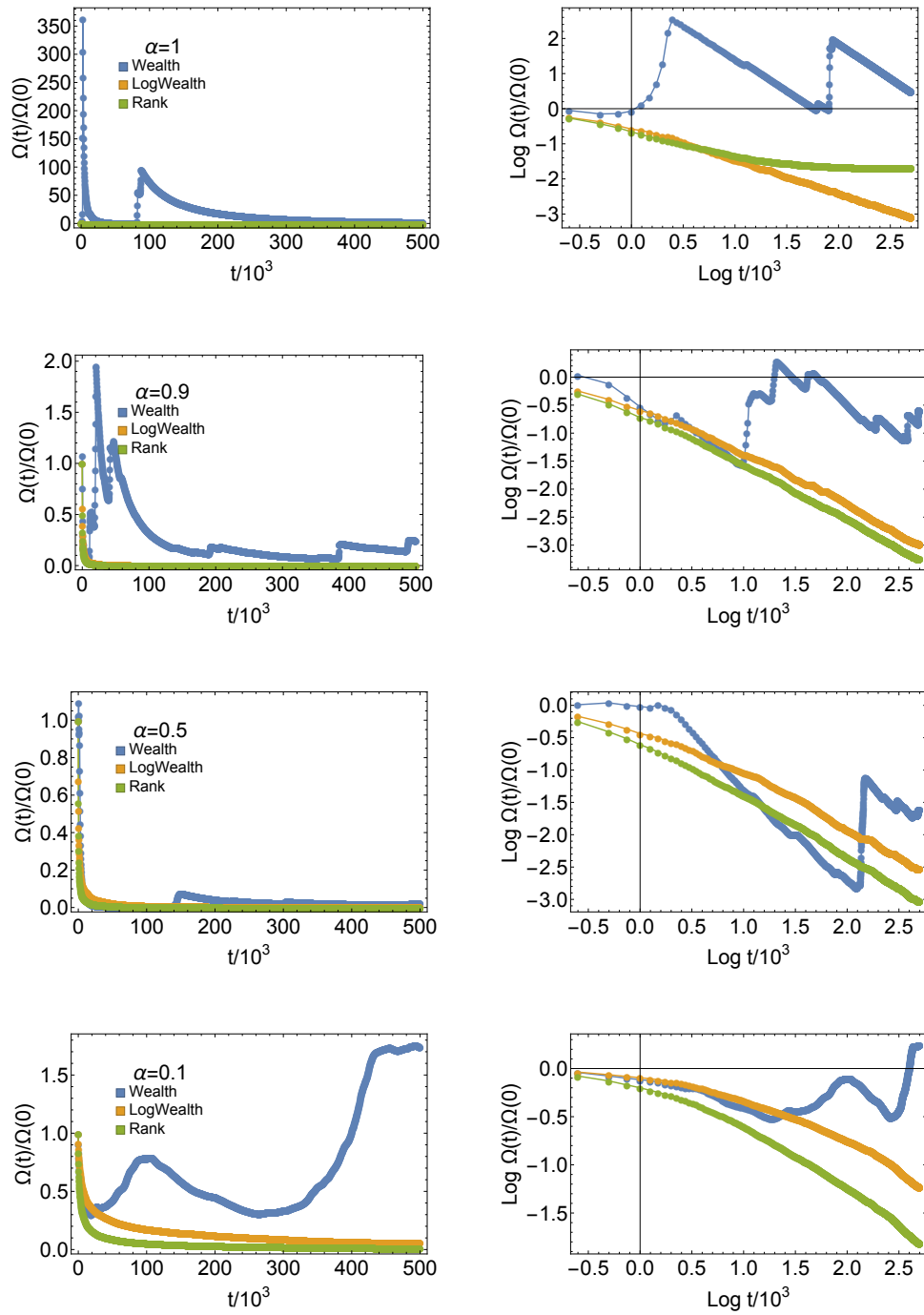


Figure 4.8: The modified metric which examines the fluctuations of all but the richest agent, for various α .

the unmodified metric; however, it may be the case for the log-wealth of the agents. For $\alpha = 0.9$ the scaling appears for both rank and log-wealth. For moderate values, $\alpha = 0.5$, the scaling form appears at late times.

For small α , the scaling form has not appeared, but is neither ruled out by the data present. It seems quite likely that the system is effectively ergodic, however, the time-scale over which this behavior is evident is beyond the reach of a simple simulation. This is corroborated by the rank-rank transfer data for small α , which indicates that the agents are diffusive among ranks. For a non-interacting particle, diffusion within a bounded domain is necessarily ergodic; for this collection of interacting particles in steady state, we expect that background can be treated as approximately stationary.

4.6 Arithmetic growth in the MT approximation

To handle the case of arithmetic growth, let us introduce a growth function $g(x)$ which gives a constant-in-time growth to agents which may generally depend on the rank of the agents. The dynamical equation becomes

$$\dot{w}(x, t) = -\beta x w + \beta \int_x^1 w(x', t) dx' + g(x) \quad (4.2)$$

In tandem to introducing $g(x)$, we introduce likewise a cumulative growth function $G(x) = \int_x^1 g(x') dx'$. Then, integrating as in the no-growth case, we see that

$$\dot{W}(x, t) = -\beta x W(x, t) + G. \quad (4.3)$$

This is solved by

$$W(x, t) = q(x) e^{-\beta x t} + \frac{1}{\beta x} G(x), \quad (4.4)$$

where $g(x)$ can be used to match the initial conditions.

Evidently, the steady-state is given by

$$W_s(x) = \frac{G(x)}{\beta x} \quad (4.5)$$

$$w_s(x) = \frac{g(x)}{\beta x} + \frac{G(x)}{\beta x^2}. \quad (4.6)$$

Notice that while the steady-state formally exists, the time required to converge to the steady-state diverges as we approach $x \rightarrow 0$, that is, for the richest agents in this economy. Except for the richest agent, every agent will eventually converge to the steady-state value. Hence, the richest agent will eventually absorb all of the growth, growing at a rate $G(0)$. Specifying uniform growth $g(x) = g_0$, we have $G(x) = g_0(1 - x)$, and the steady state is

$$w_s(x) = \frac{g_0}{\beta x^2}. \quad (4.7)$$

Notice that The cumulative wealth distribution is the inverse of the ranked wealth function, hence the cumulative distribution that asymptotically approaches $c(w) \sim w^{-1/2}$, or a Pareto index of 1/2. Note that this result is robust in that it does not depend on the MT rate β . This value of the Pareto index represents a model economy with too much wealth disparity to be realistic.

4.7 Skewed arithmetic growth

4.7.1 Constrained arithmetic growth

Alternatives to uniform growth may be considered.

If we introduce skewed arithmetic growth as a function of *relative* wealth while

fixing the overall growth, there are a few possibilities. Let us start with *constrained* growth, where the growth of the total system is fixed at a constant in time.

First, if the growth is monotonically increasing with relative wealth, all but one agent will go bankrupt; Inequities in the system are self-reinforcing. As an example, suppose that we consider a skewed distribution of growth

$$\delta w_i = \delta W \frac{w_i^\gamma}{S}, \quad (4.8)$$

where the normalization factor S is the sum

$$S = \sum_i w_i^\gamma. \quad (4.9)$$

The skew parameter γ ranges from 0 to 1; $\gamma = 0$ returns the distribution of growth to the even distribution, above. If we examine the rescaled wealth for $\gamma > 0$. As in the unskewed growth, the richest agent will eventually come to absorb a large fraction of the growth. However, in this case, the richest agent's increase will decrease the absolute growth of the other agents, thus decreasing their wealth.

On the other hand, if the growth is decreasing function of wealth, the situation may be reversed. This may depend on the precise form of the growth, but certainly for the specific model $\gamma < 0$, the poorest agents will not be impoverished, for in the limit that a set of agents becomes largely impoverished, they begin to receive the dominant fraction of the wealth. On the other hand, as the richest agent in this model will receive less and less growth as they become more and more wealthy.

4.7.2 Unconstrained growth

If we introduced skewed growth where the total growth is a function of *wealth* as opposed to of relative wealth, we obtain a developing steady-state, provided that the

growth function is non-zero in the limit where an agent's wealth approaches 0.

Let us treat growth which is a function of rank. We can work backwards to engineer what forms of arithmetic growth might lead to a realistic Pareto index. Assuming that the richest segment of the economy is well-described by a Pareto index k , we have $c(w) \sim w^{-k}$. The clear ansatz for a growth function is $G(x) \sim C - Ax^q$ near $x = 0$ for some constant C and some power q . Inserting this into Eq. 4.6 we find

$$x^{2-\frac{1}{k}} \propto A(q-1)x^q + C. \quad (4.10)$$

There are two possible solutions. The first is $q = 1$, which is the uniform growth case already covered. The second is $C = 0$, with $A < 0$ so that the total growth is positive, and $q < 0$ to ensure that $g(x)$, the agent-wise growth, is positive. Then the Pareto index given by $k = \frac{1}{2-q}$, ensuring that $k < 1/2$. The wealth disparity is even greater in this case, and which puts us even further from a realistic Pareto index.

4.7.3 On physical expectations for the growth

From a more physical perspective, if we consider modifying the growth function, we can only lower the disparity between the rich and the poor by reducing the growth function for the rich relative to the poor. The assertion that the assets of the richer agents would actually *inhibit* their ability to grow is incredibly counter to economic intuition. Hence the arithmetic growth model will always have a wealth disparity at least as strong as in uniform growth; we thus conclude that arithmetic growth models cannot give rise to realistic Pareto exponents. It is certainly the case within the context of MT theory.

Chapter 5

The YSM with geometric growth

Next, let us examine geometric growth. Economic growth rate is usually measured as a fractional growth rate. If a growth rate remains constant, then the system undergoes a geometric (exponential) growth over time. We use a growth rate μ and grow the system such that the total wealth W grows as

$$\delta W = \mu W \tag{5.1}$$

during each growth step. This assumption may reflect, for example, an economy in which some of the wealth is used to create technology which enables more efficient production of wealth.

5.1 Uniform geometric growth

We initially consider uniform growth, where each agent receives the same amount of wealth in each time step:

$$\delta w = \delta W / N \tag{5.2}$$

In this case, all agents grow without bound; see figure 5.1. The overall distribution grows at the same rate as the total system, and so when we rescale the system to

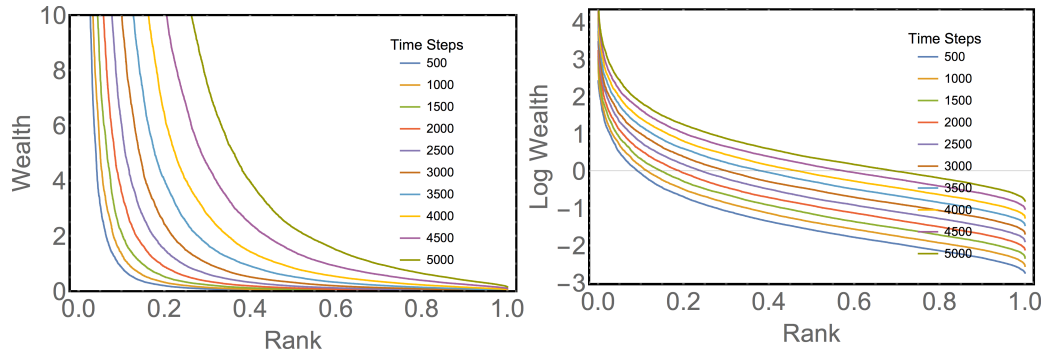


Figure 5.1: The wealth distribution for $\alpha = 0.5$, $\mu = 0.001$, $N = 10,000$, taken at different times. The growth in the system leads to a rescaled steady state, seen on the right as a constant additive change in the Log of the wealth in time.

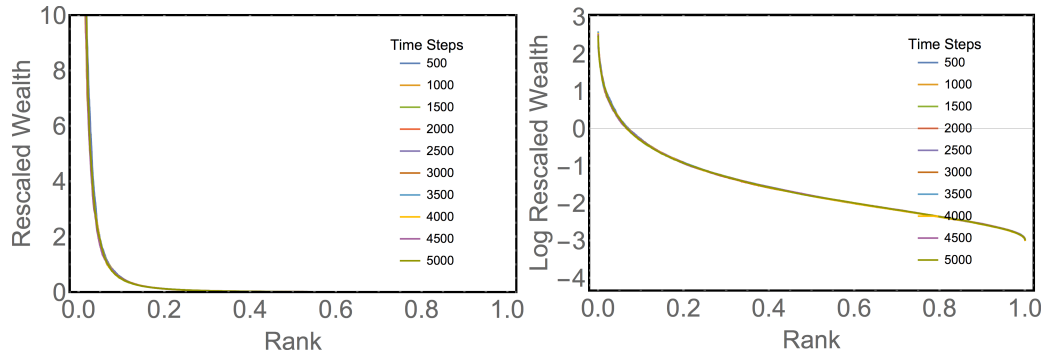


Figure 5.2: The rescaled wealth distribution for $\alpha = 0.5$, $\mu = 0.001$, $N = 10,000$, taken at different times; the rescaled wealth is in a steady-state.

wealth fractions, this distribution is in steady-state, see figure 5.2. For this reason we term the system to be in a “rescaled steady state”. This rescaled steady state includes even the richest agent, and so, unlike in arithmetic growth, the wealth condensation has been totally broken. For the rest of the chapter we will deal in rescaled wealths unless otherwise specified.

5.1.1 Wealth distribution

The rescaled steady state varies as a function of the model parameters. As shown in chapter 2, the trading drives the inequality in the system with a rate proportional to α^2 ; this force is contrasted with the geometric growth rate μ . The dimensionless

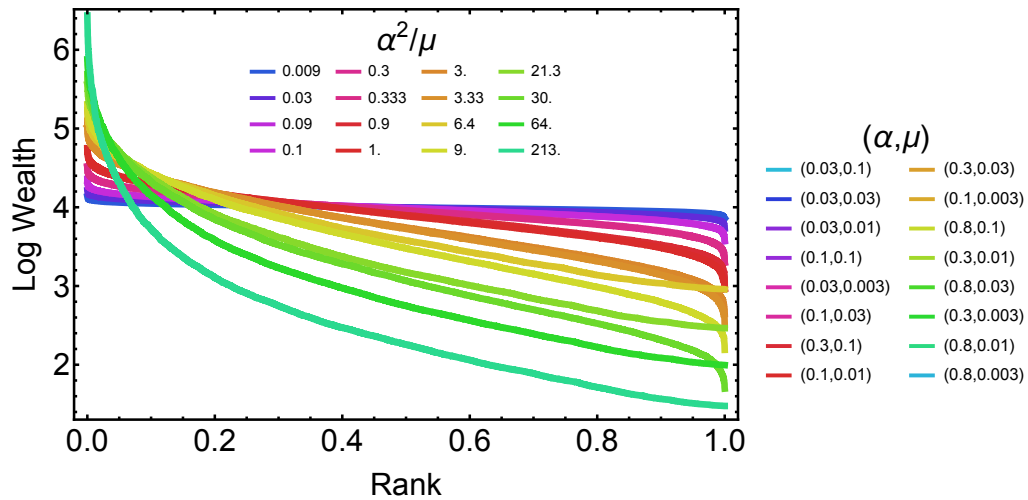


Figure 5.3: The rescaled steady state for various trading and growth parameters: α ranges over the set $(0.8, 0.3, 0.1, 0.03)$, and μ ranges over the set $(0.1, 0.03, 0.01, 0.003)$. The curves are colored with respect to α^2/μ , which reflects the inequality in the system. $N = 10,000$

constant which specifies the resulting distribution is thus α^2/μ . Figure 5.3 shows the steady state for various systems, with lines colored by the inequality parameter α^2/μ . The results show that the steady states are indeed very well sorted by α^2/μ . When $\alpha^2/\mu \gg 1$, the wealth distribution spans many orders of magnitude. When $\alpha^2/\mu \ll 1$, the agents are narrowly localized in wealth space.

The mean trade analysis of this system given in section 5.4 predicts that the wealth distribution in the system obeys that of a power law with a finite cutoff. We explore this possibility by plotting the wealth distribution as a function of the shifted rank, $x' = 1 + \alpha^2 x/\mu$. The results, shown in figure 5.4, show that when α^2/μ is large, that is, much greater than 1, the system approaches this state. Since the cut-off to the power law likewise shrinks as this limit is approached, this gracefully explains the large inequality seen in this limit.

We likewise would like to test the overall scale of the wealth distribution against the mean trade prediction. Due to deviations at the extreme edges of the distribu-

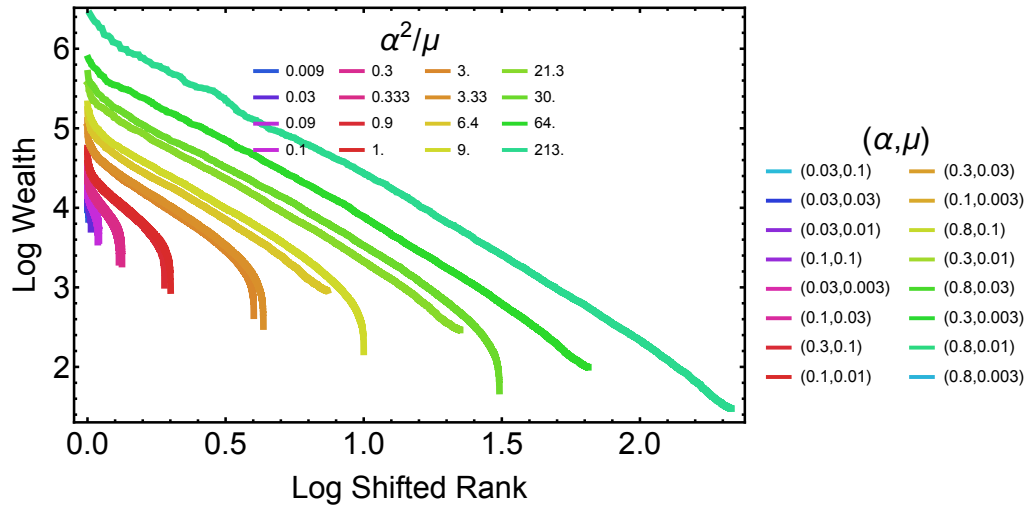


Figure 5.4: Wealth against shifted rank, showing the quality of the MT solution for uniform geometric growth: When the inequality in the system is large, the wealth distribution follows a shifted power law; a power law in the shifted rank $x' = 1 + \alpha^2 x / \mu$. Thus α^2 / μ not only reflects the inequality in the system, but is also a viable mean trade parameter which indicates the quality of the mean trade. $N = 10,000$

tions, it is most stable to test this by examining the scaling of the median agent. The comparison is shown in figure 5.5. There is very good agreement between the mean trade solution and the data. It is key to note that as the inequality increases and the power-law form of the data takes hold, the median wealth shrinks away from the mean wealth (which is always 1 in this normalization). This is characteristic of heavy-tailed distributions and so this mean-median disparity holds in real-world wealth distributions as well, as discussed in section 1.3.1.

On the other hand, we should seek a description of the regime of the system where the mean trade parameter α^2 / μ is small. In this regime, the mean-trade solution from section 5.4 confines the normalized wealths to be close to 1. The dynamics are dominated from the deviations from the mean trade approximation—the diffusive terms. This gives us a picture of an economy where the agents are able to drift multiplicatively, with fluctuations decaying due to the growth μ exceeding the drift

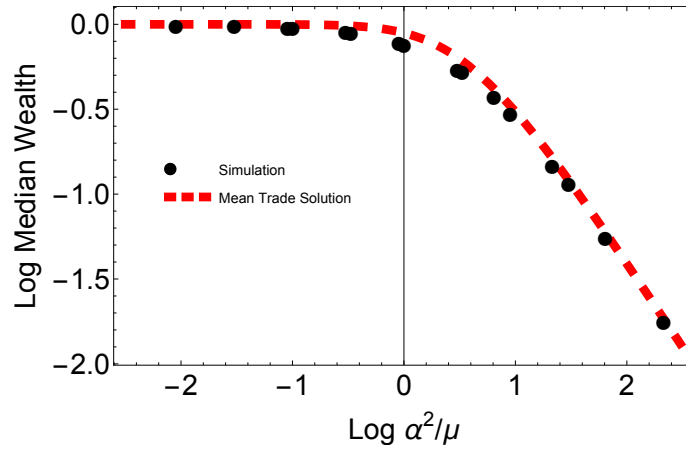


Figure 5.5: Scaling of the median wealth for geometric uniform growth. The mean trade solution, $(1 + \alpha^2/\mu)/(1 + \alpha^2/2\mu^2)^2$, (obtained in section 5.4) agrees very well with the data. The same systems are shown as in figures 5.3 and 5.4. $N = 10,000$

rate. Figure 5.6 demonstrates that this is in fact the case: For $\alpha^2/\mu \ll 1$, the moments of the log of the distribution converge to those for a normal distribution.

5.2 Skewed Growth

We now consider skewed growth parameterized by a skew parameter γ . Each agent, labeled by i , grows by an amount

$$\delta w_i = \delta W \frac{w_i^\gamma}{S}, \quad (5.3)$$

where the normalization factor S is the sum

$$S = \sum_i w_i^\gamma. \quad (5.4)$$

Tuning over the range $\gamma = 0$ to $\gamma = 1$ continuously varies the system from uniform growth to proportional growth, and as we move to $\gamma > 1$, the growth is weighted even more towards the rich agents. We take $\gamma > 0$, presuming that increasing wealth

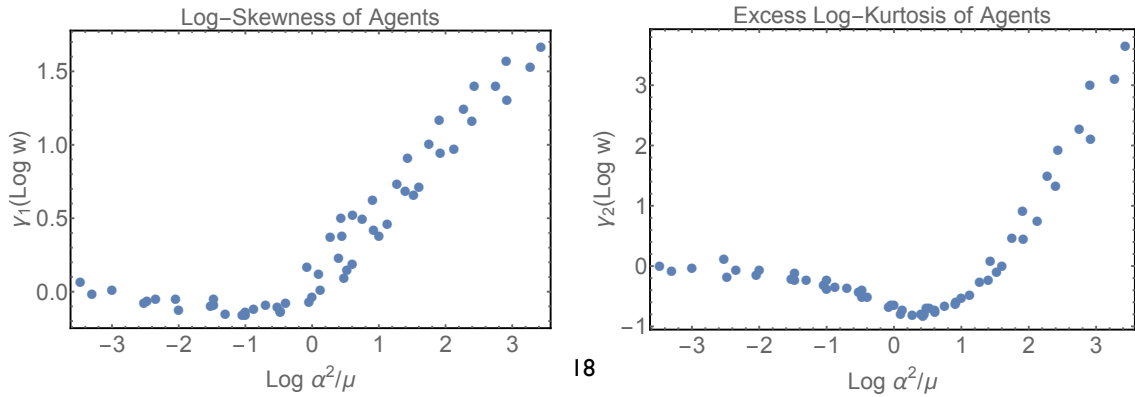


Figure 5.6: The standardized moments of the log-wealth distribution. Left: The skewness (conventionally denoted γ_1) is the third moment of the distribution nondimensionalized by the variance. It characterizes the symmetry of the distribution about the mean; $\gamma_1 = 0$ denotes no skew. Right: The excess kurtosis (conventionally denoted γ_2) is the fourth moment of the distribution nondimensionalized by the variance. It characterizes the spread of the distribution; large kurtosis indicates a distribution with tails, whereas small kurtosis indicates a distribution which ends abruptly. The excess kurtosis is defined such that the normal distribution has $\gamma_2 = 0$.

does not decrease the potential for growth.

5.2.1 Duality with wealth tax

The fact that the rescaled wealth tends towards a steady-state distribution makes it natural to examine the dynamics of rescaled wealth. We can reinterpret the system by examining the wealth fractions

$$y_i = w_i/W. \quad (5.5)$$

This change does not effect the trading dynamics because of the rescaling invariance of the YSM exchange mechanism. At each growth step, the change in the rescaled wealth becomes

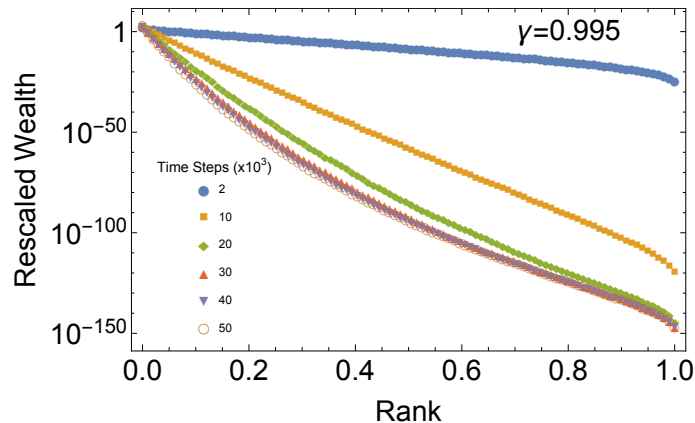


Figure 5.7: The wealth distribution for γ approaching 1, very close to the phase transition. The wealth inequality in the system is very large, with wealths spanning 150 orders of magnitude, but the system nonetheless reaches a rescaled steady state. $\gamma = 0.995$, $\alpha = 0.2$, $\mu = 0.01$, $N = 10,000$.

$$\delta y_i = \mu' \frac{y_i^\gamma}{S_y} - \mu' y_i \quad (5.6)$$

with $\mu' = \frac{\mu}{1+\mu}$, and $S_y = \sum_i y_i^\gamma$. By transforming the dynamics of the system to see how we are operating on rescaled wealths, we see that we are taking a fraction of each rescaled wealth at each time step and distributing this taxed wealth across the agents. $\gamma = 0$ is a flat redistribution of the taxes. As γ increases, the wealthy benefit more from the taxes, and as $\gamma \rightarrow 1$ the δy_i vanish because the redistribution matches the taxed amount exactly.

5.2.2 Dynamical phases

The introduction of growth skewed by the γ parameter leads to different dynamical phases of the system. Since $\gamma = 0$ reduces to the uniform growth model, it has the phase described by the previous section: a rescaled steady state. As we increase γ , we find that between 0 and 1, the system behaves much as it does when $\gamma = 0$, with a rescaled steady state distribution. This is obtained as long as $\gamma < 1$ (see figure 5.7).

$\gamma = 1$ presents a special point in the phase space. When $\gamma = 1$, the normalization factor S in equation 5.3 becomes precisely equal to the total wealth W , and hence the growth terms simplify to $dw_i = \mu w_i$, which is equivalent to a global rescaling of wealth. Because the bare YSM exchange system commutes with global wealth rescaling, this means that the dynamics of the system completely factor, and each wealth can be written as $w_i = w_{i,bare} e^{\mu t}$. This means that at this point, the steady state vanishes. There is wealth condensation in the sense that there is one agent whose fraction of the wealth approaches 1. However, if the growth rate is high enough, $\mu > \alpha^2$, even the poorest agents will continue to grow over time.

For $\gamma > 1$, the wealth quickly condenses on to the richest agent. Figure 5.8 shows the wealth of the richest x agents as γ is varied; As $\gamma \rightarrow 1$, the wealth of the richest agent approaches the wealth of the entire system approximately as a power law. Likewise, figure 5.9 shows a similar pattern in the finite size scaling for the wealth of the richest agent when using different system sizes. These figures highlight the nature of the phases: When $\gamma < 1$, the wealth distribution is scalable in the continuum limit, so that when the number of agents is large enough, the wealth distribution as a function of rank approaches a continuous distribution. When $\gamma > 1$, the wealth strongly condenses onto the richest agent.

The timescale required for the system to reach steady state is also divergent as $\gamma \rightarrow 1$. This is shown in figure 5.10. The data was obtained by observing the inequality of the system as a proxy. The inequality measure $\Phi = \frac{1}{N} \sum -\ln(w)$ (see also section 6.1.5) is at a minimum in the initial state, and increases steadily and smoothly as the system enters into the rescaled steady state. Data was taken to establish the mean value of Φ in steady state. The actual value of $\Phi(t)$ fluctuates about this mean, although very little. The timescale was then assigned by finding

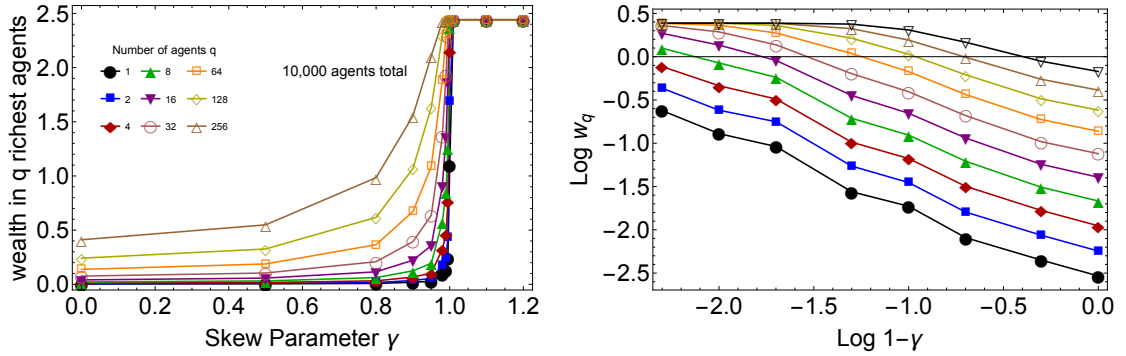


Figure 5.8: Left: The wealth in the richest segments of the economy for various growth skew parameters γ . Each line represents the amount of wealth in the top n agents. Right: The wealth of the richest agents approaches the wealth in the system as a power law in $1 - \gamma$. $\alpha = 0.2, \mu = 0.01, N = 10,000$.

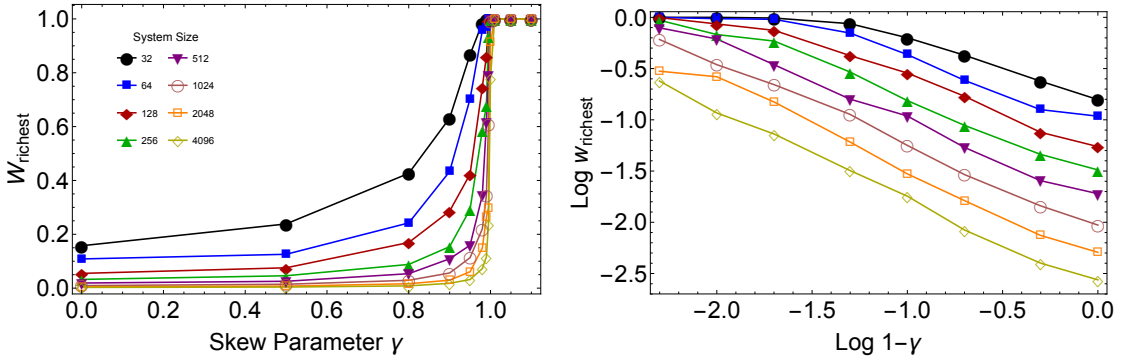


Figure 5.9: Left: The wealth of the richest agent approaching as the transition as the system size increases. Right: This wealth approaches the wealth in the system as a power law in $1 - \gamma$. $\alpha = 0.2, \mu = 0.01, N = 10,000$.

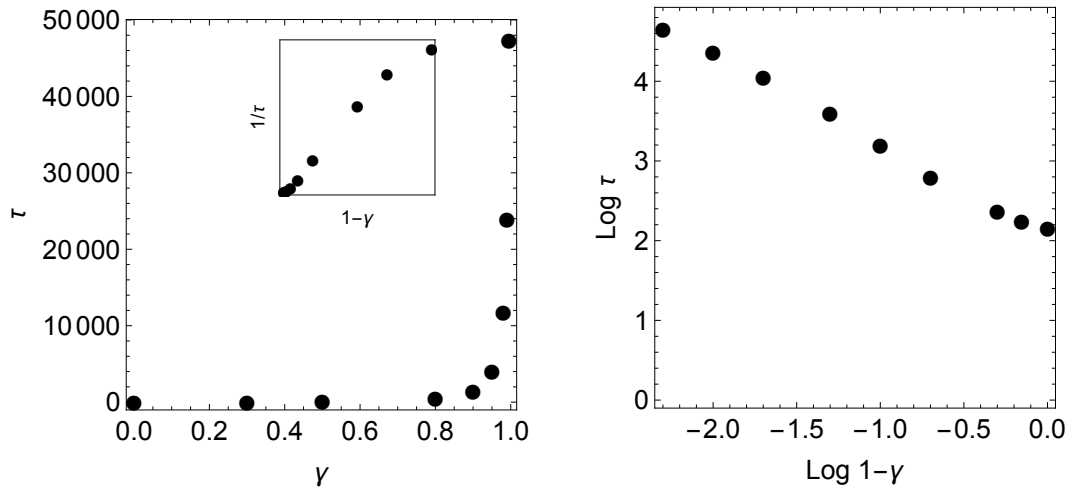


Figure 5.10: The timescale τ associated with the approach to steady state as the skew parameter γ is varied from 0 to 0.995. Left: Linear plot of the time scale τ vs. γ . Inset: $1/\tau$ vs. $1-\gamma$. Right: A log-log plot confirms that the timescale diverges with the distance between γ and 1 with a power of approximately -1 . $\alpha = 0.2, \mu = 0.01, N = 10,000$.

the first time in the data series where the value of Φ exceeded the mean steady-state value. An example is shown in figure 5.11. This process was repeated for 10 identical copies and the results log-averaged; variations in the individual data points were on order 15% or less, giving a standard deviation of the mean expected to be good to a few percent.

5.2.3 System sensitivity to μ, α

We begin by investigation the steady-state timescale for the system as a function of α, μ , and γ . Figure 5.12 shows the most significant result: The timescale τ obeys $\tau \sim \frac{1}{\epsilon}$ as $\epsilon \rightarrow 0$, regardless of the value of α or μ .

Figure 5.13 demonstrates the variation in the steady-state timescale with α . The variation of this timescale with α is given by competition between two effects. The

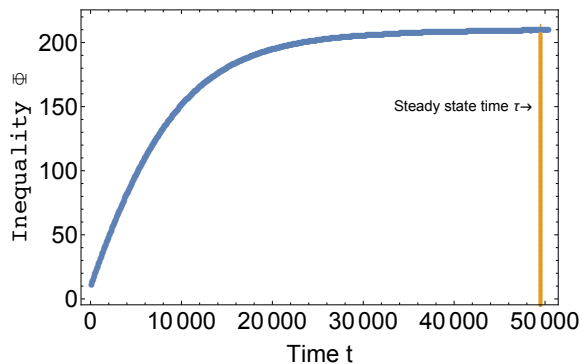


Figure 5.11: The method for obtaining steady-state times. The inequality Φ is monitored until it exceeds its steady-state value. $\alpha = 0.2, \mu = 0.01, \gamma = 0.995, N = 10,000$.

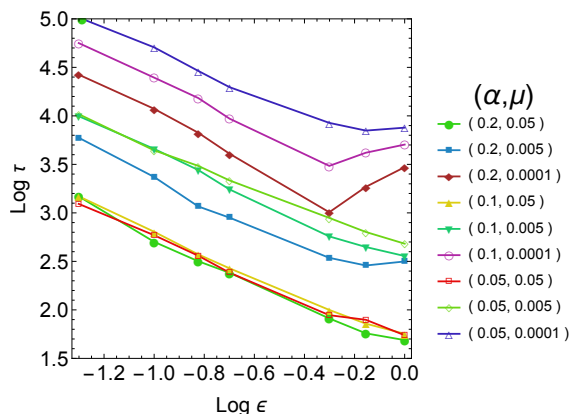


Figure 5.12: The steady-state timescale τ for different values of α and μ against the skew γ . This demonstrates that the steady-state timescale diverges with approximately the same power-law regardless of the trading and growth parameters. Average over 10 realizations per parameter point. $N = 10,000$.

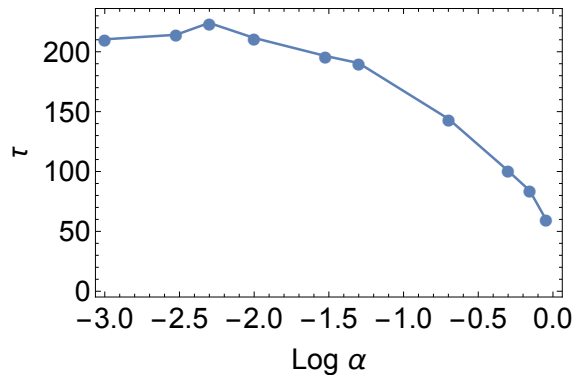


Figure 5.13: The steady-state timescale τ for $\gamma = 0$ and $\mu = 0.01$ against different values of the trading size α . Here we see that the timescale saturates as the trading rate becomes much smaller than the growth. Likewise, the timescale is not strongly dependent on α . This is because although the system slows down as α decreases, the final state is one of decreasing inequality—that is, the final state is not as different from the initial, equal state. Average over 100 realizations per parameter point. α ranges from 0.9 to 0.001. $N = 10,000$.

first is the rate that the system may evolve due to trading, which is given roughly by α^2 , as shown in section 2.6.3. This effect accounts for the increase in the timescale as the trading size is decreased. On the other hand, the timescale is also influenced by the distance between the initial, even wealth distribution, and the final state distribution. As $\alpha^2 < \mu$, in steady state the agents become confined near their initial wealth, and so this effect tends to decrease the steady state timescale as α is decreased.

Figure 5.14 shows the variation in the steady-state timescale with μ . In this case, the two effects are aligned. For one, when μ has dimension of $1/t$, so when μ is decreased, the timescale of evolution is naturally increased. However, this is the timescale associated with the *growth*, which drives the agents together as opposed to apart. The timescale appropriate to reaching the steady state is going to be driven by the force which drives the agents apart, which is the timescale associated with trading. Thus we do not expect a large effect due to this change. The second effect

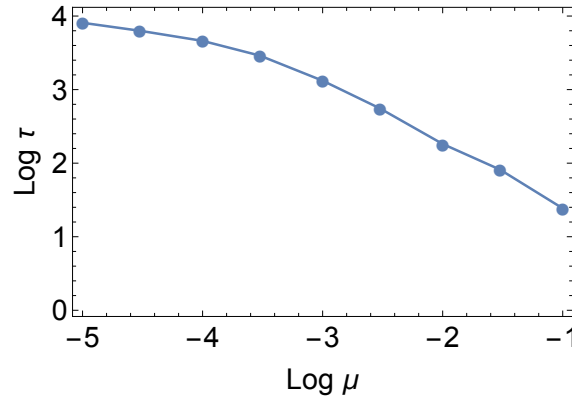


Figure 5.14: The steady-state timescale τ for $\gamma = 0$ and $\alpha = 0.1$ against different values of the growth rate μ . The time-scale increases noticeably as $\mu \rightarrow 0$, however a functional form is not readily discernable. Average over 10 realizations per parameter point. μ ranges from 0.1 to 10^{-5} . $N = 10,000$.

is that when μ is decreased, the inequality in the steady-state is increased, meaning that the initial state and the steady state are further apart. This too increases the steady-state timescale with decreasing μ .

5.3 Ergodicity

In addition to noting the steady-state properties of the system surrounding the phase transition at $\gamma = 1$, we would also like to investigate the ergodicity of the system. We use the TM metric Ω introduced in section 2.6.5. Figure 5.15 shows the TM metric for varying γ approaching the phase transition. The asymptotic form $\Omega \sim 1/t$ is clearly present for the metric applied to wealth, log-wealth, and rank. This indicates that the system is effectively ergodic when $\gamma < 1$.

On the other hand, when $\gamma > 1$, the metric is constant, as the system quickly evolves to a static wealth-condensed state.

Since the metric has the appropriate asymptotic form for $\gamma < 1$, we can also extract the mixing time from this data. The mixing time D_Ω is the coefficient of the

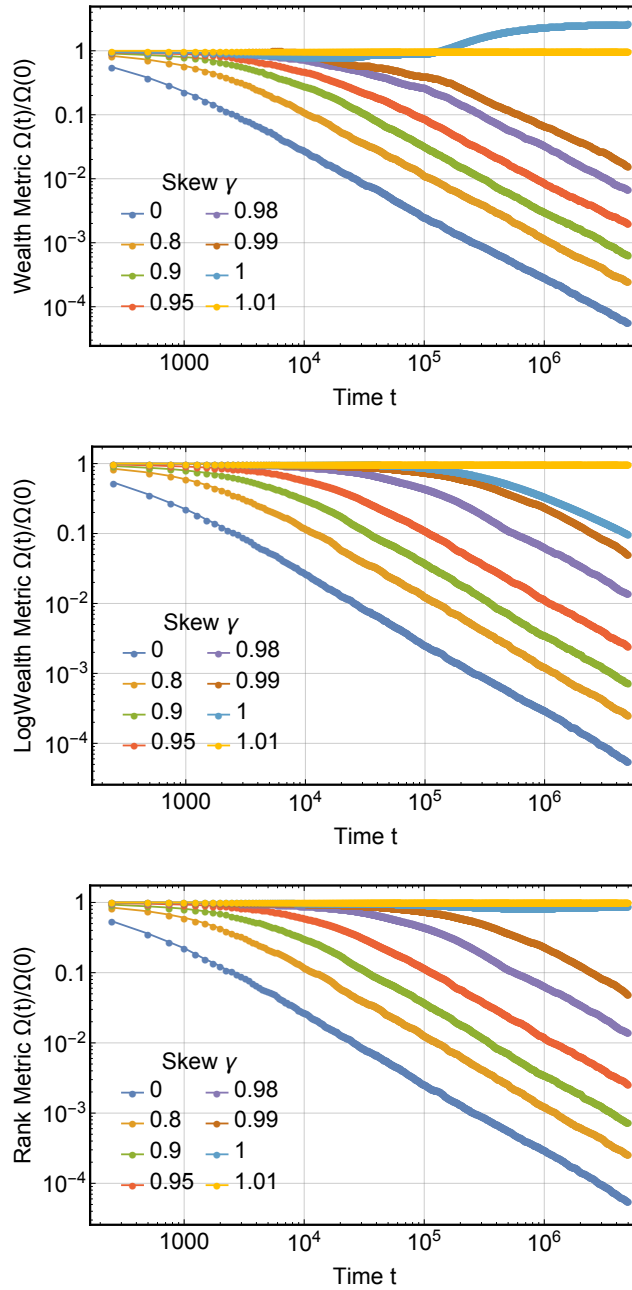


Figure 5.15: The TM metric for the Wealth, Log Wealth, and Rank of the agents against time, for different values of the skew γ approaching the phase transition. The metric demonstrates that the system is effectively ergodic only for $\gamma < 1$. The system was allowed to equilibrate for 10^5 time steps, and then the metric was recorded for 5×10^6 time steps. $\alpha = 0.1, \mu = 0.01, N = 1,000$.

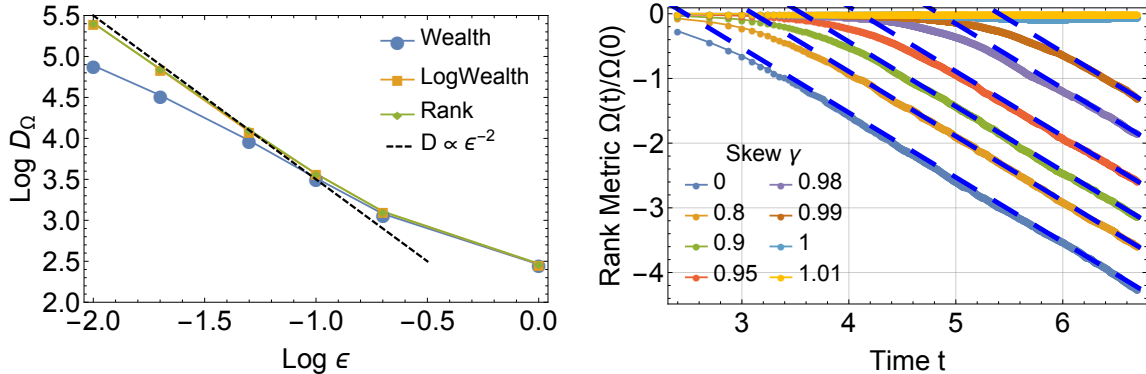


Figure 5.16: Left: The mixing time D_Ω against the skew γ extracted from the metric trajectories for the Wealth, Log Wealth, and Rank. The time was found by using least-squares methods for $\log \Omega = -\log t + \log D_\omega$ for $t > 10^6$. The data indicate that the mixing time diverges relatively strongly near the transition, suggestive of a power law with index -2 (Shown for comparison as a dashed black line). Right: An example of the fits produced using the Rank metric, showing good fit quality. $\alpha = 0.1, \mu = 0.01, N = 1,000$.

asymptotic scaling form:

$$\Omega(t) = \frac{D_\Omega}{t} \quad (5.7)$$

Measurements of D_Ω using the metric data are given in figure 5.16. They are suggestive of but not conclusive evidence for the hypothesis that the mixing time diverges as ϵ^{-2} , although it appears that the mixing time is less according to the Wealth metric. This may be because wealth is such a strongly skewed variable among the agents.

This result is also interesting because it seems to imply that if ϵ is small enough, the mixing time, which scales like ϵ^{-2} , will become larger than the time to reach steady state, which scales like ϵ^{-1} . This means that although mixing is possible, it is

very slow, and that the random bias induced in the initial trades should determine which agents are rich; In effect, the spontaneous symmetry breaking presented by the bare YSM will appear to be present on timescales much shorter than the mixing time.

5.3.1 Wealth distribution approaching the transition

Much like a thermodynamic phase transition, the phase transition in the geometric growth model occurs approaching a point of self-similarity. Near this point, the steady-state wealth distribution exhibits a scaling collapse with the distance ϵ from the phase transition. The form of this scaling collapse can be found as well in the mean trade version of the model in section 5.4. We find that the *shape* of steady-state wealth distribution $w_s(x, \epsilon)$ as a function of rank and skew obeys a relation

$$\epsilon \log \left(\frac{w_s(x, \epsilon)}{w(0, \epsilon)} \right) = -g(x). \quad (5.8)$$

The negative sign in this equation reflecting the notion that $w(x)$, a function of the sorted wealths, is inherently a decreasing function; this implies $g(x) > 0$. This scaling relation, combined with normalization of rescaled wealth, implies a further relation on *scale* of the wealth distribution:

$$w_s(0, \epsilon) = \frac{g'(0)}{\epsilon}. \quad (5.9)$$

When combined, these relations imply that near the phase transition the wealth follows the form

$$w_s(x, \epsilon) = \frac{g'(0)}{\epsilon} e^{\frac{-1}{\epsilon}g(x)} \quad (5.10)$$

This is derived in appendix A.1 . Both of these scaling relations can be seen in the data, as shown in figure 5.17.

In tandem, we find that there is not a power law for the wealthy segment of the economy, but rather a finite cutoff.

5.4 MT with geometric growth

Let us now consider geometric growth as given in section 5, where the total wealth grows by $dW = \mu W$. For generality, consider a normalized growth function $t(x)$ which distributes growth based on the agent rank. $t(x) = 1$ for uniform growth. The ranked wealth density will obey

$$\frac{dw(x, t)}{dt} = -x\beta w(x, t) + \beta \int_x^1 w(x', t) dx' + \mu t(x)W. \quad (5.11)$$

Knowing that the quantity which converges to a steady state is the rescaled wealth, we introduce the rescaled ranked wealth $y(x) = w(x)/W$. In terms of $y(x)$,

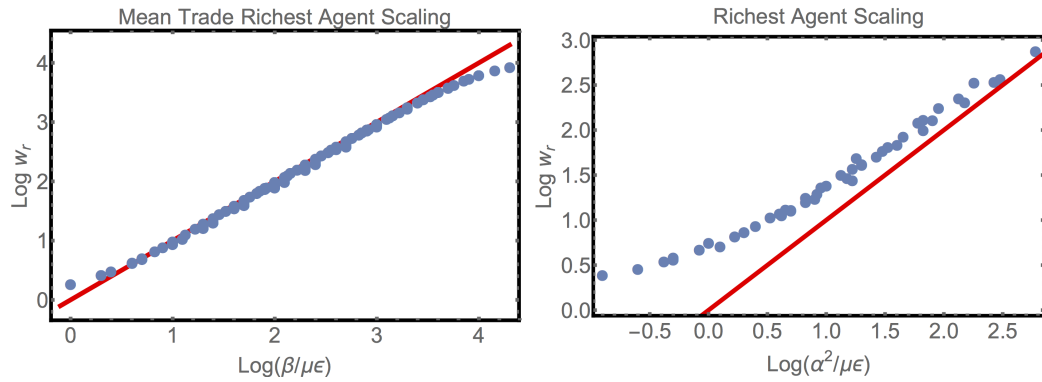
$$\frac{dy(x, t)}{dt} = -x\beta y(x, t) + \beta \int_x^1 y(x', t) dx' + \mu(t(x) - y(x)). \quad (5.12)$$

If we transform as before to the cumulative version of this equation, we have

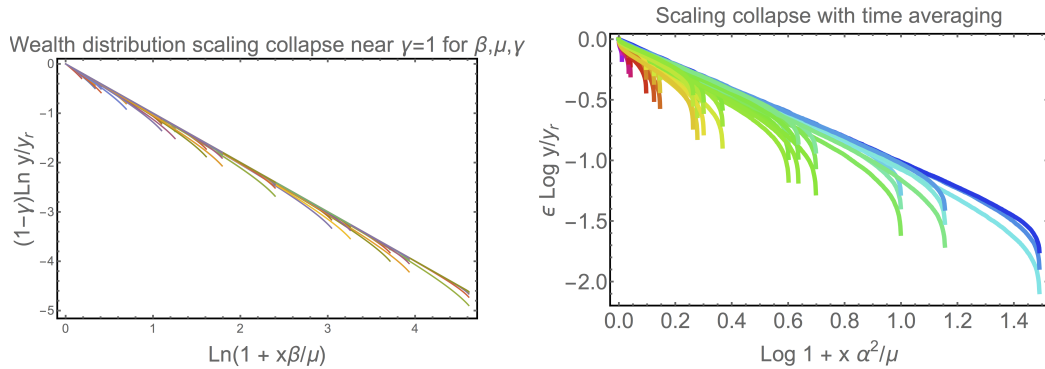
$$\dot{Y} = -(\beta x + \mu)Y + \mu T(x), \quad (5.13)$$

where $T(x) = \int_x^1 t(x)$. The time-dependent solution is

$$Y(x, t) = q(x)e^{-(\beta x + \mu)t} + \frac{\mu T(x)}{\beta x + \mu} \quad (5.14)$$



(a) Scaling relation of the richest agents in the numerical solution to the mean trade equation. (b) Scaling relation of the richest agents in trading simulations.



(c) Scaling relation of the wealth distribution in the numerical solution to the mean trade equation. (d) Scaling relation of the wealth distribution in trading simulations.

Figure 5.17: Investigation of the scaling relations for the richest agent and the wealth distribution near the tipping point. Here we simulate systems with a variety of α , μ , and γ .

with the steady state

$$Y_s = \frac{T(x)}{\frac{\beta x}{\mu} + 1} \quad (5.15)$$

$$y_s(x) = \frac{t(x)}{1 + \frac{x\beta}{\mu}} + \frac{\frac{\beta}{\mu}T(x)}{(1 + \frac{x\beta}{\mu})^2} \quad (5.16)$$

For uniform growth, this reduces to

$$Y_s = \frac{1-x}{1 + \frac{\beta}{\mu}x} \quad (5.17)$$

$$y_s = \frac{1 + \frac{\beta}{\mu}}{(1 + \frac{\beta}{\mu}x)^2} \quad (5.18)$$

This indicates that the agents obey a power law as a function of the shifted rank $x' = x + \mu/\beta$; the agents exhibit a power law up to a wealth cut-off of $y(0) = 1 + \beta/\mu$.

Now let us consider skewed growth, as in section 5.2. The growth term is

$$\left. \frac{dw(x)}{dt} \right|_{growth} = \mu \frac{w(x)^\gamma}{\int_0^1 w(x')^\gamma dx'}. \quad (5.19)$$

The rescaled system will then obey

$$\frac{dy(x)}{dt} = -x\beta y(x, t) + \beta \int_x^1 y(x', t) dx' + \mu \frac{y(x)^\gamma}{\int_0^1 y(x')^\gamma dx'} - \mu y(x) \quad (5.20)$$

This equation has been studied numerically; The properties of the instability around $\gamma = 1$ have been verified to be nearly identical to those in the YSM with the same growth distribution. This includes the scaling of the wealth of the richest agent, the scaling of the time scale, the steady-state scaling collapse. See figure 5.17.

This equation does not admit a simple steady state solution for general γ . However, there is an approximate solution near $\epsilon = 0$ found using the scaling form shown

in section 5.3.1. Solving the mean-trade equation in this regime requires some substantial algebra shown in appendix A.2. The solution form is given by a shifted power law:

$$y(x) = y(0) \left(1 + \frac{x}{\mu'}\right)^{\frac{-1}{\epsilon}} \quad (5.21)$$

Using the substitutions $\lambda = 1 - \frac{1}{\epsilon}$ and $\mu' = \frac{\mu}{\beta}$, we find that this approximate solution is valid provided that the function

$$c(\lambda, \mu') \equiv \frac{1 + \lambda}{1 + \mu' - \mu' \left(\frac{\mu'}{1 + \mu'}\right)^\lambda} \approx 0 \quad (5.22)$$

with the limit $\epsilon \rightarrow 0^+$ replaced with $\lambda \rightarrow -\infty$. We call the function c the “condensation function”, as when c shrinks to zero, the system enters into the asymptotic form approaching wealth condensation.

The denominator of c increases exponentially in this limit, hence this scaling form will eventually be approached regardless of the value of μ ; However, the rate of approach to zero depends crucially on the value of μ .

For large growth, $\mu' \gg 1$, c goes to zero slowly, meaning that the scaling form is only reached for very small values of ϵ . In this regime,

$$c(\lambda, \mu') \approx \frac{1 + \lambda}{1 - \lambda^2 \frac{\mu}{2}} \quad (5.23)$$

Which, when translated into ϵ , gives that the approximation becomes very good when $\frac{\epsilon}{\mu'} \ll 1$. The system remains in a state of relative equality until this is reached, whereupon condensation occurs.

In the case of small growth, $\mu' \lll 1$, c shrinks quickly to zero very quickly with

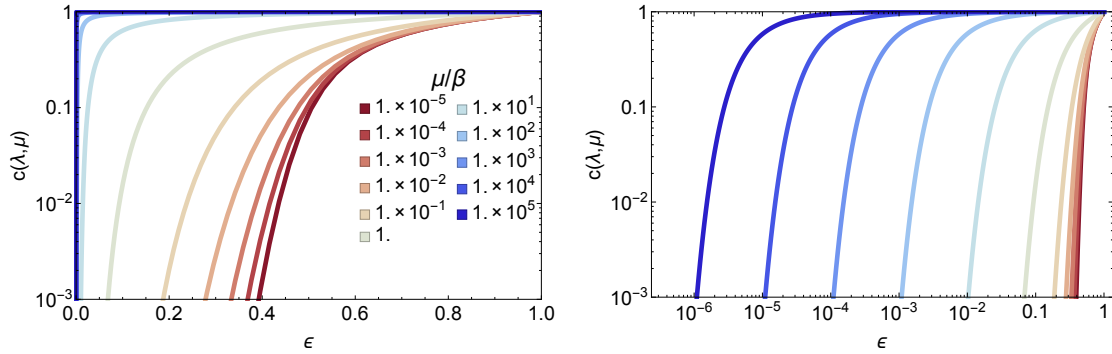


Figure 5.18: The collapse function indicating the convergence of the mean trade solution to the near-collapse shifted power law. Left: Plotted against ϵ linearly, showing saturation for small μ/β . Right: Plotted against ϵ logarithmically, showing that the collapse parameter is approximately $\epsilon\mu$.

ϵ , as here the asymptotic expansion of c is

$$c(\lambda, \mu') \approx \mu'^{1/\epsilon} \quad (5.24)$$

This makes the asymptotic solution to the mean trade equation very accurate. Nonetheless, since $c(0, \mu') = 1$ regardless of μ' , the solution can only hold for a limited range. For very small μ' , the scaling form requires approximately $\epsilon < 1/2$.

A summary showing c as a function of ϵ for various values of μ' is shown in figure 5.18, and as a phase diagram in figure 5.19. This allows us to roughly define a condensation transition near the onset of this scaling form; the scaling form indicates that we are approaching wealth condensation. Reiterating, for low growth, this occurs for any $\epsilon < 1/2$, and for high growth, it requires that $\epsilon < \mu'$.

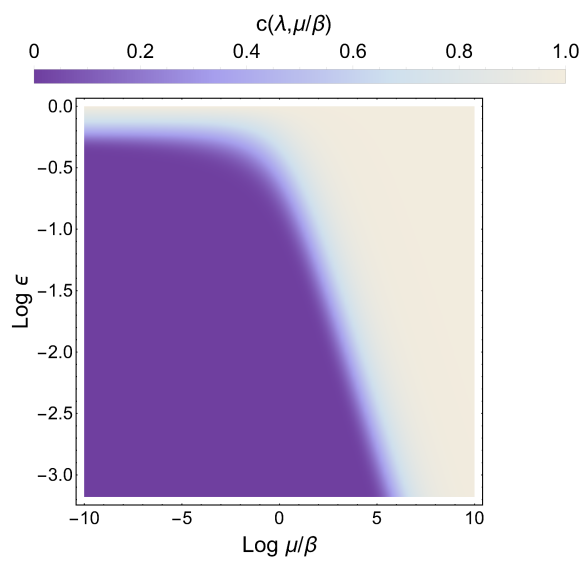


Figure 5.19: A top-down perspective on the collapse function. In the purple region, the mean-trade solution is in the scaling regime.

Chapter 6

Generalizations

6.1 Generalized Wealth Condensation

Motivated by the phase transition found in the previous chapter, in this section we develop a notion of how the mechanisms at play give rise to wealth condensation in more general asset exchanges models.

Suppose that we have an asset exchange model which is given by a generalized fair pairwise wealth transfer function f which depends on the wealth of the two agents involved in the trade and a random variable R such that $-1 < R < 1$ and the expectation value $\langle R \rangle = 0$.

$$w_1 \rightarrow w_1 + R\Delta w \quad (6.1)$$

$$w_2 \rightarrow w_2 - R\Delta w \quad (6.2)$$

$$\Delta w = \Delta w(w_1, w_2) \quad (6.3)$$

In the yard-sale model, $\Delta w = \alpha \text{Min}(w_1, w_2)$ generates losses for the poorer agent in a similar manner to the geometric random walk. In what conditions will such a system tends towards wealth condensation? To ask the question in a more active sense, is it possible for agents to choose f so that they can remain competitive and

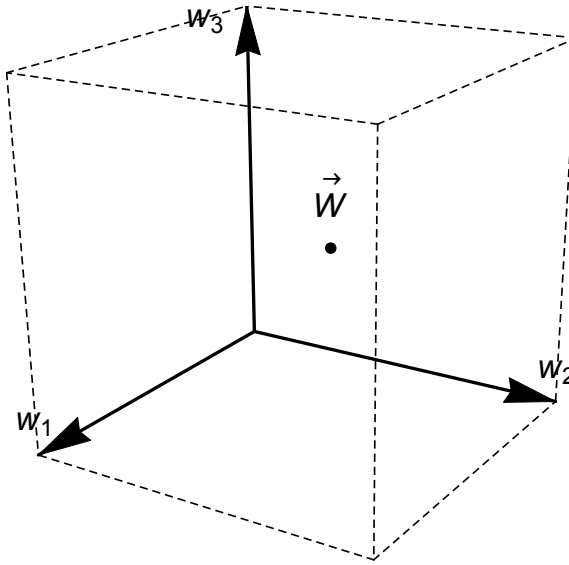


Figure 6.1: A diagram of the wealth space for 3 agents; the product space of the wealth of the individual agents.

a steady-state economy can arise? In particular, we will focus on the case where agents choose their risk separately, that is where $\Delta w(w_1, w_2) = \text{Min}(B(w_1), B(w_2))$ for a betting function $B(w)$.

6.1.1 Diffusion in Wealth Space

We can conceptualize the wealth as an N-dimensional vector $\vec{\mathcal{W}}$ (see figure 6.1) which evolves due to the trading rule specified above; random components of $\vec{\mathcal{W}}$ are selected and modified as per the trading rule by $\pm\Delta w$. In this scheme, wealth conservation is given two notions. The first is that the components of the wealth vector must add up to a constant; the dot product $\vec{\mathcal{W}} \cdot (1, 1, 1, \dots)$ is constant. The second is the notion that the ensemble of all possible $\vec{\mathcal{W}}$ has a constant centroid; if the wealth is imagined as a cloud diffusing from a point, it diffuses such that the center of mass is constant. The motion is diffusive in nature because at each step, the wealth vector is equally likely to migrate one direction or another.

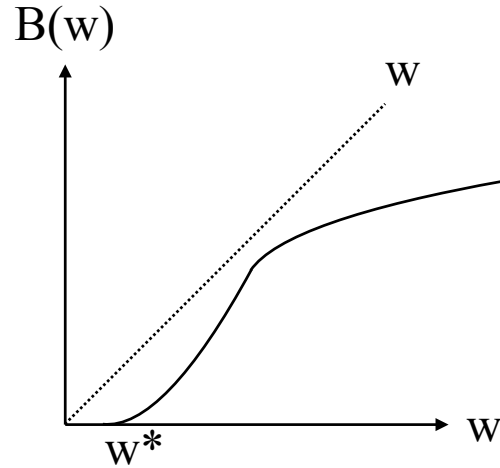


Figure 6.2: An example betting function obeying the constraint $B(w) < w$ with a zero at w^*

In this scheme, we wish to analyze the likely trajectories of the wealth through this space. Because the steps Δw depend on the wealths being exchanged, the diffusion is nonlinear in nature. This nonlinear nature gives rise to a drift term such that the typical wealth walks in a biased direction.

What we will show is that when the wealth of an agent approaches the zeros of the betting function $B(w^*) = 0$, the nonlinear drift attracts the agent towards the zero. This trapping effect drives the agents towards w^* , the location of the zero of the betting function. This trapping prevents the wealth from leaving the plane formed by $w_i = w^*$, and inevitably leads to a slowing down, or condensing of the economy; after enough time, there is an asymptotic fixed point towards which the wealth vector only approaches. Critically, if there is only one zero w^* , then all the wealths except for one must end at w^* , leaving all of the free wealth condensed onto one agent.

Importantly, physical constraints dictate that the betting function *must* have a zero, for $B(w) \leq w$, elsewise the agent is risking more wealth than they have; See

figure 6.2. This assumption requires that agents have a minimum wealth, but it does not dictate that the minimum wealth map to no assets; an asset exchange model could very well reflect an economy incorporating debt and so on. We seek to show that the nature of the approach of the betting function to zero will give rise the time-scales associated with the wealth condensation.

6.1.2 Dynamics near betting function zeros

First, consider the behavior of one of the agents closest to the zero of the betting function. Near the zero of the betting function, the amount that the agent trades will become dominated by small amount that agent is willing to risk, $B(w)$. We will show that the wealth of the poorest agent will trend down inevitably.

Because the poor agent is so dominated by these small fluctuations, we may treat their motion using the Itô calculus [75, 83–86], which allows us to treat this type of generalized Brownian motion. An Itô process for one variable is described by a stochastic differential equation $dw = \mu dt + \sigma d\eta$, with drift term μ and noise term σ . The stochastic process associated with the motion of an agent at wealth w near w^* is given by the process

$$dw = 0dt + B(w)d\eta, \quad (6.4)$$

where $d\eta$ represents underlying Gaussian noise, and the drift term $\mu = 0$ for this process. In order to understand the trajectories given by this process, we would like to find an *ergodic* measure for this process—that is, one where the noise is constant. To do this we will make use of *Itô's lemma*, which prescribes how to convert one stochastic process w into another stochastic process on a transformed variable $\chi(w)$:

$$d\chi = \left(\mu \frac{\partial \chi}{\partial w} + \frac{\sigma^2}{2} \frac{\partial^2 \chi}{\partial w^2} \right) dt + \sigma \frac{\partial \chi}{\partial w} d\eta. \quad (6.5)$$

This is the stochastic equivalent of the chain rule from ordinary calculus. The only additional term is the $\frac{\sigma^2}{2} \frac{\partial^2 \chi}{\partial w^2}$ which arises because η and t are not independent variables; η fluctuates in t in a Brownian fashion, and the repeated action of fluctuations picks up a drift term which scales as t ; see the geometric random walk in section 3.2.1; Itô's lemma merely prescribes the appropriate extension of this effect into the domain of continuous motion.

Again, we search a process with linear noise: a variable for which the fluctuations do not vary as we change the variable. From Itô's lemma, eq. 6.5, and from, eq. 6.4, we need

$$\frac{\partial \chi}{\partial w} = \frac{1}{B(w)}. \quad (6.6)$$

This gives us a stochastic differential equation for the variable χ :

$$d\chi = -\frac{1}{2} \frac{\partial B(w)}{\partial w} dt + 1d\eta \quad (6.7)$$

Typical trajectories from the linearized noise

Now that we have a process χ , we can understand the limiting state for the typical trajectory of w . The story is very similar to the geometric random walk: Although it would appear from eq. 6.4 that the average over w gives 0, this is only formally true for an *infinite ensemble average*. The reality is that the *typical* trajectory from the infinite ensemble is not stationary, but rather falls in time. The average is formally balanced by exponentially rare trajectories which grow quickly.

By transforming to the linearized variable χ , we find a variable whose fluctuations are predictable and controlled. Simple Brownian motion dictates that these fluctuations scale as \sqrt{t} . The drift term, then, will overwhelm the fluctuations for long times. Because the fluctuations are controlled, exponentially rare trajectories

cannot contribute finite contributions to the infinite ensemble average. We can thus track typical trajectory of χ by the ensemble average. This allows us to write

$$d\chi_{typ} = \mu_\chi dt = -\frac{1}{2} \frac{\partial B(w)}{\partial w}. \quad (6.8)$$

and analyze the typical trajectory χ_{typ} as a deterministic quantity. The “trapping” quality of the solutions will become apparent in the analysis that follows.

The potential function

The evolution equation for χ now follows that for a particle diffusing under the influence of an external force $f(\chi)$ and diffusion coefficient D [75]:

$$d\chi = f(\chi)dt + Dd\eta \quad (6.9)$$

$$f(\chi) = -\frac{1}{2} \frac{\partial B}{\partial w} \quad (6.10)$$

$$D = 1 \quad (6.11)$$

This analogy allows us to conceive of the stochastic nonlinearity of $B(w)$ as giving rise to a potential function V given by

$$V(\chi) = -\int f d\chi = -\int \frac{\partial B}{\partial w} d\chi \quad (6.12)$$

By making use of the defining condition of χ , Eq. 6.6, we can write

$$V(\chi) = \frac{1}{2} \int \frac{\partial B(w)}{\partial w} \frac{dw}{B} = \frac{1}{2} \int \frac{dB}{B} = \frac{1}{2} \ln(B). \quad (6.13)$$

Note that as $B \rightarrow 0$, $V \rightarrow -\infty$, regardless of the form of the approach to zero. This will help tremendously in understanding the limiting behavior of the agent.

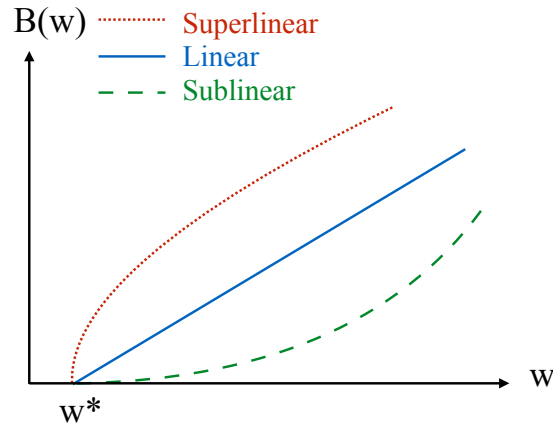


Figure 6.3: Types of betting functions behavior near w^* . The dynamic rate of condensation in a model is dependent on the shape of the approach of the betting function to zero, which can be characterized as either linear, sublinear, or superlinear.

Linear zeros and GRW

Let us suppose that the form of $B(w)$ near the zero can be written in the form

$$B(w) \approx \alpha(w - w^*). \quad (6.14)$$

Let us transform coordinates without loss of generality to shift w such that $w^* = 0$. Then $B(w) \approx \alpha w$. The transformation required to get an ergodic variable is determined by $\partial\chi/\partial w = 1/(\alpha w)$, or

$$\chi = \frac{\ln(w)}{\alpha} \quad (6.15)$$

Inserting into eq. 6.8,

$$d\chi_{typ} = -\alpha dt \quad (6.16)$$

This tells us that the typical χ scales as

$$\chi_{typ} \sim \alpha t. \quad (6.17)$$

Inverting, we find that the typical w obeys

$$dw_{typ} = -\alpha^2 w_{typ} dt \quad (6.18)$$

and so follows

$$w_{typ} \sim \exp(-\alpha^2 t) \quad (6.19)$$

A poor agent at rank x will undergo these fluctuations decreased at a rate x , so we need only replace $t \rightarrow xt$ to see the reduction of this effect with rank. The MT formulation discussed in section 3.2.3 is a further correction to this which adds back in the contributions lost by poorer agents to richer ones. There is a small caveat here in that we are assuming the betting function increases monotonically; If it does not, then we need to sort agents by the rank of $B(w)$ instead of by w .

In terms of the potential $V(\chi)$, we find that,

$$V = \frac{1}{2} \ln(\alpha w) = \frac{1}{2} \alpha \chi, \quad (6.20)$$

where we have made use of the fact that V is defined only up to a constant. The poorer walker in the trade experiences a constant force towards $\chi \rightarrow \infty$, which is $w \rightarrow 0$; this force is constant due to the self-similarity of the betting function.

Non-linear zeroes

The preceding section indicates that a linear approach $B(w)$ toward zero will give rise to wealth condensation which is much like the YSM. Here we will treat different approaches to zero of the form

$$B(w) = \alpha(w - w^*)^q \quad (6.21)$$

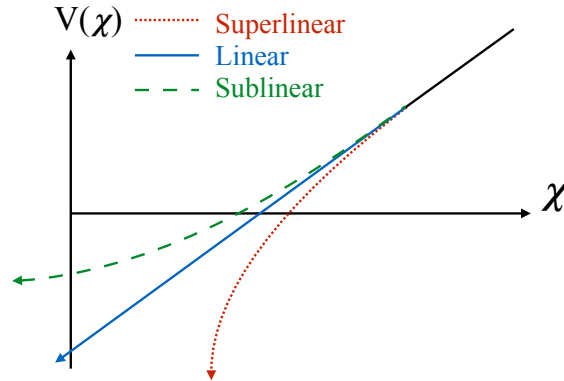


Figure 6.4: Types of potential functions. In all three cases, the potential function diverges as χ approaches its lower limit. In the case of linear and sublinear betting functions, this limit is ∞ . However, the case of a superlinear betting function, χ exhibits a lower bound.

Since $B(w)$ has dimension of wealth, we note that α is, for $q \neq 1$, a dimensionful variable. α can be associated with a wealth scale at which an agent is willing to bet all of their wealth.

As in the case of the linear approach zero, we transform w by a shift so that $w^* = 0$. The reparameterized wealth χ should satisfy $\partial\chi/\partial w = 1/(\alpha w^q)$. This gives us

$$\chi^{(q)} = \frac{1}{\alpha} \frac{w^{1-q}}{1-q} \quad (6.22)$$

(It is worth noting that χ is only determined up to an additive constant. To clean up the notation and unify these solutions with the linear case, we can assign this constant as a function of q , writing χ in terms of the q -logarithm [87, 88]:

$$\chi^{(q)} = \frac{1}{\alpha} \ln_q(w) \quad (6.23)$$

In the limit as $q \rightarrow 1$, the q -log reduces to the usual natural log: $\ln_q(w) \rightarrow \ln(w)$. However, this formulation complicates the analysis of the asymptotic motion of χ .) The form of χ exhibits a transition as q goes through 1; For $q < 1$, χ has a

lower bound but no upper bound, and for $q > 1$, χ has an upper bound but no lower bound. The presence or absence of an upper bound does not concern us greatly, as this corresponds to w far away from w^* . However, the lower bound of χ corresponds to the lower bound of w . This means that for $q < 1$ the closed nature of endpoint at w^* is preserved, but for $q \geq 1$, the closed endpoint becomes an open one. This topological change gives rise to significant differences between the two cases.

Using Itô's lemma,

$$d\chi_{typ} = -\alpha \frac{q}{2} w^{-(1-q)} dt \quad (6.24)$$

Which gives

$$\chi_{typ} d\chi_{typ} = -\frac{q}{2(1-q)} dt \quad (6.25)$$

This equation has a very different character depending on whether $q < 1$ or $q > 1$.

Furthermore, the potential V is given by

$$V = \frac{1}{2} \ln B = \frac{q}{2(1-q)} \ln(1-q)\chi, \quad (6.26)$$

which also exhibits very different characteristics depending on the sign of $q - 1$.

Sublinear (or slow) zeros

For $q > 1$, this is solved with an asymptotic solution

$$\chi_{typ}^2 \sim \frac{q}{2(q-1)} t, \quad (6.27)$$

where χ^2 grows in time, and the wealth obeys

$$w_{typ} \sim (\alpha^2 q (q-1) t)^{\frac{1}{2(1-q)}} \quad (6.28)$$

This class of solutions demonstrate a wealth which slowly shrinks in time according to a power-law. Thus, for $q > 1$, the agents inevitably approach zero, but at a very slow rate; slower than for any linear zero (see section)

The potential function V , making use of the free constant, looks like

$$V(\chi) = \frac{q}{2(1-q)} \ln(-\chi). \quad (6.29)$$

This diverges logarithmically as $\chi \rightarrow -\infty$, explaining the slow power-law approach of $w(t)$ to zero. Likewise, we can consider this the result of a renormalization process. As we scale in towards the zero of B , α decreases, and so the drift is a decelerating one.

Superlinear (or fast) zeros

On the other hand, if $q < 1$, χ^2 shrinks in time:

$$\chi_{typ}^2 = C(0) - \frac{q}{2(q-1)} t \quad (6.30)$$

The typical trajectory will reach $\chi = 0$ in a finite time. When $q < 1$, $\chi = 0$ is identified with $w = 0$. We thus have a ‘fast’ approach to zero. This can be reconciled by realizing that if $q < 1$ and $w^* = 0$, it is not actually possible to satisfy $B(w) < w$, thus agents drift downward in wealth until they inevitably risk everything they have. This process inevitably bankrupts the agents in a finite time; if the betting function approaches zero in this way, then all but one agent will reach w^* in finite time; the remaining wealth will have condensed onto the last agent.

The potential function reflects this likewise:

$$V(\chi) = \frac{q}{2(1-q)} \ln(\chi). \quad (6.31)$$

Thus V diverges drastically near the closed endpoint $\chi = 0$. Again, we can also describe this using a renormalization approach. As we scale in on the zero, α increases. This means that the drift for χ is accelerating. Coupled with the fact that χ has an endpoint, this makes it very natural to see that inevitably $\chi \rightarrow 0$ and so $w \rightarrow 0$.

6.1.3 The next-to-poorest agent and so on

In the case of linear and sub-linear betting functions where the wealth of the poorest agent is finite but ever decreasing, the next-to-poorest agent will follow approximately the same dynamics as the poorest agent, with the exception of the few interactions between the poorest and the next-to-poorest, from which the next-to-poorest will profit as the poorest diminishes. Nonetheless, the rate which the poorest agent diminishes will itself decrease steadily, leading us to the conclusion that the next-to-poorest agent will become impoverished as well. Thus, the trapping quality of the stochastic drift in the vicinity of a zero cascades up to affect even fairly rich agents; however, the rate at which richer agents are trapped may be quite slow.

Upper zeros of the betting function

We may also consider the behavior of zeros of the betting function, those points above which an agent does not participate in trading. Fortunately, these can be approached with the same analysis as zeros which form a lower bound for the betting function; The stochastic equation for w , eq. 6.4, will not change, which implies that the singularity or zero of χ will remain at w^* . However, $\partial B/\partial w$ will change sign, giving rise to a reflected positive drift in χ in Eq. 6.7. Thus the dynamics arise in the same way via the same mechanisms, but reflected, drawing the agent upwards in wealth towards the zero.

6.1.4 The thermodynamic limit and the emergence of wealth condensation

As agents fall into the traps created by zeros of the betting function, their wealth falls predictably over large time scales. These trapped agents must thus be systematically growing the wealth of un-trapped agents. Let us refer to the unbound wealth as *free wealth*. This free wealth determines the wealth of the final unbound agent in the system.

There must always be an unbound agent in the system unless a specific criteria is met: The wealth values of the zeros of the betting function must be commensurate with the number of agents in the system and the starting wealth, that is, there exists a linear diophantine combination of the w^* which adds to the total wealth in the system. This is easy to create in a deterministic model, but any small noise in the initial conditions or model parameters will destroy this process; thus we can generically expect there to be at least one unbound agent in the system. Moreover, the trapping phenomena implies that the number of unbound agents in time can only decrease. Thus, eventually the system will evolve to a state where there is only one free agent.

As the system evolves, the bound agents settle into a distribution along the traps. This limiting distribution is well-defined in the thermodynamic limit (as $N \rightarrow \infty$) because agent interactions depend only on the wealth of the pairs of agents.

This implies that the free wealth in the system *grows* linearly in the thermodynamic limit. Thus the free wealth, accumulating on the unbound agent, scales with N . Thus a thermodynamically measurable (macroscopic) amount of wealth condenses onto a single agent.

To see this behavior at finite times, we expect to see a thermodynamically signif-

icant amount of wealth condensing onto a thermodynamically insignificant number of agents. Thus, we if we plot the normalized cumulative wealth $W(x)$ in the system below a given rank x , wealth condensation means $W(x)$ is not smooth, but rather decreases very suddenly for small x .

6.1.5 Measuring Inequality

Here we consider metrics which asses the inequality in the asset exchange system. An easy form to measure wealth inequality is to use an inequality function $\phi(w)$ applied to each wealth averaged over the system to create an inequality measure Φ :

$$\Phi(\{w_i\}) = \frac{1}{N} \sum_i \phi(w_i) \quad (6.32)$$

A good inequality function will increase whenever we increase the wealth difference between agents; we want a function ϕ such that if we transfer wealth from the poorer agent to the richer agent,

$$w'_p = w_p - \Delta w \quad (6.33)$$

$$w'_r = w_r + \Delta w \quad (6.34)$$

$$\phi(w'_r) + \phi(w'_p) > \phi(w_r) + \phi(w_p). \quad (6.35)$$

It turns out that this requirement is exactly that ϕ be a *convex function* of wealth. We give a short proof in the differentiable case: Suppose we exchange the wealth continuously over the course of a time interval. In an infinitesimal time, the wealth transferred, Δw , is infinitesimal. So, the inequality Φ changes by

$$\delta\Phi = \frac{\delta w}{2} \frac{\partial}{\partial w} [\phi(w_r) - \phi(w_p)] \quad (6.36)$$

For this to be true over the entire interval of the trade, we must have, for all $w_r > w_p$,

$$\phi'(w_r) > \phi'(w_p) \tag{6.37}$$

Since we want this property to hold for any (w_r, w_p) where $w_r > w_p$, this requirement is satisfied by any convex function ϕ : One which satisfies $\frac{\partial^2}{\partial w^2}\phi > 0$ over the appropriate interval, which in this case is $w \geq 0$.

6.1.6 Inequality evolution and Jensen's Inequality

Convex functions are often characterized by the fact that the function itself lies below the secant line between any two points. The secant line itself is a structure which gives the value of the weighted average of the function applied to the two points, where different points on the line are the result of different weightings. This statement can be generalized to higher dimensional structures—first two finite lists of points and then to probability distributions. These various generalizations are referred to as Jensen's Inequality [89]. The precise statement is that the expectation of a convex ϕ function applied to a random variable X is larger than the function of the expectation of X :

$$\mathbb{E}[\phi(X)] \geq \phi(\mathbb{E}[X]) \tag{6.38}$$

Consider, now, the change in inequality after a trade:

$$\Delta\Phi(\{w_i\}, \{\Delta w_i\}) = \frac{1}{N} \sum_i \Phi(w_i + \delta w_i) - \Phi(w_i) \tag{6.39}$$

In particular, if we consider the w_i all fixed and vary the Δw_i , $\Delta\Phi$ is a convex function of the Δw_i . This implies that the expectation of the inequality is nondecreasing in

time:

$$\mathbb{E}[\Delta\Phi] \geq \Delta\Phi(\{w_i\}, E[\{\Delta w_i\}]) = \Delta\Phi(\{w_i\}, 0) = 0 \quad (6.40)$$

In terms of inequality, then, the system must tend towards maxima. We can shed more light on this evolution more carefully by treating the components of Φ using stochastic calculus:

$$d\Phi = \mu_\Phi dt + \sigma_\Phi dt \quad (6.41)$$

By examining the evolution of the inequality Φ in this way, we can understand how Eq. 6.40 arises as a result of a result of the *mechanism* of the system—the trading rules. In order to understand the tendency of the inequality to increase or decrease, we need to have some understanding of the nonlinearity of the noise σ_Φ as the inequality increases. We aim to show that

$$\frac{\partial\sigma_\Phi}{\partial\Phi} < 0 \quad (6.42)$$

and

$$\mu_\Phi > 0 \quad (6.43)$$

for the microscopic fluctuations in Φ . Together these entail that Φ will tend to increase in time, and investigating how this arises will give us insight into how an asset exchange model produces inequality.

$$d\Phi = \frac{1}{N} \sum_i d\phi_i \quad (6.44)$$

$$= \frac{1}{N} \sum_i \mu_\phi dt + \sigma_\phi d\eta_i \quad (6.45)$$

$$= \frac{1}{N} \sum_i \frac{\sigma_{w_i}^2}{2} \frac{\partial^2 \phi_i}{\partial w^2} dt + \sigma_{w_i} \frac{\partial \phi_i}{\partial w_i} d\eta_i \quad (6.46)$$

If wealth B_{jl} is traded from trader l to trader j , this gives rise to

$$d\Phi = \frac{1}{N} \left(\frac{B_{jl}^2}{2} \left(\frac{\partial^2 \phi_j}{\partial w^2} + \frac{\partial^2 \phi_l}{\partial w^2} \right) dt + B_{jl} \left(\frac{\partial \phi_j}{\partial w} - \frac{\partial \phi_l}{\partial w} \right) d\eta_{jl} \right) \quad (6.47)$$

$$= \mu_\Phi dt + \sigma_\Phi d\eta_{jl} \quad (6.48)$$

This problem was tackled in the case of the individual agents by choosing a function χ which made the noise constant for the agent which was setting the bet. Let us make, for the moment, the assumption that $B(w)$ is an increasing function of w . This means that $\chi(w)$, through equation 6.6, is a naturally concave-down function which linearizes the noise in the poorer wealth. This gives a natural choice for the inequality function $\phi(w) = -\chi(w)$, Making this substitution, the fluctuation term due to the poorer wealth will be 1, and the noise becomes

$$\sigma_\Phi = \frac{B(w_p)}{B(w_r)} + 1, \quad (6.49)$$

where we have denoted the richer wealth of j and l of w_r and the poorer with w_p . If the inequality Φ increases due to this trade, then w_p decreases and w_r increases. Using the presumption that B is monotonic in w , we have that $B(w_p)$ decreases and

$B(w_r)$ increases, which implies that the noise decreases with increasing inequality, demonstrating equation 6.42. Likewise, the convexity of ϕ ensures that the drift term in equation 6.47 will also be positive, demonstrating equation 6.43.

Thus we see how the evolution of macroscopic inequality is connected to the microscopic betting system used by the agents: The function linearizing the noise of the agents also provides an appropriate measure of inequality.

What more can be said about the inequality in the system? The form of equation 6.47 suggests that the drift can be known more precisely if we can pick ϕ such that the quantity

$$\sigma_{\Phi} = B(w_j, w_l) [\phi'(w_j) - \phi'(w_l)] \quad (6.50)$$

is invariant as the wealth of the traders changes. Even if $B(w_j, w_l)$ only locally depends on the wealth of *one* of the agents (such as the poorer agent), it will not be possible to construct ϕ such that σ_{Φ} is constant for all *pairs* of wealths; Even if σ_{Φ} is locally flat around some pair (w_1, w_2) , it will not be flat around $(w_1, w_2 + \epsilon)$, because ϕ must be strictly convex in order to be a well-formed inequality measure. Essentially, there are not enough degrees of freedom in ϕ to linearize the noise in Φ , which is inherently depends on both w_1 and w_2 even if the betting function reduces to a function of only one wealth. This entails that although a functional form such as Φ may be a good way to *measure* inequality, it is not easy (and may not be possible) to construct a generic Langevin equation which describes the evolution of the inequality in time; Φ functionally depends on the wealths as standalone objects as an inequality, but its evolution is tied to the pairs of wealths and thus to nonlocal qualities of the wealth distribution.

Supposing that the betting function is *not* strictly monotonic, how should we construct our inequality function? In this case, the bet is not necessarily determined

by the poorer agent, so let us rather refer to the agent with the lower betting function as the *controlling* agent of the bet. Let us divide the betting function into monotonic intervals, labeling the betting function in each i^{th} interval B_i . Define $\frac{\partial^2}{\partial w} \phi_i = |B'(w)|/B(w)^2$; when $B(w)$ is increasing, use $\phi_i = -\chi_i$, and when it is decreasing, adjoin it with $\phi_i = \chi_i$, using the freedom of the additive constant in χ to make ϕ continuous. In this way, $\phi(w)$ will be entirely convex, with inflections which occur at the ends of the intervals.

We find that the drift function μ_Φ is identical to equation 6.47 and therefore positive. Equation 6.50 will be given by the rather cumbersome expression:

$$\sigma_\Phi = B(w_j, w_l) \left[\frac{\text{Sgn}(B(w_j))}{B(w_j)} - \frac{\text{Sgn}(B(w_l))}{B(w_l)} \right] \quad (6.51)$$

The analytic expression for the derivative $\partial\sigma_\Phi/\partial w_i$ is even more cumbersome and not in itself particularly illuminating. The expression for ϕ is constructed so that there is no contributions to $\partial\sigma_\Phi/\partial\Phi$ for the motion of the *controlling* agent, however, the contributions from the non-controlling agent can be positive, depending on the form of $B(w)$, if either of the agents are in a region of decreasing B . So, the proof that $d\sigma_\Phi/d\Phi < 0$ falls apart, and it is no longer clear how macroscopic inequality is generated from microscopic rules.

6.1.7 Drift Terms, Growth, and Trade bias: Condensation stability

The framework above also gives an method of determining whether or not an asset exchange model breaks wealth condensation, either partially or totally.

Partially broken condensation, as in chapter 4, requires that the poorest agents remain afloat. In this case it is required that the growth terms the *typical drift* as the poorest agent approaches zero wealth. In the case of an external growth term

μ_g , the typical decay can be extracted from section 6.1.2:

$$\mu_{typ} = \mu_g - \frac{1}{2}B(w)B'(w) \quad (6.52)$$

The result is natural: Each category of condensation rate requires a growth rate which matches the strength of the decay rate near zero. Sublinear zeroes require very little external growth to prevent bankruptcy of the poorest agents.

Linear zeroes such as the YSM require a growth term which satisfies $\mu_g > \frac{1}{2}\alpha^2 w$; the growth may vanish as the wealth vanishes, so long as the growth vanishes more slowly.

Superlinear zeroes, however, can only break wealth condensation if the external growth is nonzero even when the wealth is zero; because agents will risk their entire wealth at some given point of impoverishment, the poorest agents will require finite growth just to stay active in the system.

As a further generalization, it is interesting to consider asset exchange models where the trading is biased towards either the poorer or the richer agent. Using the framework described here, the appropriate bias can be inserted into the drift term of the Itô calculus, and the dynamics analyzed in a similar fashion.

6.1.8 Example system simulations

We give examples of the behavior described by implementing three models: the critical model (the yard sale model), a super-linear model (fast condensation), and a sub-linear model (slow condensation). The models can be parameterized by q into the form:

$$B_q(w) = \begin{cases} \alpha w^q & w \leq 1 \\ \alpha w & w > 1 \end{cases}, \quad (6.53)$$

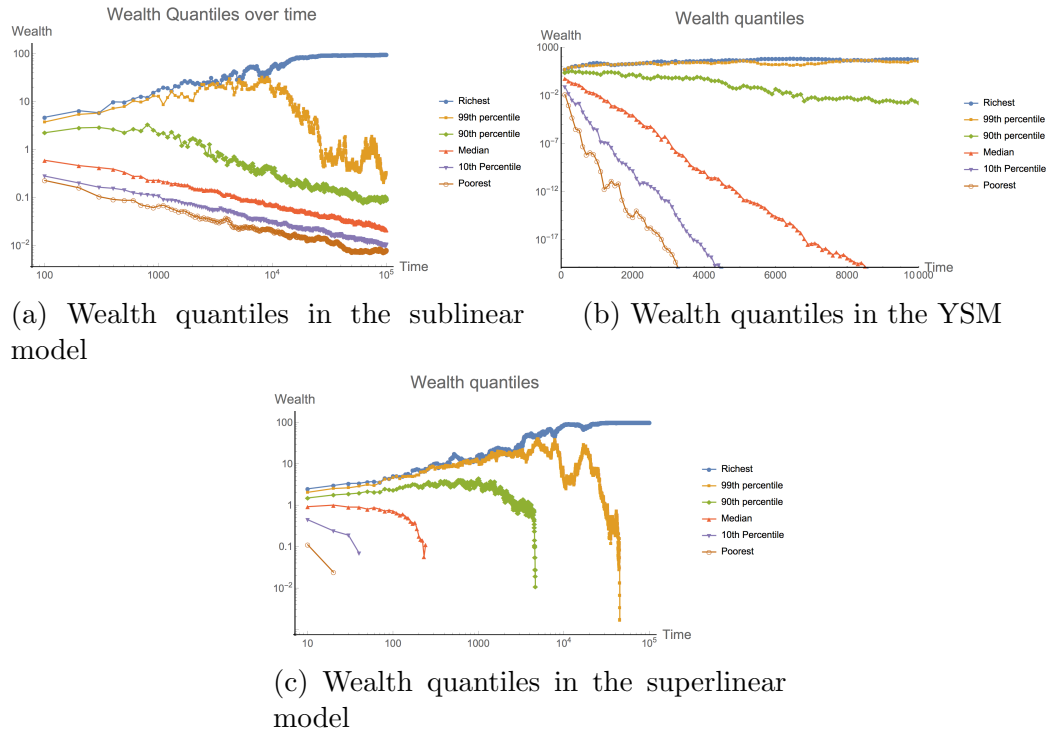


Figure 6.5: Wealth quantiles versus time for various types of wealth condensation. The simulations use $N = 100$ agents and a trading parameter $\alpha = 0.1$. Note the differing axes scales for the different behaviors.

We run simulations for $q = 0.5, 1, 2$, corresponding to fast condensation, the yard sale model, and slow condensation respectively, and using $N = 100$ agents and $\alpha = 0.1$. Figure 6.5 shows the quantiles of wealth for the various models. The slow condensation model generates wealths which decay in time with an exponent of roughly $-1/2$; the wealth in YSM agents decays exponentially in time; and the agents in the fast condensation fall to exactly zero wealth over the course of the simulation. Likewise, figure 6.6 shows the number of active agents in the system above a very small wealth threshold; From this we see the expected fast rate for the fast model, an interrim rate for the YSM, and that in the slow condensation model, agents do not fall to numerically unmeasurable values of wealth in the simulation time frame.

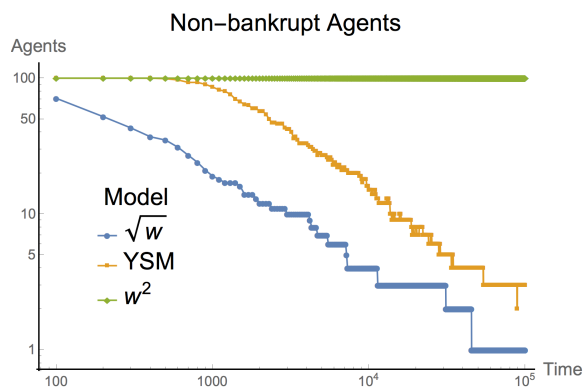


Figure 6.6: The number of nonbankrupt agents (those whose wealth exceeds 10^{-5} times their initial wealth), plotted for the various models implemented.

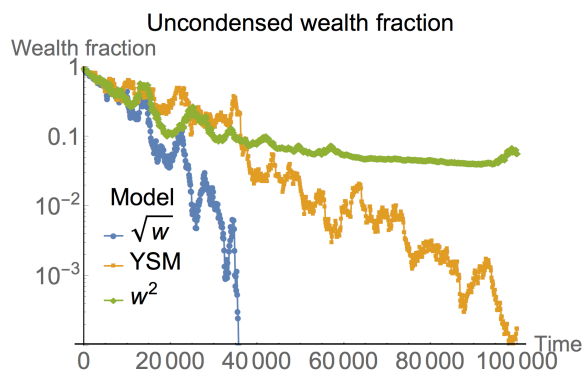


Figure 6.7: The fraction of the wealth not held by the richest agent in the system; In all systems this becomes small, however, the class of model determines the rate at which the condensation occurs.

Chapter 7

Concluding remarks and further directions

So ends our journey through extensions to the yard-sale model. Although there are many technical results which are of some interest when examining the model in careful detail, here I give a condensed set of the most important conclusions in this dissertation with special attention to the contextual importance within the related work outlined in the introductory chapter.

7.1 The Yard-Sale Model

In chapters 2 and 3, I analyze the Yard Sale Model (YSM). As an asset exchange model (AEM), the YSM differs from traditional economic models of wealth and income in that transitions are made by way of interactions with other agents; the distribution of wealth is not externally imposed but internally generated by the model. The key difference between the YSM and many other AEMs is that transactions are limited to the scale of the poorer agent's wealth. This is a key physical assumption which reflects the inability of a poor agent to spontaneously grow by many orders of magnitude in a single transaction.

The YSM results in wealth condensation, where the richest agent continually accretes all of the wealth in the system. This is found to be a result of the Itô drift associated with the nonlinear character of fluctuations in the YSM. This is similar

to the St. Petersburg Paradox [90], the poor agent is exponentially unlikely to gain wealth, but the amount of wealth gained may be exponentially large. This effect is in proportion to the number of agents which are richer than the agent of interest, and so it is proportionally smaller on rich agents. The longer a system is run, the larger the inequality in the wealth distribution. I thus characterize the YSM as a non-ergodic system, and quantify this using the TM metric for effective ergodicity. This non-ergodicity can be ascribed to the Itô drift in combination with open boundary character of the phase space; drift encourages poorer agents to lose wealth, and multiplicatively speaking, there is always room for them to do so. This is in contrast to the classical model of Champernowne [39] and similar models in the lineage of Kesten [52] that incorporate lower-boundedness, which prevents the collapse of the wealth distribution.

The YSM also exhibits power-law scaling for a number of quantities. Of foremost interest is the Pareto exponent, which for the bare YSM is asymptotically zero, which is far *more* unequal than is observed in typical empirical data. This is a result of the diverging inequality. It is related to the result that YSM suffers a breakdown in *mobility*, as evidenced in the rank correlation function. This shows that the non-ergodic wealth transfer mechanism applies to every strata in the wealth distribution, so that all agents become separated from each other as time goes on—inequality increases between every combination of agents in the YSM.

Further developments focus on the development of effective dynamics. The Itô drift gives rise to a characteristic timescale of the YSM which is proportional to α^{-2} , where α is the trade fraction parameter, and this manifests in many measurements, including the the condensation fraction, the bankruptcy rate, and the economic mobility.

I write the mean-field version of the wealth transfer mechanism in the YSM, which I called here “Mean Trade” (MT) theory. In the MT, I find that the effective wealth transfer between rich and poor can be succinctly expressed in the cumulative distribution of the wealth, which solves the dynamics of the mean-field version of the Itô drift, and allows for simple incorporation of growth into the model.

The MT also bridges the gap with non-interacting models of the economy by allowing one to predict the behavior of single agents with a minimal number of variables, explicitly eschewing detailed knowledge of the distribution of wealth. The MT formalism shows that approximately speaking, the dynamics of an individual agent can be represented in terms of that agent’s current wealth as well as the rank of the agent in the economy. Thus, the YSM as a statistical mechanical model has two relevant parameters for any given agent, the wealth and the rank.

I furthermore show that the MT is also the first term in an infinite series expansion of a complex integro-differential equation describing the YSM in terms of its kinetic equation. Although solutions to the full equation appear difficult, each term can be written in closed form. This provides a starting point for further analytical analysis, such as evaluation of the error involved in the MT approximate theory.

7.2 Extending the Yard-Sale Model with growth:

This work extends the YSM with growth of two forms. The first is arithmetic (constant in time), and the second is geometric (exponential in time).

7.2.1 Arithmetic growth

Uniform arithmetic growth is characterized by a single growth rate parameter. We find that the growth rate is equivalent to an initial condition on the total wealth. The

long term wealth distribution is independent of this initial condition, except for the wealth of the richest agent. This is remarkable in itself because it means that in the long time limit the YSM with uniform arithmetic growth is exactly as parsimonious as the original YSM, effectively having no more tuning parameters.

The system acquires a steady state in a time-scale which depends on system size—a quasi-steady state—which starts with the wealth of the poorest agents, and propagates upwards rank-wise to the richest agents. The steady state has a form which is reminiscent of real economic data; the rich segment of the economy has a power-law distribution of wealth, and the poor segment is concentrated together. The size of the poor segment, and thus the overall scale of the wealth distribution, is set by α^2 . However, the Pareto index of the distribution is approximately $1/2$, which is a stronger inequality than exhibited in real-world data. Both the Pareto exponent and the scale of the poor agents are explained by the MT effective theory.

Mobility in the arithmetic growth model is highly rank-dependent, with wealth agents being less mobile. The mixing time scales up with decreasing trading fractions. For large α , the poor segment of the economy can mix in only a few trade steps. For small α , the rich agents can take tens of thousands of trades to mix with the bulk of the economy.

The TM metric shows that the richest agent, which absorbs the growth in the system, gives rise to a non-ergodic system. For a finite system, the metric applied only to the rest of the agents indicates that over long times, the system is effectively ergodic, in line with the rank-rank mobility data.

7.2.2 Geometric growth

Geometric growth is given by a rate which changes multiplicatively in time. For uniform growth, this gives rise to a *rescaled steady state*, where wealth is steady-state when rescaled by the factor $e^{\mu t}$. The distribution of rescaled wealth is given by a dimensionless parameter α^2/μ . The steady state is ergodic: Wealth condensation is totally broken by geometric growth. When the inequality is low, the wealth distribution is approximately normal. For high inequality, the form of the wealth distribution is a *shifted* power law—a power-law with a finite cutoff—that is predicted by the MT theory. The form of the wealth distribution, similar to arithmetic growth, is reminiscent of real wealth distributions, but not identical to them. An exhaustive search of the parameter space might identify some regions where the model feasibly fits data, but this would require fine tuning.

Also explored is a non-uniform distribution of growth, where richer agents are able to use their capital to generate wealth more quickly. This is accomplished using an inequality parameter γ by apportioning the exponential growth among the agents in proportion to their wealth to the power of gamma. When $\gamma = 0$, the original uniform growth is recovered. Increasing values of γ lead to increasing inequality of the wealth distribution. A steady state is maintained until $\gamma = 1$ (the point where growth becomes proportional to wealth), whereupon the steady state disappears, and wealth condensation is restored. This phase-transition-like behavior is associated with a divergence of the steady-state time, the wealth inequality, the mobility, and the mixing timescale of effective ergodicity. These divergences have a power-law form which is reminiscent of second order phase transitions. We show that the form of the wealth distribution obeys a scaling relation. Both the form and the scaling can be predicted by the MT theory. The form is given by a power-law with a finite upper

cutoff, similar to the uniform growth case, but with variable Pareto index. The index shrinks to zero as the transition is approached, and the system returns to a wealth condensing state.

Although the system is effectively ergodic below the condensation transition, the mixing time diverges quite rapidly. This leads one to ask whether or not it is important that mixing times are related to human timescales. A system which is formally ergodic, but only on the scale of centuries, will not appear ergodic to agents which live in human timespans.

There is a duality of the geometric growth model with a wealth tax model; the wealth tax model is identical to the growth model after rescaling. This implies that the two models can be mixed together by appropriately combining parameters.

7.3 Extensions to generalized trading schemes

The final extension considered to the YSM is to modify the trading scheme. This is done to investigate the universality of the dynamics of the YSM. This is accomplished by examining a more generalized *betting function* which allows the wealth set forth for trading to be an arbitrary function of an agent's current wealth. In this framework the YSM has a linear betting function. By analyzing repeated transactions between two agents as a stochastic process, we find that exchange between agents can be written as a potential function with diffusion terms, much as in a Fokker-Planck equation.

Wealth Condensation behavior is tied to the fairly natural assumption that the only zero of the betting function is at a lower bound on the agent's wealth. Condensation is direct (i.e. there is no metastable state before condensation) if the betting function is monotonically increasing. The long-term rate of Wealth Condensation

is tied to the form of the betting function near zero. Sub-linear (conservative) betting processes result in a *slow condensation*, exhibiting power-law dynamics in time. Super-linear (aggressive) betting processes exhibit *fast condensation*, where wealth condenses onto a single agent in finite time. The YSM is the critical dividing line between these cases, where condensation trajectories are exponential.

7.4 Future directions

The Pareto index is the most intriguing empirical observation in the study of wealth and income distributions, and it is typically in the range of 1 to 3. The findings here indicate that external growth in YSM leads to a typical index of 0.5. Further work on asset exchange models would do quite well to seek a model with a natural index in the typical range for real economies. The difficulty here is to find models which give rise to such an index naturally, that is, without fine-tuning model parameters. Furthermore, extensions should keep in the statistical mechanical spirit of the YSM: they should represent a microscopic process that agents undergo in the economy. The MT theory demonstrates that these interactions are likely to be approximately solvable if they are in some way a function of the agents' ranks.

Potential modifications to the bare YSM may include a notion of trading rate attached to different wealths or ranks, or the notion of connectivity between agents of differing wealths.

The form of growth considered in this dissertation is an as an external process which influences agents individually. It also would be interesting to consider economic growth which is the result of transactions, that is, some rule which allows the total wealth after agent exchange to actually be larger (or smaller) than before. Depending on the form, such a growth may give rise to an effective version of the growth functions

used here, or it may give rise to a new phenomena. Another thing to consider is that the skewed geometric growth given here has a constraint on the total growth, which is then portioned out to agents. This fixes the overall system to mimic real economic data, but it could prove useful to write down growth whose total value is not externally constrained, but rather emergent-generated within the dynamics of the system.

Likewise, alternative taxation systems can be considered. The taxation herein is a wealth tax. One alternative is redistribution which originates from transactions, similar to a sales tax. Another would be redistribution of earned wealth over time, i.e. an income tax.

Other novel couplings to the YSM might include the incorporation of social institutions. For example, an unemployment support scheme which prevents agents from bankrupting, but does not act on richer segments of the economy. There is also a body of work related to agent-based simulation of markets [18, 91]. It may be interesting to consider a hybrid YSM and market model, which incorporates the effects of individuals trading with pools and with individuals.

The difficulty in extending theoretical models is the draw towards complexity. It is quite simple to write models which are completely intractable. In other cases, complex models are tractable but uninterpretable, as they have many more parameters than can be actually measured. Even the purely theoretical analysis of a model is very difficult when there are many parameters. This means that regardless of the direction of further work, it should focus on models which have an interpretation of a known economic interaction. The models should contain a few parameters at most, and the parameters should be readily interpretable. Furthermore, the aim should be to explain empirical observations, such as the appearance of Pareto exponents

without fine tuning.

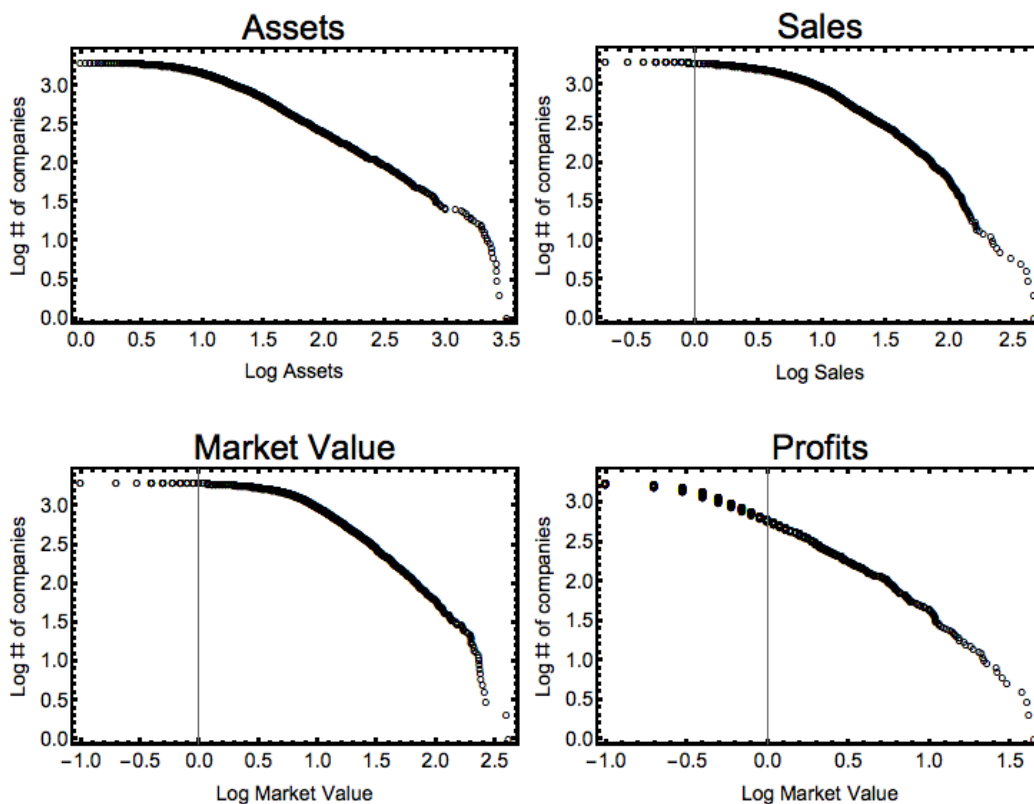


Figure 7.1: The 2013 Forbes Global 2000 dataset. Ranked plots of Assets, Sales, Market Value, and Profits given in billions of dollars. The Assets and Market Value plots show strong evidence of an upper cutoff to pareto behavior.

From an empirical standpoint, it is interesting that the growth models in this dissertation lead to a power law with a cutoff which is dependent on the growth, trade, and inequality parameters. Many physics models result in power-law distributions with exponential cutoffs, but the economic literature predominantly imagines Pareto behavior as having no cutoff. It would be useful to do some careful statistical work to determine whether or not there is an upper cutoff to Pareto behavior. This kind of behavior can certainly be seen for some datasets: shown in Fig. 7.1 are data for the year 2013 Forbes Global 2000 list of largest public companies [92]. This list

is constructed by using a combination of company assets, sales, market value, and profits over the year. Strong evidence of upper cutoff behavior is visible for plots of company assets and market value, and possible evidence is visible in company profit. While distributions of sales and profits do show some turnover in the upper ranks, it is not large, and may be due to statistical fluctuations. This tantalizing data indicates that further, more comprehensive statistical analysis should be carried out both for this data and other datasets.

Chapter 8

Part II: Inferring low-dimensional microstructure representations using convolutional neural networks

Chapter Abstract I apply recent breakthroughs in computer vision and machine learning to a central problem in materials informatics: The statistical representation of microstructural images. I present dimensionality reduction on a set of related texture images through a two-step process which involves high-dimensional characterization of the textures of using a pre-trained convolutional neural network, and low dimensional embedding of the results using manifold learning. I demonstrate that the low-dimensional embedding faithfully captures the relevant parameters of the input image set, and demonstrate superior fidelity when compared to the commonly used spectral representation of microstructure.

8.1 Introduction

An central outstanding problem in materials science is the characterization of materials microstructure. Microstructure is generated by non-equilibrium processes during the formation of the material, and plays a large role in the bulk material's properties [93–97].

In recent years, machine learning and informatics based approaches to materials design have generated much interest [98–100]. These frameworks are powered by

quantitative representations of materials, and so effective statistical representation of microstructure have become a central problem [96, 101–103].

The standard approach [101, 104–107] to characterizing microstructure are based on n-point correlation functions, and is typically restricted to pair correlations. Pair correlations are essentially capable of assessing the scale of domains in a system, but do not capture complexities such as the relative shape or relative orientation of nearby domains [106, 108, 109]. However, three-point functions (and their successors) are generally computationally infeasible approaches to capturing a texture. Instead, many approaches involve engineering a set of modified two-point functions to better capture certain microstructural features [106, 110–112].

Machine learning approaches to computer vision have developed extensive technology for the purpose of automated analysis of image content [113–117] and texture reconstruction and modeling [118–124]. I present a new framework for characterizing materials microstructure based on state-of-the-art convolutional neural networks [125] (CNNs). As a test of its capability, I demonstrate that it produces low dimensional representations of microstructure manifolds which are superior to traditional methods based on pair correlations.

I use the CNN feature vector introduced by Gatys *et al.* [118, 119] as a rich characterization of texture images. The feature vector synthesizes stunningly accurate resampled materials micrograph images, see figure 8.1. This can be attributed to the hierarchical and non-linear aspects of a CNN, which are capable of describing higher order dependencies in the data which are not available to two point correlations.

As a framework for the characterization of microstructure, I demonstrate that for an ensemble of similar images, this CNN vector is ripe for embedding into low-dimensional spaces to characterize textures; the latent variables which are used to

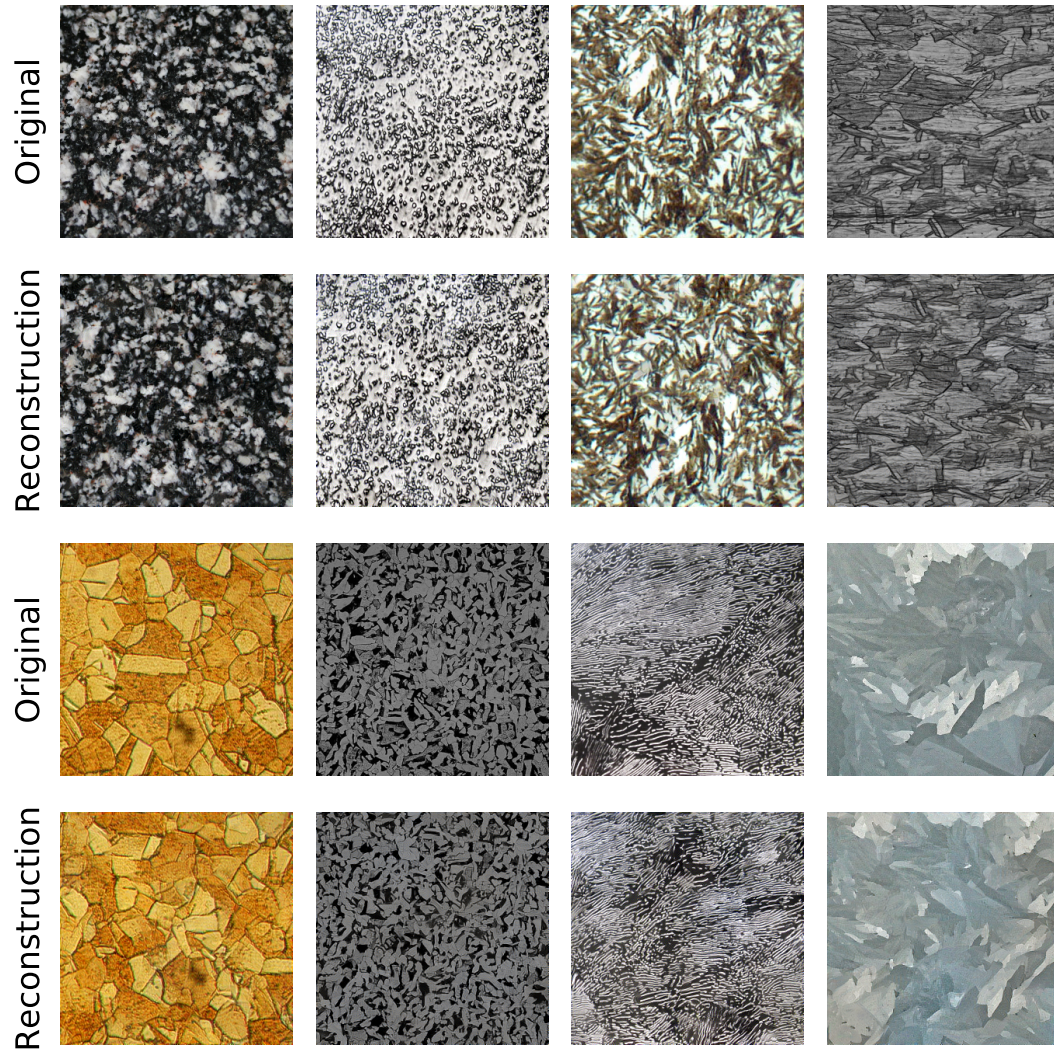


Figure 8.1: Texture synthesis of materials microstructures using the CNN texture synthesis algorithm of Gatys *et al.* [118] The algorithm synthesizes each image by characterizing a single sample.

generate images are the primary sources of variation in the low-dimensional representation, and the correlations between the generating and CNN representations are robust even in the presence of noisy, varied patterns.

I establish these characteristics in an unsupervised learning context—the algorithm does not need to be guided by targets—and on small data sets. These are very desirable properties for further informatic analysis, such as regression between materials microstructure and materials properties or processing techniques. It is particularly important to generate high-quality low dimensional features for materials analysis because generating new samples is an expensive process, and I anticipate that this framework will provided an excellent basis for design of high-performance materials.

Our approach exemplifies a technique from Machine Learning known as *transfer learning*, wherein the data processing capabilities developed in one machine learning effort are used to boot-strap the capabilities of another. Here, the neural network is trained on the task of classifying a database of a million natural images into a thousand classes [126]. I are thus leveraging the power of deep learning on very large, high-dimensional datasets to generate an appropriate framework for the processing of small, high-dimensional datasets. This leveraging is not without a cost—this methodology is limited to the domain of the origin network, in this case two-dimensional RGB channel images.

8.1.1 Structure of this chapter

The remainder of the paper is organized as follows: Section II gives background on CNNs for image recognition. Section III details our methods for image ensemble analysis, and Section IV demonstrates the results of these methods on test datasets. Section V discusses the primary reasons for the success of this approach, and Section

VI offers some concluding remarks and directions for further research.

8.2 Background

8.2.1 Convolutional Neural Networks for image processing

Convolutional Neural Networks have emerged in recent years as state-of-the-art systems for computer vision tasks [113–117]. They form a modern basis for image recognition and object detection tasks [126], and in some cases now outperform humans [117, 127].

The basic computational structure is that of a deep neural network (for a brief overview, see Ref. [125], for comprehensive text, see Ref. [128]). These networks consist of layers of artificial computational units called neurons. The neurons are fed weighted inputs and compute a simple nonlinear function (known as the activation function) of those inputs, and pass that output as input to further neurons in the network. The weights and parameters of the activation function can be tuned in order to adjust the behavior of the network. Deep structures include many layers, allowing for the network to perform complex data processing tasks. In the common supervised learning framework, the network is trained to perform a task by being shown input data with a desired output, and the network is trained to produce the correct output by some variation on gradient descent.

Image recognition tasks require an algorithm to analyze very high dimensional datasets. Furthermore, the relevant information in the image is hidden in the complex correlations between the pixels, which give rise to the shapes and textures of the objects to be recognized. However, CNNs are particularly suited to analyzing this type of data by encoding the concept of locality into the neural network. Natural images often have features which are stationary with respect to translation, meaning

that many patterns which appear in a given image are likely to recur in the same image or a different image at a different location. By convolving the image with a filter, one can identify the locations in an image which correspond to a given local correlated pattern. The CNN is a neural network whose neurons consist of stacks of nonlinear convolutional kernels, which are scanned across the image, forming a higher-order image plane whose channels constitute the features of the image in that region. Also commonly introduced is a pooling operation, which coarse-grains the image plane. By interleaving convolutional and pooling layers, CNNs are able to develop features which incorporate complex correlations over large scales. These complex features encode relevant information about the content of the image as information about large regions, and can be fed into classification architectures. In addition, CNNs can be thought of as a regularization via parameter sharing—adding the appropriate constraints to a fully connected network based on locality greatly decreases the number of parameters in the network.

8.3 Methods

8.3.1 Baseline method: Power spectrum for texture characterization

As a baseline for texture characterization, I use the power spectrum (PS), which measures the two-point correlations in the image. I use grayscale (single-component) images, corresponding to a single scalar field referred to as ϕ . The two-point correlation function of the order parameter is

$$P_2(\Delta\vec{x}) = \int \phi(\vec{y})\phi(\vec{y} + \Delta\vec{x}) d\vec{y}. \quad (8.1)$$

The structure factor or power spectrum $S(\vec{k})$ is the Fourier transform of P_2 , which can be expressed in terms of the Fourier representation of the order parameter, $\tilde{\phi}(\vec{k})$

as

$$S(\vec{k}) = \phi(\vec{k})\tilde{\phi}(-\vec{k}). \quad (8.2)$$

For this analysis, I compute the structure factor after normalizing the datasets with the mean of ϕ to zero, and the range from -1 to 1 .

8.3.2 CNNs for texture characterization

Intermediate representations of a neural network can reveal the hierarchy of features learned by the network [129, 130]. Gatys et al. [118, 119] have developed a robust algorithm for texture synthesis by using the statistics of the activations in intermediate layers of a CNN as a feature vector. Examples of the algorithm applied to create synthetic versions of materials microstructure are shown in Figure 8.1.

They construct a feature vector as follows: Suppose we desire to construct a texture vector out of the intermediate activations on layer l . They will consist of a bank of features across a hyper-image planes. We can then label the activation of the i th feature on the j th pixel of the hyper-image plane F_{ij}^l . This object is equivariant with respect to translations in the source image plane—a suitable translation can be performed by translating the filter bank in the same direction. To construct a texture vector, one desires an object invariant to translations in the image plane—this can then be constructed by any suitable summary statistics of the F_{ij}^l over the image plane.

For the construction of a texture vector, we use the Gram matrix summarizing the correlations between feature i and feature k :

$$G_{ik}^l = \sum_j F_{ij}^l F_{kj}^l \quad (8.3)$$

The inclusion of the correlations between features greatly increases richness of the

representation. It is also a logical with respect to the architecture of the CNN—the weight structure of neural networks dictate that individual features need not carry meaning directly, but rather combinations of the features, which are selected by deeper layers for further processing. Thus it is desirable to construct a summary statistic which considers correlations between features. The Gram matrix is then viewed elementwise as a layer-wise texture vector \vec{G}^l for the purposes of further analysis by treating the matrix elementwise.

For the purposes of texture synthesis, Gatys et. al introduce a scalar, positive-definite loss between two images x and x' with Gram matrices \vec{G}^l and \vec{G}'^l :

$$L^l(x, x') = \frac{1}{A_l} (\vec{G}^l - \vec{G}'^l)^2. \quad (8.4)$$

$A_l = 4N_l^2 M_l^2$ is a normalization factor for the loss on layer l with N_l features and M_l hyperpixels. The factor 4 was introduced for convenience of the expression for the derivatives used in their optimization.

I use the square root of this loss function for the comparison of similar textures, introducing a distance matrix d_{ij} :

$$(d_{ij})^2 = \sum_l w_l L^l(x_i, x_j) \quad (8.5)$$

where w_l is a weighting factor for each layer. In this work, I use the same normalized version of the VGG network [115] used in [118,119], using layers “conv1_1”, “conv2_1”, “conv3_1”, “conv4_1”, and “conv5_1”, with equal weighting for each layer.

It is notable that there are several free parameters in this which may subtly modify this process, of which the layer weighting is only one. For example, one might also scale the activations within the layers according to the mean activation strength on each layer, either individually according to each image or over the set

of images. Dissimilarities can be generated using a variety of norms, such as L^p norms or cosine distances. The conventions used here define a Euclidean distance over the features, which ensures that a set of N images can be embedded into an N -dimensional euclidean space.

8.3.3 Manifold Learning with Multidimensional Scaling

To assess the quality of the texture vectors for characterizing images, I perform unsupervised dimensionality reduction—manifold learning. The goal of manifold learning is to find a low-dimensional structure which represents the data.

Because the dimensionality of the texture vector is large (roughly $k \sim 2^{18}$ or 2.5×10^5), one desires to work with methods which do not scale poorly with respect to the number of input features. Multidimensional scaling [131–133] (MDS) is well-suited to this task, as it minimizes a reconstruction objective on an $N \times N$ distance matrix over the data set. I factor out the stage of the problem which scales with k by computing the distances between data points in the high-dimensional space, and can then very quickly assess the ability of MDS to capture the structure of the data.

The goal of multidimensional scaling is to reproduce a distance (or dissimilarity) matrix over a dataset while embedding the data points in a low dimensional space. In particular, I use *Kruskal-Shephard* scaling, for which the objective is to minimize the *stress* S between the input distances d_{ij} and the embedded distances \hat{d}_{ij} :

$$S = \sqrt{\frac{\sum (d_{ij} - \hat{d}_{ij})^2}{\sum d_{ij}^2}} \quad (8.6)$$

MDS is conceptually simpler than many other nonlinear manifold learning schemes available, and its conceptual clarity aids us to better understand the morphology of the high-dimensional data being compared. The aim is not to produce the absolutely

most effective low dimensional basis for a specific manifold of images but to demonstrate the general viability of this scheme of microstructure data processing and pave the way for further work. I use the implementation of MDS found in scikit-learn [134] which seeks low-stress configurations by an iterative majorization algorithm [135].

8.4 Tasks

8.4.1 Image generation process

Microstructural evolution can be viewed as a process governed by low-dimensional latent generating variables (e.g. material composition, thermodynamic conditions during formation) which manifest in a high dimensional space by way of smooth, local noise.

As a prototype for microstructural analysis, I generate a synthetic dataset which factors into latent variables and noise. The latent variables govern the abstract qualities of the image, and when the noise vanishes, the latent variables define a unique image; A small number of variables sets the statistical qualities of the texture, but raw dimensionality of the resulting manifold of images is exponentially large.

I use the procedural texture generation method due to Perlin [136] known as *turbulence* to generate images conforming to this scheme. The turbulence patterns are constructed by generating a lattice of coordinate values, and distorting the values on the lattice using smooth multi-scale noise. A template function is applied to these distorted values to generate textures—in this case, a sine function with an angle and a scale parameter. By controlling the amplitude of the noise, one can tune the images from exactly periodic stripes to a noisy, marble-like pattern of stripes.

In this work I vary three generating parameters for the textures- the angle of the texture, the amplitude of the noise, and the scale at which the texture is viewed.

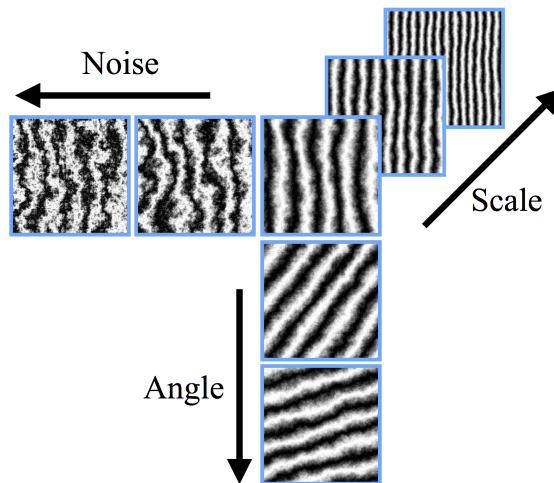


Figure 8.2: The space of synthetic textures, generated by three tunable parameters.

Figure 8.2 demonstrates these explicitly. I parameterize noise amplitude as relative to the stripe scale, as opposed to the pixel size, so that images with the same noise parameter but different scale parameters will appear visually to be the same pattern viewed from a different distance.

8.4.2 Angle reconstruction task

The first task is to reconstruct a manifold of images of fixed noise and stripe scale, but varying angle. For each trial, the stripe parameter was fixed to 15 (shown in fig.8.3). A number of images were generated by stepping the angles uniformly from 0 to π . I place the images on a manifold by computing their distance via the CNN procedure in section 8.3.2 and embedding the resulting distance matrix into a two dimensional space with MDS.

Even when the embedded manifold reflects the structure of the generating manifold very well, there are two things necessary to align them for quantitative analysis. The first is that the generating angle is periodic over the range 0 to π , whereas the embedded manifold places points over an angular range of 0 to 2π . Therefore

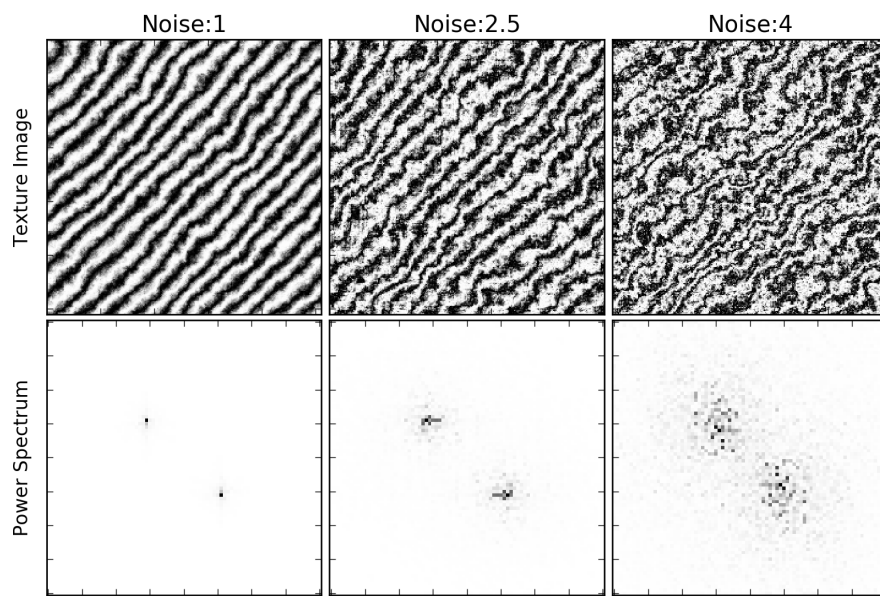


Figure 8.3: Samples images at different noise values. Top: Image textures. Bottom: Associated power spectrum, zoomed to show relevant area. For the purposes of this visualization, the power spectra images are increased in brightness by factors of approximately 2, 5, and 240, associated with the relative magnitude of their maxima.

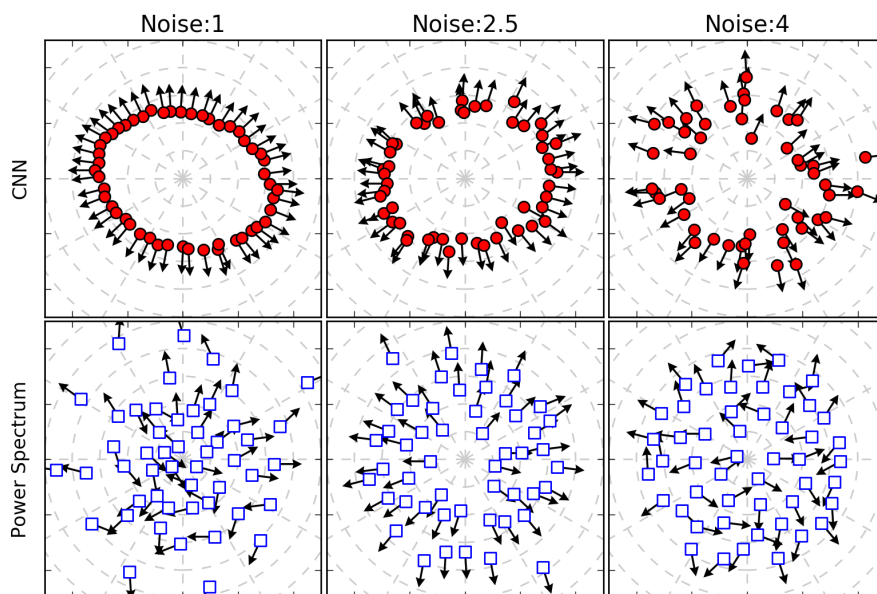
we double the generating angles to make the ranges commensurate with each other. Furthermore, the origin of the angular coordinates is not necessarily aligned. I rotate about the embedded manifold to maximally align it with the generating manifold using a least-squares procedure on the error between the generating and embedded angles.

Samples of this embedding procedure are shown in Figure 8.4 for ensembles of 50 images with varying noise.

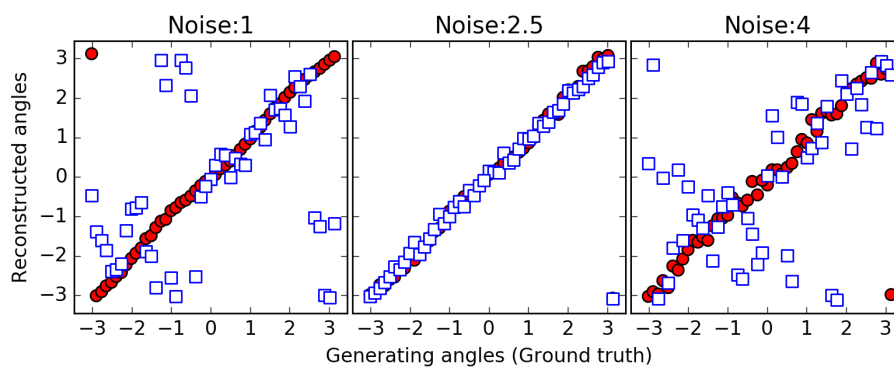
Quality of embeddings

Qualitatively, we find that the CNN reconstructions to be quite favorable to the spectral ones. For low noise, the CNN produces a continuous ring structure which reflects. The CNN representation is not perfectly rotationally symmetric, and so there is some bias in the reconstruction, evident in the skewed shape of the ring. As the noise is raised, the ring widens somewhat, however, the CNN performs well up across a large range of noise. The CNN is also very robust to small datasets. Conversely, the PS performs poorly for low and high noise values. There is a narrow band of mid-range noise amplitudes where the PS can perform comparably to the CNN, but only if it has access to a large number of images.

I quantify reconstruction error by measuring the root-mean-square deviation of the embedded angles from the target generating angles. (This is the quantity minimized when rotating the manifold.) The results are shown in Figure 8.5 for a variety of number of images, and a variety of noise values when generating the images. I note that for 5 images in the ensemble, (not shown in the figure to decrease clutter) the neural network performs just as well, but the spectral method performs roughly equally badly for all noise values.



(a) Visualization of target and reconstructed angles. Marks give the location of the reconstructed image, and arrows emanating from the marks indicate the generating angle for the image.



(b) Direct comparison of target and reconstructed angles.

Figure 8.4: The reconstructions of the angle image manifold (cf. Fig. 8.2) using the CNN and PS representations. CNN reconstruction (red filled circles) dramatically outperforms the PS (blue unfilled squares).

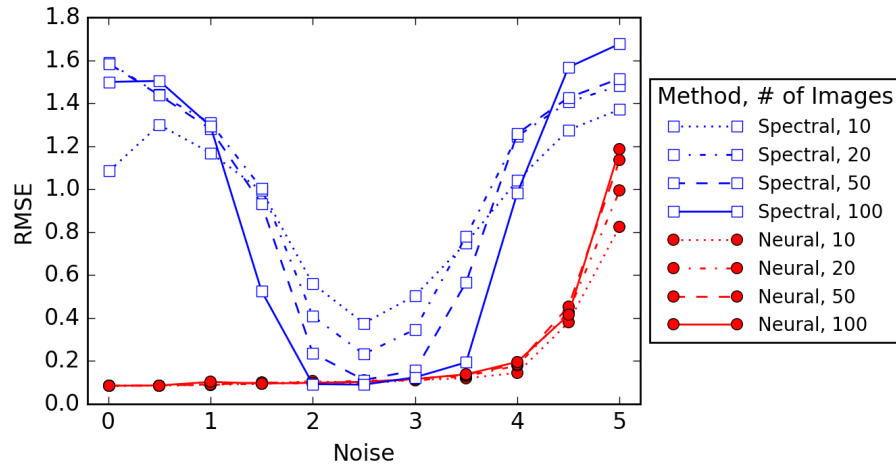


Figure 8.5: The reconstruction error of the angle reconstruction task as a function of noise. Each data point is an average over 100 trials.

The data shows that the CNN reliably reconstructs the image manifold regardless of the number of images in the manifold, and with a high degree of tolerance to noise. On the other hand, the power spectrum method is capable of reconstructing this manifold only for a window of noise ranges, and requires a much larger number of images to reach a high degree of accuracy.

Stress of embeddings

We can also assess the quality of the embedding procedure by examining the residual stress (Eq. 8.6) of the embedded configuration found by MDS, shown in Figure 8.6. The data indicate that the CNN texture vector, though of very high dimension ($\sim 2.5 \times 10^5$), can be captured much more effectively in two dimensions than the PS embedding.

The stress of the embeddings grows with the noise, and this is to be expected. With zero noise, the subset of images specified by this procedure is exactly a ring which can be embedded exactly into a two dimensional plane. However, adding the

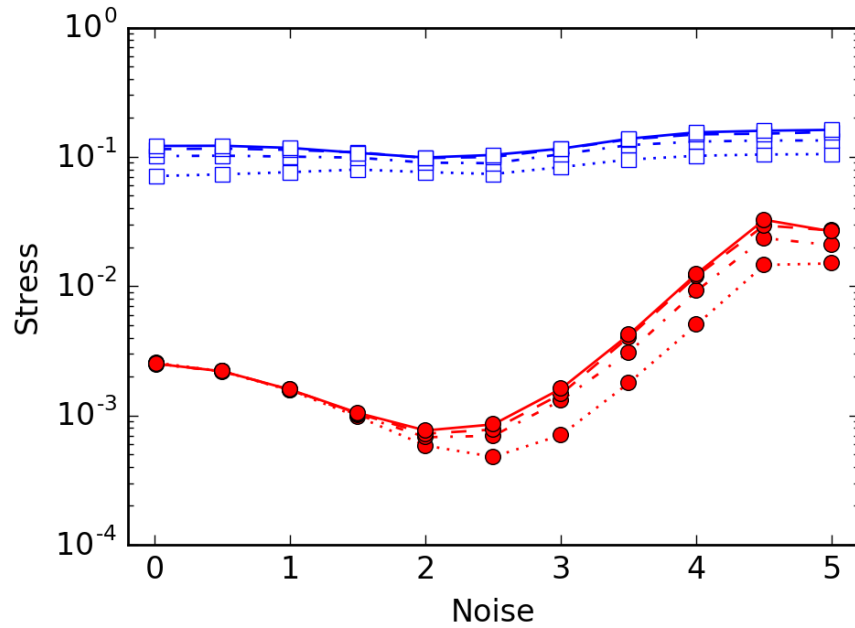


Figure 8.6: The MDS stress of the embedding into two dimensions for the angle reconstruction task as a function of noise. Markers are the same as in fig 8.5.

high-dimensional noise to the image perturbs this ring into a very high dimensional space. The phase space of the noise grows rapidly with its amplitude, and so a highly noisy image manifold has a very large volume. The CNN texture embedding is resilient to this noise, mapping two images with the same latent parameters to very similar texture vectors; in the CNN representation, the volume of space associated with different realizations of the noise is much smaller than the volume associated with angle. The power spectrum features, however, are quite susceptible to the noise (see fig 8.3), and thus the effective dimensionality of the power spectrum representation greater (cf. similar results in later section 8.4.3, Fig. 8.7).

8.4.3 Three dimensional manifold reconstruction task

The second task is the reconstruction of a 3-D manifold of images, of varying angle, scale, and noise parameters, each in 10 increments, for a 1000-image manifold. The angle parameter spans the gamot from 0 to π , the scale parameter ranges from 5 to 14, and the noise parameter varies from 0.5 to 2. As before, we determine the distances between images using the CNN texture vector and the power spectrum, and embed the resulting distances into a low dimensional space using MDS.

Stress of embedding

The embedding stress is shown as a function of dimension in fig 8.7. The data indicate that the CNN vectors can be more easily embedded into a much lower dimensional space than the spectral vectors.

The embedding stress of the CNN approach decays rapidly and roughly exponentially over the first few dimensions, implying that they capture a very large fraction of the variation in the data. As an unsupervised analysis, choosing the appropriate embedding dimension is not an exact science. While from an exponential standpoint, there are diminishing returns on embedding into any dimension greater than 3, it seems reasonable to choose an embedding into any dimension between 3 and 6 to produce good fidelity while minimizing the number of parameters used to describe each image.

The embedding stress of the spectral method, on the other hand, decays roughly as a power law. This implies that the intrinsic dimensionality of the space is very large, and the scale-free nature likewise implies that there is no natural dimensionality of the data in this representation.

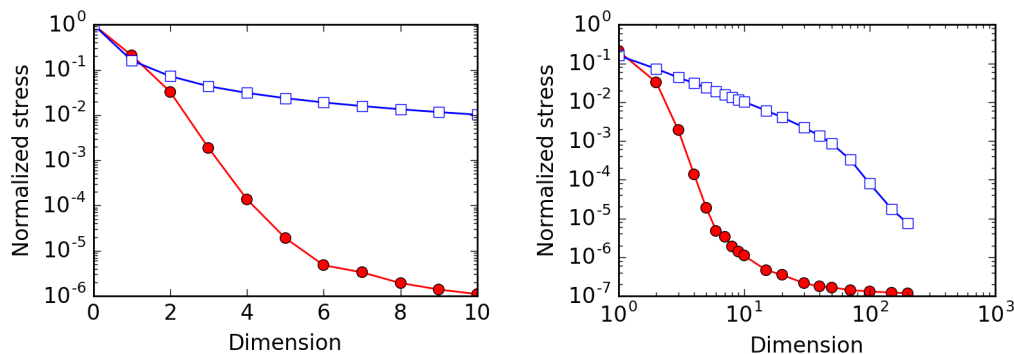


Figure 8.7: The MDS embedding stress for the three dimensional manifold reconstruction as a function of embedding dimension. Red: Using CNN texture vector. Blue: Using power spectrum. Left: Low-dimensional embedding highlights the approximately exponential gain in fit quality with dimension for the CNN method. Right: Higher dimensional embeddings demonstrate that the power spectrum cannot be easily embedded into a lower dimensional space.

Three dimensional embedding

Here, I present visualizations and explore the results of the embedding of the CNN method into a three dimensional space, matching the latent dimensionality of the images. The CNN embedding is highly structured with respect to the generating parameters. The manifold as a whole has a cone-like structure elucidated in Figure 8.8. The noise parameter varies roughly according to the depth from the outer surface of the cone, and the scale parameter roughly as an arc length away from the axis of the cone. Figure 8.9 shows the angular variable is distributed in sharp regions which are uniformly around a central axis, capturing the angular distribution of the images with very high fidelity.

Higher dimensional embeddings

The three dimensional embedding produces a coherent manifold which smoothly embeds the generating parameters, however, as indicated in fig. 8.7, the distance

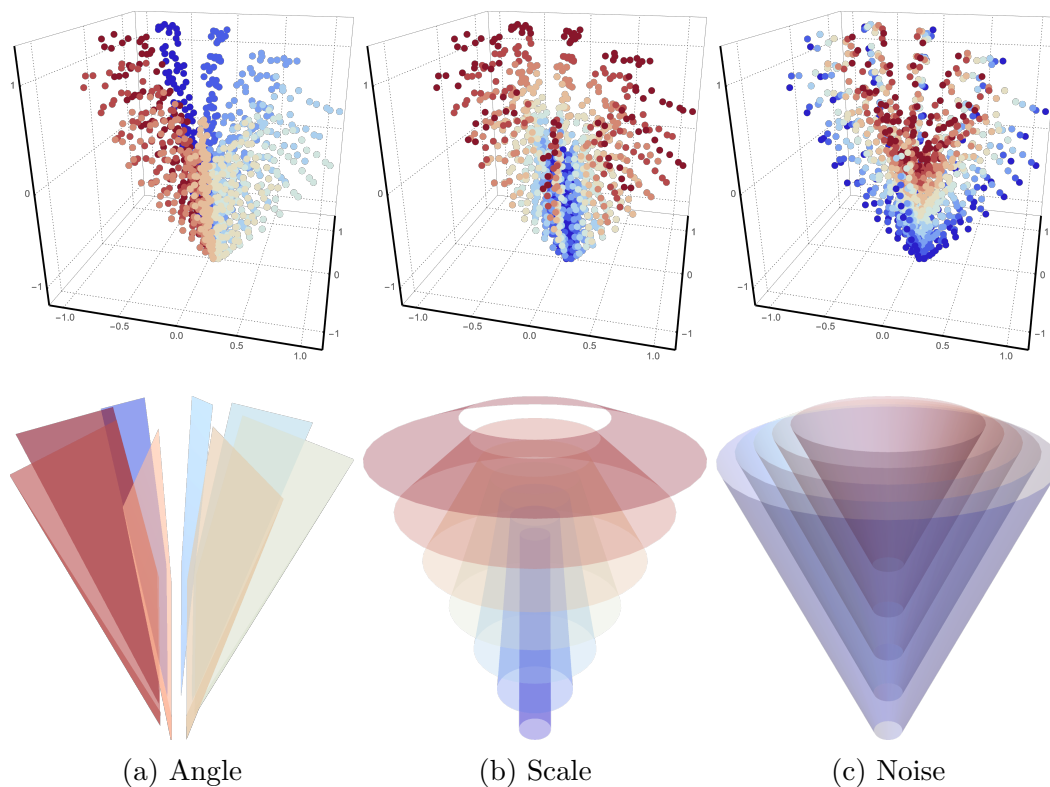


Figure 8.8: The three dimensional embedding of the three dimensional image manifold. The cone axis was manually rotated to align with the z-axis. Top: Views of the embedding colored by generating parameter. Bottom: Corresponding schematic representations of the manifold.

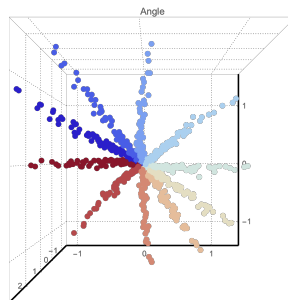


Figure 8.9: Axis-aligned view of the 3-D embedding colored by angle, demonstrating strong separation of images with differing angles.

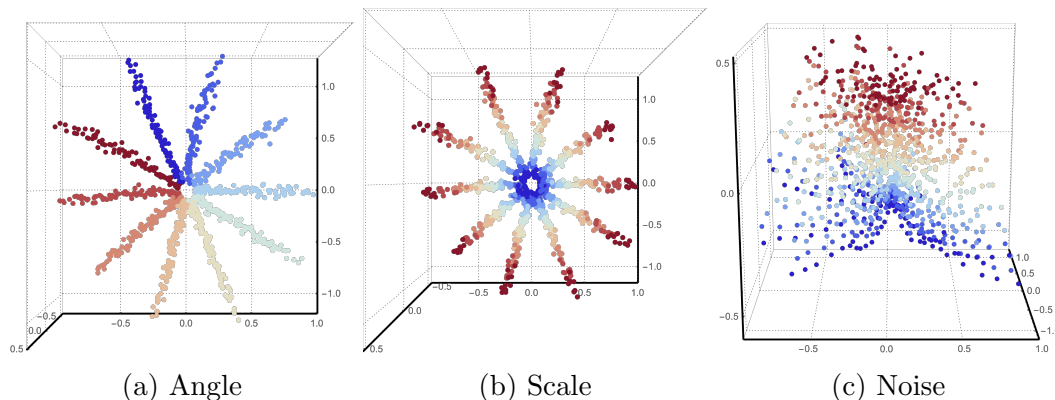


Figure 8.10: Images of the 3-D image manifold embedded into four dimensions; this is a particular linear projection of the data into three dimensions. This three dimensional projection coordinatizes the generating parameters in an approximately cylindrical coordinate system, where angle is mapped to the polar angle, scale is mapped to the radial variable, and noise is mapped to the longitudinal variable.

data can be embedded with exponentially smaller stress in four dimensions. With a higher number of dimensions, it is easier to find directions which represent the generating parameters in a regular fashion. Figure 8.10 shows a projection of this 4-D embedding into three dimensional space where the conic nature of the manifold is almost negligible, and the generating variable are approximately encoded as a cylindrical coordinate system.

CNNs invoke complicated nonlinear processing techniques which entangle information from the source image to produce their output. Though it is clear that the embedded manifolds are smooth, one may be interested in the type and extent of entanglement in these representations between the various generating parameters of the image. In the cases above, the scale parameter is entangled with the angle parameter as a radius and azimuthal angle. Is this always the case? What are the linear subspaces which best represent the generating parameters, and how well do they fit the data?

To investigate these questions, I explored simple linear regression of the generat-

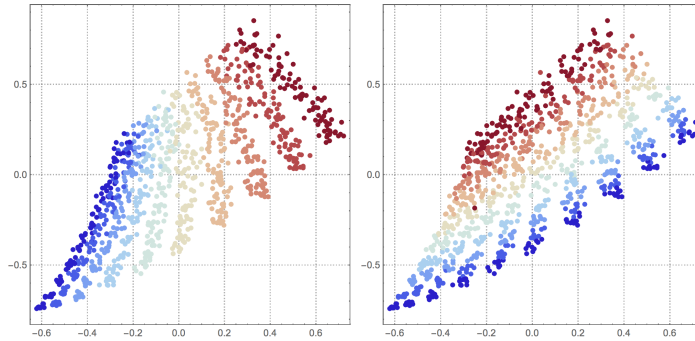


Figure 8.11: Projection from the six dimensional embedding into the two dimensions which best capture scale and noise variations using linear regression. Left: Colored by scale value. Right: Colored by noise value.

Dim.	Angle	Scale	Noise
3	.437	.720	.231
4	.464	.901	.908
5	.487	.916	.950
6	.522	.916	.951
10	.671	.930	.972
50	.787	.980	.983

Table 8.1: R^2 coefficients for linear regression between the manifold coordinates and generating parameters for varying embedding dimensions.

ing parameters in higher dimensional embeddings. Figure 8.11 shows a two dimensional projection from a six dimensional embedding space using the space spanned by the regression vectors. There is global cross-correlation of the noise and scale regressions in that the regression vectors are not orthogonal, visible in the figure by the skew of the structure. Furthermore, there is some local entanglement within the manifold, evident in the curvature of the manifold with respect to the variables.

Table 8.1 gives the Pearson R^2 coefficients as a for several higher dimensional embeddings, which demonstrates that for modest embedding dimensions, scale and noise parameters can be isolated as a single manifold coordinate.

The global cross-correlation was found consistently between the scale and noise parameters, but little was found between the angle parameter and the others. Lin-

ear regression of the angle parameter, due to its cyclical topology, proves difficult. Multi-class Linear discriminant analysis (LDA) [133], which can handle the cyclical structure better, was also investigated for the angle parameter. Although it was more successful than linear regression, for dimensions larger than 4, LDA did not find subspaces which captured the distribution of angles more faithfully than the embeddings shown in figs. 8.9 and 8.10-this is likely because LDA is a somewhat coarse procedure for this data: It does not seek an explicitly angular representation (it penalizes radial variance), and it treats all classes equally, rather than incorporating angular locality. The two dimensional linear subspace found by LDA on the angle parameter did not correlate with the subspaces found for the noise and scale parameters, indicating that the discriminant plane for angle is effectively orthogonal to scale and noise regardless of embedding dimension.

8.5 Discussion

8.5.1 Power spectrum performance

The effectiveness of the spectral method and the stress of the embeddings are best for moderate values of the noise. Since the images consist of perturbed sine functions, it would seem that the power spectrum would be the appropriate basis for examining these images. Indeed, inspection of the power spectrum provides a indication of the information in the image in regimes where the manifold learning procedure does not succeed to capture the structure of the images.

I offer the following explanation: When the noise is very low, the spectral peaks between images have little to no overlap, and so the distance matrix is roughly uniform; all points are equidistant from each other, as in an n -dimensional simplex, and relationship between generating and reconstruction angles is essentially random, with

no correlation. As the noise blurs the spectral peaks, they begin to overlap. As they do, this brings adjacent points in the generating space closer together, allowing for a lower-dimensional space to capture some of the distance structure between points. However, the noise strongly influences the individual features of the power spectrum, and as the noise amplitude grows, adjacent points in the generating space again become orthogonal, such that spectral distances are again no longer meaningful.

This paradigm is backed up by the increased effectiveness of the spectral method for a larger number of images, and likewise reflected in a dip in stress of the embeddings near the optimal effectiveness of the spectral method. While the problem can be to some extent mitigated using larger datasets, it cannot overcome the intrinsic large dimensionality of the images in the power spectrum representation.

This highlights a failure mode for spectral methods when used for automatic processing: Although the basis functions for the power spectrum are orthogonal, there is a geometry to the basis functions provided by the reciprocal space. This relationship allows one to extract meaningful relationships between nearby components (even when they are formally orthogonal) by the application of small spatial transformations such as rotation and dilation.

Understanding of this geometry serves the knowledgeable observer well, however, it is not incorporated into machine learning frameworks. By incorporating this form of domain expertise, it is possible to solve this particular simple problem using automatic methods; one can characterize these power spectra by computing statistics under the assumption that they consist of noise with two diametrically opposed spatial peaks for an envelop. One can then derive formulae to extract the center of position and width of the peaks. However, such an approach will not easily generalize to complex microstructures, which contain nontrivial power spectra. It also does

not overcome the limitations of two-point statistics—it is made simple in this case because the parameters of interest aside from the noise, correspond to single points in the power spectrum.

These concerns will apply to any unitary basis transformations used to process the images—distances in the transformed space will only be meaningful to the extent that the basis is aligned with meaningful aspects of the image. This basis alignment problem prevents information-preserving (or almost-information preserving) transformations from being useful for detecting similarity unless the basis is very well tailored to the features of interest. In the case of the power spectrum, the detectable features of interest are relevant reciprocal space vectors characterizing length scales and anisotropy angles. I have shown that even when the microstructural features are length scales and anisotropy angles, the power spectrum approach on its own does not lend itself to dimensionality reduction.

8.5.2 CNN performance

The performance of the CNN texture vector is much better, achieving high accuracy and consistent performance across the spectrum of noise. This can be attributed to several advantages of the CNN-based approach.

Local feature support The CNN uses local features with finite support. The global nature of the spectral basis means that when similar patterns appear at different locations, there can be a beating effect which actually decreases the response at the wave vectors in question and pushes the feature response (which ought to be aggregated due to their similarity) into neighboring modes. The CNN, on the other hand, will respond to a similar pattern a long distance away and produce the same response to that pattern. When averaging over the hyperimage plane, these

responses are aggregated.

Richness of features Secondly, the neural network exhibits a very rich variety of features, on account of the fact that the filter complexity is higher than that of a fourier transform, and that filters are hierarchically composed.

Convolutional filters can represent arbitrary cross-correlations between the pixels within their receptive fields, such that individual filters themselves can estimate higher order statistics. This stands in contrast to the Fourier basis: although the Fourier basis is complete, individual components are completely insensitive to sensitive to higher order statistics.

Curved filters can assist in the identification of features in an images when the noise parameter is large, and linear correlation lengths become diluted. Higher order filters provide another benefit which is particularly showcased when the noise parameter is low. In this case, a curved filter may respond to two images of differing angles. Curves and other higher-n-point features can give rise to correlated features between similar images which are uncorrelated in the real space or fourier domains. This explains the ability of the neural network to reconstruct the proper angles even when there are very few images in the ensemble.

The hierarchical composition of filters after pooling enables the CNN to generate highly complex responses patterns [137] which aid the network in its design goal—recognition of objects in natural images. The complexity of these features is what allows for the reconstruction of complex textures with large correlation lengths and hierarchical patterning. This is exhibited in fig. 2 from [118], where reconstructions of the texture are generated using different layers from the network, affirming using higher layers is necessary for the reconstruction of larger and more intricate correlation structures.

The intrinsic difficulty in dealing with these higher-order correlations statistics is to decide which statistics are important to compute. The space of two-point statistics is already the same size as the original image space, and the dimensionality of three-point statistics (requiring the specification of two separation vectors) is the square of that for two-point statistics. Many of them may not be informative about the set of images of interest, and so a brute-force approach will waste a lot of effort.

The neural network architecture represents a prior about the statistics of interest, in that all short-range statistics can be computed, but longer range correlations must factor into combinations of short-range correlations, which helps prune down the space of higher-order correlations.

Still, the neural structure is a very high-dimensional space, and random points in that space do not lend themselves to an appropriate basis for texture reconstruction [118]. The image space itself is also a very high-dimensional space, however, the subset of all natural images is much smaller; A given image with completely random pixels will always be distinguishable from a photograph. This enables us to distill a good basis for natural image analysis by training of the neural network.

Feature Pooling As a general scheme, pooling similar features is an useful tool for data analysis. Although not usually phrased in this language, the supposition that textures can be represented by stationary statistics with respect to translation gives rise to natural pooling in analysis. Pixel-level correlations are aggregated together based on the difference vector between the pixels. Mathematically phrased, we use the stationarity assumption to justify pooling the raw two-point configuration function $P(\vec{x}_1, \vec{x}_2)$ to the two-point correlation function, with the pooled variable being

the center of the points, $\vec{y} = (\vec{x}_1 + \vec{x}_2)/2$:

$$P(\vec{x}_1, \vec{x}_2) = \phi(\vec{x}_1)\phi(\vec{x}_2) \quad (8.7)$$

$$P_2(\Delta\vec{x}) = \int P(\vec{y} - \Delta\vec{x}/2, \vec{y} + \Delta\vec{x}/2) d\vec{y} \quad (8.8)$$

Likewise, in Fourier space, where spatial translations correspond to phase modulation, and a translationally stationary signal is constructed by considering only the amplitude of the components, i.e. pooling over the phase variables, and the result is the power spectrum of the signal.

In the texture-vector approach using a CNN, local correlations are constructed by the neurons, and a translational stationary texture vector is constructed by pooling across the entire image plane.

The pooling layers of the CCN serve to reduce the complexity of the spatial information in higher levels of the network, a process usually known to physicists as *coarse-graining*. Coarse-graining has proven to be an enormously effective tool for the analysis of physical systems and the construction of field theories which explain universality of phase transitions.

In the context of power spectra (two-point functions), coarse graining is a trivial procedure which simply discards high-frequency (short distance) information. This can provide for sophisticated action, however, in the context of hierarchical analysis, such as in a neural network. Here, statistics are computed, the system is coarse-grained, and further statistics are computed. Coarse-graining (pooling layers) pool long range composite features over perturbations to the local configuration of their component features. This gives high-complexity, long-range features a higher degree of flexibility—activations on higher levels correspond to a whole set of spatially similar correlations in the image plane, related by small deformations of the com-

ponent features. Furthermore, increasing flexibility is associated with longer-range correlations, whose phase space is inherently much higher. It is in these high-volume regions of phase space that a unitary approach to feature selection will be proportionally more sensitive to alignment of basis, and cross-correlations become infeasible to compute. So, spatial pooling allots feature flexibility in measure to its need.

It is worth noting that for all the advantages of the lossy, many-to-one aspects of pooling, it is disadvantageous from the perspective of a physical analysis, and the nonlinearities in the CNN compound this problem. Individual activations in CNNs cannot be deterministically inverted to generate a response function, and so it becomes difficult to understand concretely what a particular activation in a CNN may represent.

The neural embedding’s RMSE in the angular reconstruction task reflects a consistent degree of bias due to the lopsided shape of the reconstructed manifold. This is itself due to the fact that the neural network architecture does not explicitly capture rotational symmetry, but rather it is implicitly encoded in the variation of learned filters in the network. However, systematic but smooth deviations do not provide any large obstacle to effective regression between neural embeddings and parameters of interest—processing parameters or material parameters. Furthermore, one may seek rotationally invariant features by averaging the texture vector applied to several passes of rotated images through the network, or the use of Cyclic Symmetry CNNs [138] or Deep Symmetry networks [139], which can architecturally encode features which are robust to rotation.

8.6 Conclusions and future directions

I have introduced a method for detecting the low-dimensional structure of a distribution of similar texture images using CNN. Although the manifold of noisy texture images is inherently of very large dimension, I show that the CNN can embed these images meaningfully into a low dimensional manifold which reflects the structure of the latent variables used to generate the image, performing extreme dimensionality reduction. I present this as a framework for the analysis of materials microstructure to determine the dimensionality, topology, etc. of materials microstructures, characterizing materials directly by state instead of by processing. By faithfully capturing the variations in microstructure using an unsupervised low dimensional representation, this approach forms a platform for further model development to connect processing to microstructure, and microstructure to properties.

I demonstrate the superiority of our approach to a similar pipeline using more traditional statistical approaches to microstructure characterization. The CNN-based approach demonstrates a pattern recognition sensitivities with a much wider range of response, including conditions of very high stochasticity as well as very low sample size. The latter is a common constraint many disciplines, such as materials science, where data is expensive. The low sample size is circumvented by the use of transfer learning, reaping the benefits from image characterization of large datasets.

In addition, I discuss the features of CNNs which allow for these remarkable capabilities, with an emphasis on the relationship between these techniques and the standard physics approach. These pave the way for future microstructure characterization techniques which synthesize physics-based and machine learning approaches. For example, the the incorporation of frameworks which obey the appropriate physical symmetries of a given system [138–141]. Another avenue is the incorporation of

latent variable models (e.g. [142]) which reflect the microstructural generation process. It may also be feasible to construct or tune CNNs which are optimized for the detection of texture elements which are particular to materials microstructure.

Appendices

Appendix A

Mean Trade Equations Approaching the Phase Transition

A.1 Scaling of the richest agent

Given the scaling relation:

$$\epsilon \log \left(\frac{w_s(x, \epsilon)}{w(0, \epsilon)} \right) = -g(x), \quad (\text{A.1})$$

or equivalently,

$$w_s(x, \epsilon) = w_s(0, \epsilon) e^{-\frac{1}{\epsilon} g(x)} \quad (\text{A.2})$$

and the normalization of rescaled wealth:

$$\int_0^1 w_s(x, \epsilon) dx = 1 \quad (\text{A.3})$$

We can factor out the wealth scale $w_s(0, \epsilon)$ from the integral and evaluate the integral:

$$I = \int_0^1 \exp(-\epsilon^{-1} g(x)) dx \quad (\text{A.4})$$

As $\epsilon \rightarrow 0$, the contributions to the integral will become dominated by the behavior of $g(x)$ near $x = 0$, so expand g in a Taylor series. Note that $g(0) = 0$ by the original

scaling relation.:

$$I = \int_0^1 \exp \left[-\epsilon^{-1} \left(xg'(0) + \frac{x^2}{2}g''(0) + \dots \right) \right] dx \quad (\text{A.5})$$

Using the substitution $u = \frac{xg'(0)}{\epsilon}$:

$$I = \int_{x=0}^{x=1} \exp \left[-u + \frac{\epsilon u^2}{2g'(0)^2}g''(0) + \dots \right] \frac{\epsilon}{g'(0)} du \quad (\text{A.6})$$

Equation A.3 insists that the equation $w_s(0)I = 1$ is independent of ϵ . Moreover the u^2 term in the exponent cannot dominate the integral because $g(x)$ is increasing.

The ratio of the second term of the expansion to the first is

$$r = \frac{\epsilon u g''(0)}{2g'(0)^2} \quad (\text{A.7})$$

So as long as r remains small while u is on order 1, this contribution to the integral will be negligible, which will always occur for sufficiently small ϵ . We can then evaluate the integral straightforwardly, giving:

$$I \approx \frac{\epsilon}{g'(0)} \quad (\text{A.8})$$

$$w(0, \epsilon) \approx \frac{g'(0)}{\epsilon} + O(1) \quad (\text{A.9})$$

Further analysis gives the integral to another order proceeds by the usual method of completing the square:

$$I' = \int_0^\infty \exp \left(-u - \frac{ku^2}{2} \right) du \quad (\text{A.10})$$

$$I' = \frac{\sqrt{\frac{\pi}{2}} e^{\frac{1}{2}/k} \operatorname{erfc} \left(\frac{1}{\sqrt{2}\sqrt{k}} \right)}{\sqrt{k}} \quad (\text{A.11})$$

Analysis of this in the limit as $k \rightarrow 0$ requires examining only a right-handed limit $k \rightarrow 0^+$, as I_2 acquires an imaginary component for $k < 0$. This is not actually a problem for our case since we are looking only to find the perturbative correction to this integral for small k , knowing that the correction contributions come from deformations to the exponential shape around $x = 0$. Moreover, we will eventually find that the solution satisfies $k > 0$. We may then expand to find:

$$I'(k \approx 0) \approx 1 - k + 3\frac{k^2}{2} + \dots \quad (\text{A.12})$$

The k^2 component is not reliable since we have not included the $g'''(0)$ term to our correction, which should contribute at the same order in ϵ . In our case, $k = -\frac{\epsilon g''(0)}{g'(0)^2}$. Including the first two orders gives:

$$I \approx \frac{\epsilon}{g'(0)} \left(1 + \frac{\epsilon g''(0)}{g'(0)^2} \right) \quad (\text{A.13})$$

Which can be rearranged to the equivalent expansion

$$w(0, \epsilon) \approx \frac{g'(0)}{\epsilon} + \frac{g''(0)}{g'(0)} + O(\epsilon) \quad (\text{A.14})$$

A.2 Solution to the scaling form near the phase transition

For the YSM with skewed geometric growth, and the scaling form

$$\epsilon \log \left(\frac{w_s(x, \epsilon)}{w(0, \epsilon)} \right) = -g(x), \quad (\text{A.15})$$

near the phase transition at $\gamma = 1; \epsilon = 0$. Let us insert the function

$$g(x) = \log(1 + x\beta/\mu) \quad (\text{A.16})$$

into the mean-trade equation at steady state:

$$0 = -x\beta y(x) + \beta \int_x^1 y(x') dx' + \mu \frac{y(x)^\gamma}{\int_0^1 y(x')^\gamma dx'} - \mu y(x) \quad (\text{A.17})$$

For convenience, we divide out by β and set $\mu' = \mu/\beta$.

The form of $g(x)$ gives us a form for y :

$$y(x) = y(0) \left(1 + \frac{x}{\mu'}\right)^{\frac{-1}{\epsilon}} \quad (\text{A.18})$$

This allows us to compute:

$$\int_x^1 y(x') dx' = y(0) \int_x^1 \left(1 + \frac{x'}{\mu'}\right)^{\frac{-1}{\epsilon}} dx' \quad (\text{A.19})$$

$$= \frac{\mu' y(0)}{1 - \epsilon^{-1}} \left[\left(1 + \frac{1}{\mu'}\right)^{1 - \epsilon^{-1}} - \left(1 + \frac{x}{\mu'}\right)^{1 - \epsilon^{-1}} \right] \quad (\text{A.20})$$

and likewise, the integral for S can be computed similarly with the substitution

$\frac{1}{\epsilon} \rightarrow \frac{\gamma}{\epsilon}$:

$$S = \int_0^1 y^\gamma dx = \frac{\mu' y(0)^\gamma}{1 + \frac{\gamma}{\epsilon}} \left[\left(1 + \frac{1}{\mu'}\right)^{1 - \frac{\gamma}{\epsilon}} - 1 \right] \quad (\text{A.21})$$

Likewise, we can use normalization to compute $y(0)$:

$$\frac{1}{y(0)} = \int_0^1 \left(1 + \frac{x}{\mu'}\right)^{\epsilon^{-1}} dx \quad (\text{A.22})$$

$$y(0) = (1 - \epsilon^{-1}) \frac{(1 + \mu')^{\epsilon^{-1}}}{\mu'^{\epsilon^{-1}} (1 + \mu') - \mu' (1 + \mu')^{\epsilon^{-1}}} \quad (\text{A.23})$$

$$= \frac{\lambda \mu'^{\lambda-1}}{(1 + \mu')^\lambda - \mu'^\lambda} \quad (\text{A.24})$$

where $\lambda = 1 - \epsilon^{-1}$ is a notational convenience. $0 < \epsilon < 1$ is mapped to the domain $-\infty < \lambda < 0$.

We take the derivative of the mean trade steady state equation with respect to x , and regroup. y' denotes $\frac{dy}{dx}$.

$$0 = -xy' - 2y + \mu'y' \left(\frac{\gamma y^{\gamma-1}}{S} - 1 \right) \quad (\text{A.25})$$

which can be further rearranged to

$$\frac{2y}{\mu'y'} + 1 + \frac{x}{\mu'} = \frac{\gamma y^{\gamma-1}}{S} \quad (\text{A.26})$$

(Dividing by y' is not perilous because $y(x)$ is a strictly decreasing function). At this point we insert the solution from eq. A.18, which has the convenient property that

$$\frac{y}{y'} = -\epsilon \mu' \left(1 + \frac{x}{\mu'} \right) \quad (\text{A.27})$$

Simplifying the steady-state equation to

$$(1 - 2\epsilon) \left(1 + \frac{x}{\mu} \right) = \frac{\gamma}{S} y(0)^{-\epsilon} \left(1 + \frac{x}{\mu'} \right) \quad (\text{A.28})$$

$$(1 - 2\epsilon) = \frac{\gamma}{S} y(0)^{-\epsilon} \quad (\text{A.29})$$

$$\frac{\frac{\gamma}{S} y(0)^{-\epsilon} - 1}{\epsilon} = -2 \quad (\text{A.30})$$

With $y(0)$ determined by the expression in eq. A.24 and S by eq. A.21. This cumbersome expression can be algebraically manipulated to the statement that

$$c(\lambda, \mu') \equiv \frac{1 + \lambda}{1 + \mu' - \mu' \left(\frac{\mu'}{1 + \mu'} \right)^\lambda} = 0 \quad (\text{A.31})$$

with the limit $\epsilon \rightarrow 0^+$ replaced with $\lambda \rightarrow -\infty$.

Bibliography

- [1] Online Etymology Dictionary. Entry: Statistics. <http://www.etymonline.com/index.php?term=statistics>, 2016.
- [2] Z. Burda, J. Jurkiewicz, and M. A. Nowak. Is Econophysics a Solid Science? *Acta Physica Polonica B*, 34:87, January 2003.
- [3] Dean Rickles. Econophysics for philosophers. *Studies in History and Philosophy of Science Part B: Studies in History and Philosophy of Modern Physics*, 38(4):948 – 978, 2007.
- [4] Franck Jovanovic and Christophe Schinckus. The emergence of econophysics: A new approach in modern financial theory. *History of Political Economy*, 45(3):443–474, 2013.
- [5] Mauro Gallegati, Steve Keen, Thomas Lux, and Paul Ormerod. Worrying trends in econophysics. *Physica A: Statistical Mechanics and its Applications*, 370(1):1–6, 2006.
- [6] Joseph L McCauley. Response to “Worrying trends in econophysics”. *Physica A: Statistical Mechanics and its Applications*, 371(2):601–609, 2006.
- [7] Jean-Philippe Bouchaud. The (unfortunate) complexity of the economy. *Physics World*, 22(04):28, 2009.

- [8] J. Doyne Farmer and Duncan Foley. The economy needs agent-based modelling. *Nature*, 460(7256):685–686, 08 2009.
- [9] Christophe Schinckus. Is econophysics a new discipline? The neopositivist argument. *Physica A: Statistical Mechanics and its Applications*, 389(18):3814 – 3821, 2010.
- [10] Christophe Schinckus. Econophysics and economics: Sister disciplines? *American Journal of Physics*, 78(4):325–327, 2010.
- [11] Victor M. Yakovenko and J. Barkley Rosser. *Colloquium*: Statistical mechanics of money, wealth, and income. *Rev. Mod. Phys.*, 81:1703–1725, Dec 2009.
- [12] Wataru Souma. Physics of personal income. In Hideki Takayasu, editor, *Empirical Science of Financial Fluctuations: The Advent of Econophysics*, pages 343–352. Springer Japan, Tokyo, 2002.
- [13] V Pareto. Cours d'économie politique. *Droz, Geneva*, 1896.
- [14] MEJ Newman. Power laws, Pareto distributions and Zipf's law. *Contemporary Physics*, 46(5):323–351, 2005.
- [15] Brian Hayes. Computing science: Follow the money. *American Scientist*, pages 400–405, 2002.
- [16] Zhi-Feng Huang and Sorin Solomon. Stochastic multiplicative processes for financial markets. *Physica A: Statistical Mechanics and its Applications*, 306:412 – 422, 2002. Invited Papers from the 21th IUPAP International Conference on Statistical Physics.

- [17] Anirban Chakraborti, Ioane Muni Toke, Marco Patriarca, and Frédéric Abergel. Econophysics review: I. Empirical facts. *Quantitative Finance*, 11(7):991–1012, 2011.
- [18] Anirban Chakraborti, Ioane Muni Toke, Marco Patriarca, and Frédéric Abergel. Econophysics review: II. Agent-based models. *Quantitative Finance*, 11(7):1013–1041, 2011.
- [19] J. Kelly. A new interpretation of information rate. *IRE Transactions on Information Theory*, 2(3):185–189, September 1956.
- [20] Sitabhra Sinha. Stochastic maps, wealth distribution in random asset exchange models and the marginal utility of relative wealth. *Physica Scripta*, 2003(T106):59, 2003.
- [21] C. F. Moukarzel, S. Gonçalves, J. R. Iglesias, M. Rodríguez-Achach, and R. Huerta-Quintanilla. Wealth condensation in a multiplicative random asset exchange model. *The European Physical Journal Special Topics*, 143(1):75–79, 2007.
- [22] Cristian F. Moukarzel. Multiplicative asset exchange with arbitrary return distributions. *Journal of Statistical Mechanics: Theory and Experiment*, 2011(08):P08023, 2011.
- [23] The World Bank. World development indicators. <http://data.worldbank.org/indicator/NY.GDP.MKTP.KD.ZG>, September 2014.
- [24] Wataru Souma. Universal structure of the personal income distribution. *Fractals*, 09(04):463–470, 2001.

- [25] Anthony B. Atkinson, Thomas Piketty, and Emmanuel Saez. Top incomes in the long run of history. Working Paper 15408, National Bureau of Economic Research, October 2009.
- [26] Makoto Nirei and Wataru Souma. A two factor model of income distribution dynamics. *Review of Income and Wealth*, 53(3):440–459, 2007.
- [27] Moshe Levy and Sorin Solomon. New evidence for the power-law distribution of wealth. *Physica A: Statistical Mechanics and its Applications*, 242(1-2):90 – 94, 1997.
- [28] Fabio Clementi and Mauro Gallegati. Pareto’s law of income distribution: Evidence for germany, the united kingdom, and the united states. In Arnab Chatterjee, Sudhakar Yarlagadda, and Bikas K. Chakrabarti, editors, *Econophysics of Wealth Distributions*, pages 3–14. Springer Milan, Milano, 2005.
- [29] Sitabhra Sinha. Evidence for power-law tail of the wealth distribution in India. *Physica A: Statistical Mechanics and its Applications*, 359:555 – 562, 2006.
- [30] Géza Hegyi, Zoltán Nédá, and Maria Augusta Santos. Wealth distribution and Pareto’s law in the Hungarian medieval society. *Physica A: Statistical Mechanics and its Applications*, 380:271 – 277, 2007.
- [31] A. Y. Abul-Magd. Wealth distribution in an ancient egyptian society. *Phys. Rev. E*, 66:057104, Nov 2002.
- [32] Oren S. Klass, Ofer Biham, Moshe Levy, Ofer Malcai, and Sorin Solomon. The Forbes 400 and the Pareto wealth distribution. *Economics Letters*, 90(2):290 – 295, 2006.

- [33] D Kondor, M Pósfai, I Csabai, and G Vattay. Do the rich get richer? An empirical analysis of the Bitcoin transaction network. *PLoS ONE*, 9(2):e86197, 02 2014.
- [34] Sidney Redner. Random multiplicative processes: An elementary tutorial. *Am. J. Phys*, 58(3):267–273, 1990.
- [35] Henri Theil. *Economics and information theory*, volume 7 of *Studies in mathematical and managerial economics*. Amsterdam : North-Holland, 1967.
- [36] C. E. Shannon. A mathematical theory of communication. *The Bell System Technical Journal*, 27(4):623–656, Oct 1948.
- [37] Robert Gibrat. *Les inégalités économiques*. Recueil Sirey, 1931.
- [38] Michael H. R. Stanley, Luis A. N. Amaral, Sergey V. Buldyrev, Shlomo Havlin, Heiko Leschhorn, Philipp Maass, Michael A. Salinger, and H. Eugene Stanley. Scaling behaviour in the growth of companies. *Nature*, 379(6568):804–806, 02 1996.
- [39] D. G. Champernowne. A model of income distribution. *The Economic Journal*, 63(250):318–351, 1953.
- [40] Moshe Levy, Sorin Solomon, and Givat Ram. Dynamical explanation for the emergence of power law in a stock market model. *International Journal of Modern Physics C*, 07(01):65–72, 1996.
- [41] Didier Sornette and Rama Cont. Convergent multiplicative processes repelled from zero: Power laws and truncated power laws. *J. Phys. I France*, 7(3):431–444, 1997.

- [42] Xavier Gabaix. Zipf's law for cities: An explanation. *The Quarterly Journal of Economics*, 114(3):739–767, 1999.
- [43] Gerhard Sorger. Income and wealth distribution in a simple model of growth. *Economic Theory*, 16(1):23–42, 2000.
- [44] Jayasri Dutta, J. A. Sefton, and M. R. Weale. Income distribution and income dynamics in the United Kingdom. *Journal of Applied Econometrics*, 16(5):599–617, 2001.
- [45] William J Reed. The Pareto, Zipf and other power laws. *Economics Letters*, 74(1):15 – 19, 2001.
- [46] Jeremy Greenwood, Nezih Guner, and John A. Knowles. More on marriage, fertility, and the distribution of income. *International Economic Review*, 44(3):827–862, 2003.
- [47] Moshe Levy. Market efficiency, the Pareto wealth distribution, and the Lévy distribution of stock returns. *The Economy As an Evolving Complex System, III: Current Perspectives and Future Directions*, page 101, 2005.
- [48] Urna Basu and PK Mohanty. Modeling wealth distribution in growing markets. *The European Physical Journal B*, 65(4):585–589, 2008.
- [49] Juan Carlos Córdoba. A generalized Gibrat's law. *International Economic Review*, 49(4):1463–1468, 2008.
- [50] Jess Benhabib, Alberto Bisin, and Shenghao Zhu. The distribution of wealth and fiscal policy in economies with finitely lived agents. *Econometrica*, 79(1):123–157, 2011.

- [51] Guglielmo D’Amico, Giuseppe Di Biase, and Raimondo Manca. Income inequality dynamic measurement of Markov models: Application to some European countries. *Economic Modelling*, 29(5):1598–1602, 2012.
- [52] Harry Kesten. Random difference equations and renewal theory for products of random matrices. *Acta Mathematica*, 131(1):207–248, 1973.
- [53] Yoshi Fujiwara, Wataru Souma, Hideaki Aoyama, Taisei Kaizoji, and Masanao Aoki. Growth and fluctuations of personal income. *Physica A: Statistical Mechanics and its Applications*, 321(3–4):598 – 604, 2003.
- [54] A. F. Shorrocks. Income mobility and the Markov assumption. *The Economic Journal*, 86(343):566–578, 1976.
- [55] Frank Bickenbach and Eckhardt Bode. Markov or not Markov—This should be a question. Technical report, Kieler Arbeitspapiere, 2001.
- [56] Frank Bickenbach and Eckhardt Bode. Evaluating the Markov property in studies of economic convergence. *International Regional Science Review*, 26(3):363–392, 2003.
- [57] J. Doyne Farmer and John Geanakoplos. The virtues and vices of equilibrium and the future of financial economics. *Complexity*, 14(3):11–38, 2009.
- [58] John Angle. The surplus theory of social stratification and the size distribution of personal wealth. *Social Forces*, 65(2):293–326, 1986.
- [59] S. Ispolatov, P. L. Krapivsky, and S. Redner. Wealth distributions in asset exchange models. *Eur. Phys. J. B*, 2(2):267–276, 1998.

- [60] Jean-Philippe Bouchaud and Marc Mézard. Wealth condensation in a simple model of economy. *Physica A: Statistical Mechanics and its Applications*, 282(3â4):536 – 545, 2000.
- [61] A. Dragulescu and V.M. Yakovenko. Statistical mechanics of money. *The European Physical Journal B - Condensed Matter and Complex Systems*, 17(4):723–729, 2000.
- [62] A. Chakraborti and B.K. Chakrabarti. Statistical mechanics of money: how saving propensity affects its distribution. *The European Physical Journal B - Condensed Matter and Complex Systems*, 17(1):167–170, 2000.
- [63] Arnab Chatterjee, Bikas K. Chakrabarti, and S.S. Manna. Pareto law in a kinetic model of market with random saving propensity. *Physica A: Statistical Mechanics and its Applications*, 335(1â2):155 – 163, 2004.
- [64] František Slanina. Inelastically scattering particles and wealth distribution in an open economy. *Phys. Rev. E*, 69:046102, Apr 2004.
- [65] A. Chatterjee and B. K. Chakrabarti. Kinetic exchange models for income and wealth distributions. *The European Physical Journal B*, 60(2):135–149, 2007.
- [66] Arniban Chakraborti. Distributions of money in model markets of economy. *International Journal of Modern Physics C*, 13(10):1315–1321, 2002.
- [67] Bruce M. Boghosian. Kinetics of wealth and the Pareto law. *Phys. Rev. E*, 89:042804, Apr 2014.
- [68] J.R. Iglesias, S. Gonçalves, G. Abramson, and J.L. Vega. Correlation between risk aversion and wealth distribution. *Physica A: Statistical Mechanics and its*

- Applications*, 342(1â2):186 – 192, 2004. Proceedings of the VIII Latin American Workshop on Nonlinear Phenomena.
- [69] JR Iglesias. How simple regulations can greatly reduce inequality. *arXiv preprint arXiv:1007.0461*, 2010.
- [70] R Bustos-Guajardo and Cristian F Moukarzel. Yard-sale exchange on networks: Wealth sharing and wealth appropriation. *Journal of Statistical Mechanics: Theory and Experiment*, 2012(12):P12009, 2012.
- [71] M. L. Bertotti and G. Modanese. Discretized kinetic theory on scale-free networks. *ArXiv e-prints*, February 2015.
- [72] K. Liu, N. Lubbers, W. Klein, J. Tobochnik, B. Boghosian, and H. Gould. The Effect of Growth On Equality in Models of the Economy. *ArXiv e-prints*, May 2013.
- [73] Roman Frigg, Joseph Berkovitz, and Fred Kronz. The ergodic hierarchy. In Edward N. Zalta, editor, *The Stanford Encyclopedia of Philosophy*. The Metaphysics Research Lab, Center for the Study of Language and Information, Stanford University, summer 2014 edition, 2014.
- [74] A. Ishihara. *Statistical Physics*. Academic Press, 1971.
- [75] N. G. Van Kampen. *Stochastic processes in physics and chemistry*. Elsevier, third edition, 2007.
- [76] J. J. Binney, N. J. Dowrick, A. J. Fisher, and M. Newman. *The Theory of Critical Phenomena: An Introduction to the Renormalization Group*. Oxford University Press, Inc., New York, NY, USA, 1992.

- [77] John G Kemeny, James Laurie Snell, et al. *Finite Markov chains*, volume 356. van Nostrand Princeton, NJ, 1960.
- [78] James R Norris. *Markov chains*. Cambridge university press, 1998.
- [79] D. Thirumalai, Raymond D. Mountain, and T. R. Kirkpatrick. Ergodic behavior in supercooled liquids and in glasses. *Phys. Rev. A*, 39:3563–3574, Apr 1989.
- [80] D. Thirumalai and Raymond D. Mountain. Ergodic convergence properties of supercooled liquids and glasses. *Phys. Rev. A*, 42:4574–4587, Oct 1990.
- [81] C. Spearman. The proof and measurement of association between two things. *The American Journal of Psychology*, 15(1):72–101, 1904.
- [82] O. Peters and W. Klein. Ergodicity breaking in geometric brownian motion. *Phys. Rev. Lett.*, 110:100603, Mar 2013.
- [83] Kiyosi Itô. 109. stochastic integral. *Proceedings of the Imperial Academy*, 20(8):519–524, 1944.
- [84] Kiyosi Itô. *Diffusion Processes*. Wiley Online Library, 1974.
- [85] N. G. Kampen. Itô versus Stratonovich. *Journal of Statistical Physics*, 24(1):175–187, 1981.
- [86] Ioannis Karatzas and Steven Shreve. *Brownian motion and stochastic calculus*, volume 113. Springer Science & Business Media, 2012.
- [87] Constantino Tsallis. What are the numbers that experiments provide. *Quimica Nova*, 17(6):468–471, 1994.

- [88] Constantino Tsallis, Renio S Mendes, and Anel R Plastino. The role of constraints within generalized nonextensive statistics. *Physica A: Statistical Mechanics and its Applications*, 261(3):534–554, 1998.
- [89] J. L. W. V. Jensen. Sur les fonctions convexes et les inégalités entre les valeurs moyennes. *Acta Mathematica*, 30(1):175–193, 1906.
- [90] Ole Peters. Menger 1934 revisited. *arXiv preprint arXiv:1110.1578*, 2011.
- [91] Egle Samanidou, Elmar Zschischang, Dietrich Stauffer, and Thomas Lux. Agent-based models of financial markets. *Reports on Progress in Physics*, 70(3):409, 2007.
- [92] Forbes. Forbes Global 2000: The world’s biggest public companies. <http://www.forbes.com/global2000/list/>, April 2013.
- [93] H. Kumar, C.L. Briant, and W.A. Curtin. Using microstructure reconstruction to model mechanical behavior in complex microstructures. *Mechanics of Materials*, 38(8–10):818 – 832, 2006. Advances in Disordered Materials.
- [94] Martin Ostojca-Starzewski. *Microstructural randomness and scaling in mechanics of materials*. CRC Press, 2007.
- [95] Moran Wang and Ning Pan. Predictions of effective physical properties of complex multiphase materials. *Materials Science and Engineering: R: Reports*, 63(1):1 – 30, 2008.
- [96] David T. Fullwood, Stephen R. Niezgodza, Brent L. Adams, and Surya R. Kalidindi. Microstructure sensitive design for performance optimization. *Progress in Materials Science*, 55(6):477 – 562, 2010.

- [97] S. Torquato. Optimal Design of Heterogeneous Materials. *Annu. Rev. Mater. Res.*, 40(1):101–129, 2010.
- [98] Turab Lookman, Francis J. Alexander, and Krishna Rajan, editors. *Information Science for Materials Discovery and Design*. Springer International Publishing, 2016.
- [99] Surya R. Kalidindi. Data science and cyberinfrastructure: critical enablers for accelerated development of hierarchical materials. *International Materials Reviews*, 60(3):150–168, 2015.
- [100] Krishna Rajan. *Informatics for materials science and engineering: data-driven discovery for accelerated experimentation and application*. Butterworth-Heinemann, 2013.
- [101] Surya R. Kalidindi, Stephen R. Niezgoda, and Ayman A. Salem. Microstructure informatics using higher-order statistics and efficient data-mining protocols. *JOM*, 63(4):34–41, 2011.
- [102] Yu Liu, M. Steven Greene, Wei Chen, Dmitriy A. Dikin, and Wing Kam Liu. Computational microstructure characterization and reconstruction for stochastic multiscale material design. *Computer-Aided Design*, 45(1):65 – 76, 2013. Computer-aided multi-scale materials and product design.
- [103] Stephen R. Niezgoda, Anand K. Kanjarla, and Surya R. Kalidindi. Novel microstructure quantification framework for databasing, visualization, and analysis of microstructure data. *Integr. Mater. Manuf. Innov.*, 2(1):3, 2013.

- [104] Y. Jiao, F. H. Stillinger, and S. Torquato. Modeling heterogeneous materials via two-point correlation functions: Basic principles. *Phys. Rev. E*, 76:031110, Sep 2007.
- [105] David T. Fullwood, Stephen R. Niezgod, and Surya R. Kalidindi. Microstructure reconstructions from 2-point statistics using phase-recovery algorithms. *Acta Materialia*, 56(5):942 – 948, 2008.
- [106] Y Jiao, F H Stillinger, and S Torquato. A superior descriptor of random textures and its predictive capacity. *Proc. Natl. Acad. Sci. U. S. A.*, 106(42):17634–17639, 2009.
- [107] Dongdong Chen, Qizhi Teng, Xiaohai He, Zhi Xu, and Zhengji Li. Stable-phase method for hierarchical annealing in the reconstruction of porous media images. *Phys. Rev. E*, 89(1):1–10, 2014.
- [108] Y. Jiao, F. H. Stillinger, and S. Torquato. Geometrical ambiguity of pair statistics: Point configurations. *Phys. Rev. E*, 81:011105, Jan 2010.
- [109] Yang Jiao, Frank H. Stillinger, and Salvatore Torquato. Geometrical ambiguity of pair statistics. ii. heterogeneous media. *Phys. Rev. E*, 82:011106, Jul 2010.
- [110] S.R. Niezgod, D.T. Fullwood, and S.R. Kalidindi. Delineation of the space of 2-point correlations in a composite material system. *Acta Materialia*, 56(18):5285 – 5292, 2008.
- [111] Chase E. Zachary and Salvatore Torquato. Improved reconstructions of random media using dilation and erosion processes. *Phys. Rev. E*, 84(5):1–5, 2011.

- [112] Kirill M. Gerke, Marina V. Karsanina, Roman V. Vasilyev, and Dirk Mallants. Improving pattern reconstruction using directional correlation functions. *EPL (Europhysics Letters)*, 106(6):66002, 2014.
- [113] Y. Lecun, L. Bottou, Y. Bengio, and P. Haffner. Gradient-based learning applied to document recognition. *Proceedings of the IEEE*, 86(11):2278–2324, Nov 1998.
- [114] Alex Krizhevsky, Ilya Sutskever, and Geoffrey E Hinton. ImageNet classification with deep convolutional neural networks. *Adv. Neural Inf. Process. Syst.*, pages 1097–1105, 2012.
- [115] Karen Simonyan and Andrew Zisserman. Very deep convolutional networks for large-scale image recognition. *arXiv preprint arXiv:1409.1556*, 2014.
- [116] Christian Szegedy, Wei Liu, Yangqing Jia, Pierre Sermanet, Scott Reed, Dragomir Anguelov, Dumitru Erhan, Vincent Vanhoucke, and Andrew Rabinovich. Going deeper with convolutions. *arXiv preprint arXiv:1409.4842*, 2014.
- [117] K. He, X. Zhang, S. Ren, and J. Sun. Deep Residual Learning for Image Recognition. *ArXiv e-prints*, 2015.
- [118] Leon A. Gatys, Alexander S. Ecker, and Matthias Bethge. Texture synthesis and the controlled generation of natural stimuli using convolutional neural networks. *CoRR*, abs/1505.07376, 2015.
- [119] Leon A. Gatys, Alexander S. Ecker, and Matthias Bethge. A neural algorithm of artistic style. *arXiv*, abs/1508.06576, 2015.

- [120] Tele Hao, Tapani Raiko, Alexander Ilin, and Juha Karhunen. Gated Boltzmann machine in texture modeling. In Alessandro E.P. Villa, Włodzisław Duch, Péter Érdi, Francesco Masulli, and Günther Palm, editors, *Artif. Neural Networks Mach. Learn. – ICANN 2012*, volume 7553 of *Lecture Notes in Computer Science*, pages 124–131. Springer Berlin Heidelberg, 2012.
- [121] Jyri J Kivinen and Christopher Williams. Multiple texture boltzmann machines. In *International Conference on Artificial Intelligence and Statistics*, pages 638–646, 2012.
- [122] Heng Luo, Pierre Luc Carrier, Aaron Courville, and Yoshua Bengio. Texture Modeling with Convolutional Spike-and-Slab RBMs and Deep Extensions. *Proc. 16th Int. Conf. Artif. Intell. Stat.*, 31:415–423, 2013.
- [123] Qi Gao and Stefan Roth. Texture Synthesis: From Convolutional RBMs to Efficient Deterministic Algorithms. In Pasi Fränti, Gavin Brown, Marco Loog, Francisco Escolano, and Marcello Pelillo, editors, *Struct. Syntactic, Stat. Pattern Recognit.*, volume 8621 of *Lecture Notes in Computer Science*, pages 434–443. Springer Berlin Heidelberg, 2014.
- [124] Lucas Theis and Matthias Bethge. Generative image modeling using spatial lstms. In C. Cortes, N. D. Lawrence, D. D. Lee, M. Sugiyama, and R. Garnett, editors, *Advances in Neural Information Processing Systems 28*, pages 1927–1935. Curran Associates, Inc., 2015.
- [125] Yann LeCun, Yoshua Bengio, and Geoffrey E Hinton. Deep learning. *Nature*, 521(7553):436–444, 2015.

- [126] Olga Russakovsky, Jia Deng, Hao Su, Jonathan Krause, Sanjeev Satheesh, Sean Ma, Zhiheng Huang, Andrej Karpathy, Aditya Khosla, Michael Bernstein, Alexander C. Berg, and Li Fei-Fei. ImageNet large scale visual recognition challenge. *International Journal of Computer Vision*, 115(3):211–252, 2015.
- [127] Kaiming He, Xiangyu Zhang, Shaoqing Ren, and Jian Sun. Delving deep into rectifiers: Surpassing human-level performance on imagenet classification. In *The IEEE International Conference on Computer Vision (ICCV)*, December 2015.
- [128] Ian Goodfellow, Yoshua Bengio, and Aaron Courville. Deep learning. Book in preparation for MIT Press, 2016.
- [129] Jason Yosinski, Jeff Clune, Anh Nguyen, Thomas Fuchs, and Hod Lipson. Understanding neural networks through deep visualization. *arXiv preprint arXiv:1506.06579*, 2015.
- [130] Dumitru Erhan, Aaron Courville, and Yoshua Bengio. Understanding representations learned in deep architectures. Technical Report 1355, Université de Montréal/DIRO, 2010.
- [131] J. B. Kruskal. Multidimensional scaling by optimizing goodness of fit to a nonmetric hypothesis. *Psychometrika*, 29(1):1–27, 1964.
- [132] I. Borg and P. J. F. Groenen. *Modern Multidimensional Scaling: Theory and Applications*. Springer Series in Statistics. Springer-Verlag New York, 2005.
- [133] James Franklin. The elements of statistical learning: data mining, inference and prediction. *The Mathematical Intelligencer*, 27(2):83–85, 2008.

- [134] F. Pedregosa, G. Varoquaux, A. Gramfort, V. Michel, B. Thirion, O. Grisel, M. Blondel, P. Prettenhofer, R. Weiss, V. Dubourg, J. Vanderplas, A. Passos, D. Cournapeau, M. Brucher, M. Perrot, and E. Duchesnay. Scikit-learn: Machine learning in Python. *Journal of Machine Learning Research*, 12:2825–2830, 2011.
- [135] Jan De Leeuw. Recent developments in statistics. *Chapt. Applications of convex analysis to multidimensional scaling*, Amsterdam: North-Holland, pages 133–145, 1977.
- [136] Ken Perlin. An image synthesizer. *SIGGRAPH Comput. Graph.*, 19(3):287–296, July 1985.
- [137] The Keras Blog. How convolutional neural networks see the world. <http://blog.keras.io/how-convolutional-neural-networks-see-the-world.html>, January 2016.
- [138] Sander Dieleman, Jeffrey De Fauw, and Koray Kavukcuoglu. Exploiting cyclic symmetry in convolutional neural networks. *CoRR*, abs/1602.02660, 2016.
- [139] Robert Gens and Pedro M Domingos. Deep symmetry networks. In Z. Ghahramani, M. Welling, C. Cortes, N. D. Lawrence, and K. Q. Weinberger, editors, *Advances in Neural Information Processing Systems 27*, pages 2537–2545. Curran Associates, Inc., 2014.
- [140] Stéphane Mallat. Group invariant scattering. *Communications on Pure and Applied Mathematics*, 65(10):1331–1398, 2012.
- [141] Taco S. Cohen and Max Welling. Transformation properties of learned visual representations. *CoRR*, abs/1412.7659, 2014.

- [142] D. P Kingma and M. Welling. Auto-Encoding Variational Bayes. *ArXiv e-prints*, December 2013.

Curriculum Vitae

Nicholas Lubbers

Boston University, Physics Department
590 Commonwealth Avenue
Boston, Massachusetts 02215 USA

Telephone: 617-353-3845
Cellphone: 719-244-2622
E-mail: nlubbers@bu.edu

EDUCATION

- 2016, Ph.D. Physics, Boston University, Boston, MA, USA

Advisor: Professor William Klein

Dissertation: *A STATISTICAL MECHANICAL MODEL OF ECONOMICS*

- 2008, B.S. Engineering Physics, Colorado School of Mines, Golden, Colorado, USA

RESEARCH EXPERIENCE

- Aug 15 – Present, Research Assistant, Theoretical Division and Center for Nonlinear Studies, Los Alamos National Laboratory, Machine learning applied to statistical physics systems
- Aug '12 – Present, Research assistant, Boston University Physics Department, W. Klein Group, Statistical physics of heterogenous systems, earthquakes, and econophysics.

- Sept '10 – July '12, Research assistant, Boston University Physics Department, High energy theory group, Dark matter direct detection and signatures of Technicolor physics.

TEACHING EXPERIENCE

- September '09 – May '15, Teaching assistant, Boston University Physics Department, Teaching Lab and Discussion sections for the follow undergraduate physics courses: PY103, PY105, PY106, PY212, PY251, PY252, PY313.
- Spring 2012, Grader, Boston University, PY551: Particle Physics.
- September '06 – December '08, Tutor, Colorado School of Mines, Walk-in tutoring services for various undergraduate science and engineering courses.

AWARDS

- 2008, Physics Faculty Distinguished Graduate Award, Colorado School of Mines.

COMPUTER SKILLS

- \LaTeX
- Python, Mathematica, Fortran, Java, C++

TALKS

- October 2013, **contributed talk**, “An Asset Exchange Model with Tunable Pareto Index” Greater Boston Area Statistical Mechanics Meeting, Brandeis University.

- May 2013, **preliminary oral exam**, “Agent-based Economics and the Relationship Between Growth and Wealth Inequality,” Boston University.
- November 2014, **contributed talk**, “Growth and stability in an asset exchange model economy” Greater Boston Area Statistical Mechanics Meeting, Brandeis University.
- November 2014, **departmental seminar**, “The Statistical Mechanics of Wealth: Agent-based economics with ergodic transitions.” Boston University.
- November 2015, **student talk**, “Deep Learning, Image Processing, and Materials Microstructure” CNLS Students Seminar, Center for Nonlinear Studies, Los Alamos National Laboratory, Los Alamos, NM.
- April 2016, **invited talk**, “Machine Learning Capabilities and Concepts” Workshop: Machine Learning and Earthquakes, Center for Nonlinear Studies, Los Alamos National Laboratory, Los Alamos, NM.
- July 2016, **dissertation defense**, “Inferring low-dimensional microstructure representations using convolutional neural networks,” Boston University.

POSTERS

- January 2016, “Learning low-dimensional representations of textures using convolutional networks ,” Workshop: Physics Informed Machine Learning, Santa Fe, NM.
- May 2016, “Learning low-dimensional representations of textures using convolutional networks ,” Workshop: Data Science and Optimal Learning for Materials Discovery and Design, Santa Fe, NM.

PUBLICATIONS

1. M. Coffey and N. Lubbers, “On generalized harmonic number sums,” *Applied Mathematics and Computation* **216**, 689-698 (2010)
2. A. Liam Fitzpatrick, Wick Haxton, Emanuel Katz, Nicholas Lubbers, Yiming Xu “The Effective Field Theory of Dark Matter Direct Detection”, 2012 arXiv:1203.3542 [hep-ph]
3. A. Liam Fitzpatrick, Wick Haxton, Emanuel Katz, Nicholas Lubbers, Yiming Xu “Model Independent Direct Detection Analyses”, 2012 arXiv:1211.2818 [hep-ph]
4. Kang Liu, N. Lubbers, W. Klein, J. Tobochnik, B. Boghosian, and H. Gould, “The effect of growth on equality in models of the economy,” 2013 arXiv:1305.0794 [q-fin]
5. N. Lubbers, K. Liu, W. Klein, J. Tobochnik, B. Boghosian, and H. Gould, “Phase transitions in the modified asset exchange model,” manuscript in preparation.
6. N. Lubbers, T. Lookman, K. Barros, “Inferring low-dimensional microstructure representations using convolutional neural networks,” manuscript in preparation.
7. Bertrand Rouet-Leduc, Claudia Hulbert, Nicholas Lubbers, Kipton Barros, and Paul A. Johnson, “Learning the Physics of Failure,” manuscript in preparation
8. N. Lubbers, K. Liu, W. Klein “Universality and Wealth Condensation in generalized yard-sale models of the economy,” manuscript in preparation.